

EVALUATION OF PUNCHING SHEAR STRENGTH DESIGN AND  
MODELLING APPROACHES FOR SLAB-COLUMN CONNECTIONS

A THESIS SUBMITTED TO  
THE GRADUATE SCHOOL OF NATURAL AND APPLIED SCIENCES  
OF  
MIDDLE EAST TECHNICAL UNIVERSITY

BY

MERVE ZORLU

IN PARTIAL FULFILLMENT OF THE REQUIREMENTS  
FOR  
THE DEGREE OF MASTER OF SCIENCE  
IN  
CIVIL ENGINEERING

SEPTEMBER 2012

Approval of the thesis:

**EVALUATION OF PUNCHING SHEAR STRENGTH DESIGN AND  
MODELLING APPROACHES FOR SLAB-COLUMN CONNECTIONS**

submitted by **MERVE ZORLU** in partial fulfillment of the requirements for the  
degree of **Master of Science in Civil Engineering Department, Middle East  
Technical University** by,

Prof. Dr. Canan Özgen

Dean, Graduate School of **Natural and Applied Sciences**

Prof. Dr. Güney Özcebe

Head of Department, **Civil Engineering**

Prof. Dr. Barış Binici

Supervisor, **Civil Engineering Dept., METU**

**Examining Committee Members:**

Prof. Dr. Güney Özcebe

Civil Engineering Dept., METU

Prof. Dr. Barış Binici

Civil Engineering Dept., METU

Assoc. Prof. Dr. Erdem Canbay

Civil Engineering Dept., METU

Assist. Prof. Dr. Özgür Kurç

Civil Engineering Dept., METU

Dr. Hakan Erdoğan

Civil Engineering Dept., Kocaeli University

**Date: 13.09.2012**

**I hereby declare that all information in this document has been obtained and presented in accordance with academic rules and ethical conduct. I also declare that, as required by these rules and conduct, I have fully cited and referenced all material and results that are not original to this work.**

Name, Surname : MERVE ZORLU

Signature :

## **ABSTRACT**

### **EVALUATION OF PUNCHING SHEAR STRENGTH DESIGN AND MODELLING APPROACHES FOR SLAB-COLUMN CONNECTIONS**

Zorlu, Merve  
M.Sc., Department of Civil Engineering  
Supervisor: Prof. Dr. Barış Binici

September 2012, 96 pages

Flat plate systems are constructed with slabs directly supported on columns. Since there are no beams in the system, the behavior of connections between the slabs and columns play a crucial role. Due to the sudden and brittle nature of punching shear failures, slab-column connection design must be conducted with proper safety precautions. The first part of this study aims to evaluate the safety level of different design expressions in the codes. For this purpose, the ability of ACI 318-11, TS-500 and Eurocode-2 to estimate punching shear strength was examined in light of experimental results compiled from previous research. Interior and exterior connections were examined in the course of the study. In the second part of the study, beam and shell models were calibrated to simulate the load-deformation response of interior slab-column connections in light of experimental results. In the final part of this thesis, a typical floor plan of a flat plate system was analyzed to investigate the possibility of a progressive failure mechanism after punching failure takes place at a slab-column connection. Minimum post-punching capacity required to avoid progressive punching failure in a floor was estimated. It is believed that, the results of this study can be helpful in guiding engineers in understanding the safety inherent in punching shear design expressions and to take necessary precautions against progressive collapse.

**Key Words:** Punching shear, effective stiffness, modeling, progressive collapse

## ÖZ

### KOLON DÖŞEME BİRLEŞİMLERİNDE ZİMBALAMA TASARIM VE MODELLEME ESASLARININ İRDELENMESİ

Zorlu, Merve  
Yüksek lisans, İnşaat Mühendisliği Bölümü  
Tez Yöneticisi: Prof. Dr. Barış Binici

Eylül 2012, 96 sayfa

Plak döşemeler döşemelerin doğrudan kolonlar üzerinde taşındığı sistemlerdir. Kirişlerin olmayışı sebebi ile, döşeme-kolon bağlantı bölgelerinin davranışı yapı sistemi için oldukça önemlidir. Bağlantı bölgelerinde ani ve gevrek olarak meydana gelme olasılığı bulunan zımbalama göçmesine karşı yeterli güvenlik payları ile tasarım yapılması gerekir. Bu tezin ilk kısmı, iç ve dış kolon-döşeme bağlantı bölgeleri için ACI 318-08, EC-2 ve TS500 tarafından önerilen tasarım denklemlerinin güvenlik paylarını deney verileri ışığında irdelemektedir. İkinci kısımda ise kiriş ve plak eleman modelleme teknikleri ile zımbalama davranışının nasıl modellenebileceği araştırılmış ve basit bir etkin rijitlik yaklaşımı önerilmiştir. Çalışmanın son kısmında, bu yaklaşım kullanılarak incelenen bir plak döşeme sisteminde oluşabilecek bir zımbalama sonrası ardışık zımbalama etkisinin sistemin nasıl göçmesine yol açabileceği ve açmaması için gereken zımbalama rezidüel taşıma kapasitesi belirlenmeye çalışılmıştır. Çalışmanın sonuçları hem zımbalama tasarım yaklaşımlarının güvenlik payları hem de zımbalama sonrası göçmeye karşı alınabilecek tedbirler hakkında fikir vermektedir.

Anahtar Kelimeler: Zımbalama, rezidüel kapasite, etkin rijitlik, göçme

## **ACKNOWLEDGEMENTS**

I am most thankful to my mother Merzuka and father Ramazan Zorlu for their endless support, love and altruism. Without of them, I would lose my way, they are always my light. Also, I want to thank to my brother Emre Zorlu, his existence makes me always more powerful.

I am grateful to my advisor, Prof. Dr. Barış Binici for his invaluable guidance, assistance, support and insight throughout the research and it was a privilege to work with him.

I would like to thank my mother-in-law Hatice, father-in-law Kemal Kazım and sister-in-law Gamze Silay for their valuable support and love.

I would like to thank my all my friends, especially Sema Melek Yılmaztürk and Burhan Aleessa Alam for their support and help during the research.

Finally, I have a special thanks to my husband Umut Silay. During this journey, I always feel your love, friendship and encouragement. I am the luckiest woman in the world because of being your wife. I love you so much.

*To My Family...*

## TABLE OF CONTENTS

<b>ABSTRACT .....</b>	<b>iv</b>
<b>ÖZ .....</b>	<b>v</b>
<b>ACKNOWLEDGEMENTS.....</b>	<b>vi</b>
<b>TABLE OF CONTENTS.....</b>	<b>viii</b>
<b>LIST OF TABLES .....</b>	<b>x</b>
<b>LIST OF FIGURES .....</b>	<b>xi</b>
<b>CHAPTERS</b>	
<b>1. INTRODUCTION.....</b>	<b>1</b>
1.1. Flat Plate Systems: .....	1
1.2. Literature Survey .....	9
1.3. Design Approaches.....	17
1.3.1. ACI 318-08 .....	18
1.3.2. TS-500(2000) .....	20
1.3.3. Eurocode-2(2003) .....	23
1.4. Objectives and Scope: .....	27
<b>2. EVALUATION OF DESIGN GUIDELINES IN LIGHT OF EXPERIMENTAL RESULTS.....</b>	<b>28</b>
2.1. Introduction: .....	28
2.2. Concentric Loading: .....	28
2.3. Eccentric Loading: .....	45
2.3.1. Interior Slab-Column Connections: .....	45
2.3.2. Exterior Slab-Column Connections .....	53



<b>3. ANALYSIS OF PUNCHING FAILURE EXPERIMENTS FOR FLAT PLATES .....</b>	<b>62</b>
3.1. General: .....	62
3.2. Approach1: Shell Method .....	64
3.3. Approach 2:Beam Method .....	72
<b>4. A NUMERICAL STUDY TO EXAMINE THE POST-PUNCHING CAPACITY REQUIRED TO AVOID PROGRESSIVE PUNCHING .....</b>	<b>79</b>
4.1. Introduction: .....	79
4.2. Explanation of Collapse Analysis Steps:.....	82
4.2.1. Step 1: .....	83
4.2.2. Step 2: .....	84
4.2.3. Step 3: .....	85
4.3. Results: .....	88
<b>5. CONCLUSIONS AND RECOMMENDATIONS.....</b>	<b>91</b>
<b>REFERENCES.....</b>	<b>94</b>

## LIST OF TABLES

### TABLES

Table 1.1 Values of k for rectangular loaded areas(Eurocode 2-2003, 2003) .....	24
Table 2.1 Comparison of punching loads according to ACI-318, Eurocode-2 and TS-500 on concentric loading .....	32
Table 2.2 Unbalanced moments from ACI-318, Eurocode-2 and TS500 for interior slab-column connections on eccentric loading .....	48
Table 2.3 Comparison of unbalanced moments with ACI-318, Eurocode-2 and TS500 for exterior slab-column connections on eccentric loading.....	56
Table 3.1 General properties of used experiment .....	64

## LIST OF FIGURES

### FIGURES

Figure 1.1 Major types of flat plates, (The Constructor Org) .....	1
Figure 1.2 Change of the floor height by using flat plate, (The Constructor Org) .....	2
Figure 1.3 Collapse moment of Sampoong Department Store, (McLean, et al.).....	3
Figure 1.4 Sampoong Department Store after collapse, (Park T. W., 2011) .....	4
Figure 1.5 The view of the Bullock's Department Store after the collapse, (Dewey, 1994) .....	5
Figure 1.6 J.C Penney Building after Alaska Earthquake, (Bertero, 1982) .....	6
Figure 1.7 Collapse of Harbour Cay Condominium, (Corley, 2010) .....	7
Figure 1.8 Punching Failures in Switzerland, .....	8
Figure 1.9 Jaya Supermarket after the collapse, (Rashita, et al., 2009). .....	8
Figure 1.10 Example of collapse of waffle slab building failures in New Mexico (Rosenblueth, et al., 1986) .....	9
Figure 1.11 Comparison of recommended performance based seismic design limits with slab-column connection test data, (Hueste, et al., 2007).....	16
Figure 1.12 Location of critical punching perimeter in ACI 318. ....	19
Figure 1.13 Assumed distribution of shear stress in ACI 318(ACI Committee 318, 2011) .....	20
Figure 1.14 Eccentricity calculation in TS500, (Turkish Standards Institutes, 2000)22	
Figure 1.15 Location of critical punching perimeter in TS500.....	22
Figure 1.16 Typical control parameters, (Eurocode 2-2003, 2003).....	23
Figure 1.17 Shear distribution due to unbalanced moment at a slab-internal column connection, (Eurocode 2-2003, 2003).....	24
Figure 1.18 Equivalent control perimeter $u_1^*$ (Eurocode 2-2003, 2003).....	25
Figure 2.1 Distribution of the Column Size for Slab-Column Connections in the Concentric Loading Database .....	29
Figure 2.2 Distribution of the Effective Depth of the Slabs in the Concentric Loading Database .....	30

Figure 2.3 Distribution of the Reinforcement Ratio for Slab-Column Connections in the Concentric Loading Database .....	30
Figure 2.4 Distribution of the Compressive Strength of the Concrete for Slab-Column Connections in the Concentric Loading Database .....	31
Figure 2.5 Comparison of punching loads between ACI-318 and experimental values .....	43
Figure 2.6 Comparison of punching loads between TS500 and experimental values	44
Figure 2.7 Comparison of unbalanced moments between Eurocode-2 and experimental.....	44
Figure 2.8 Distribution of the Column Size for Interior Slab-Column Connections for the Database .....	46
Figure 2.9 Distribution of the Effective Depth of the Slab for Interior Slab-Column Connections for the Database .....	46
Figure 2.10 Distribution of the Reinforcement Ratio for Interior Slab-Column Connections for the Database .....	47
Figure 2.11 Distribution of the Compressive Strength of Concrete ( $f_c$ ) for Interior Slab-Column Connections for the Database .....	47
Figure 2.12 Comparison of Unbalanced Moments between ACI-318 and Experimental Values .....	51
Figure 2.13 Comparison of Unbalanced Moments between TS500 and Experimental Values.....	52
Figure 2.15 Distribution of the Column Size for Exterior Slab-Column Connections .....	53
Figure 2.16 Distribution of the Effective Depth of the Slab for Exterior Slab-Column Connections.....	54
Figure 2.17 Distribution of the Reinforcement Ratio of the Slab for Exterior Slab-Column Connections.....	54
Figure 2.18 Distribution of the Compressive Concrete Strength ( $f_c$ ) for Exterior Slab-Column Connections.....	55
Figure 2.19 Comparison of unbalanced moments between ACI and experimental values.....	59

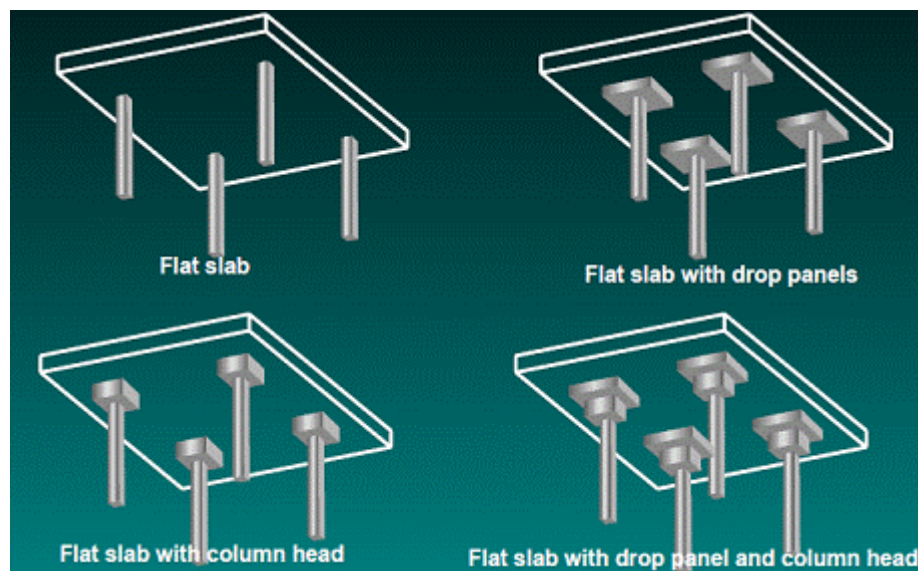
Figure 2.20 Comparison of unbalanced moments between TS500 and experimental values.....	60
Figure 2.21 Comparison of unbalanced moments between Eurocode and experimental values.....	61
Figure 3.1 Distribution of $f_c$ .....	63
Figure 3.2 Distribution of reinforcement ratio ( $\rho$ ) .....	63
Figure 3.3 General view of the test specimen .....	65
Figure 3.4 Punching stage of the specimen.....	66
Figure 3.5 Summary of the load deformation curves for shell method .....	68
Figure 3.6 Summary of the load deformation curves for shell method .....	69
Figure 3.7 Summary of the load deformation curves for shell method .....	70
Figure 3.8 Ductility versus reinforcement ratio curve .....	71
Figure 3.9 Correction factor versus reinforcement ratio curve .....	71
Figure 3.10 The General Model for Beam Method.....	72
Figure 3.11 The Final Stage of Shear Hinges .....	73
Figure 3.12 Summary of the load deformation curves for beam method .....	75
Figure 3.13 Summary of the load deformation curves for beam method .....	76
Figure 3.14 Summary of the load deformation curves for beam method .....	77
Figure 3.15 Ductility versus reinforcement ratio curve .....	78
Figure 3.16 Correction factor versus reinforcement ratio curve .....	78
Figure 4.1 Analysis procedure of slab column connections .....	80
Figure 4.2 The general view of the system and its member .....	82
Figure 4.3 Applied Load to the column S1 .....	83
Figure 4.4 Shear distribution of the system .....	84
Figure 4.5 System View and Loading Path of Step 2 .....	85
Figure 4.6 Summary of Steps1-2 and 3.....	87
Figure 4.7 The relationship between $V_{pp}/V_p$ and $R/V_p$ .....	89
Figure 4.8 The summary of the relationship between $V_{pp}/V_p$ and $R/V_p$ .....	90

## CHAPTER 1

### INTRODUCTION

#### 1.1. Flat Plate Systems:

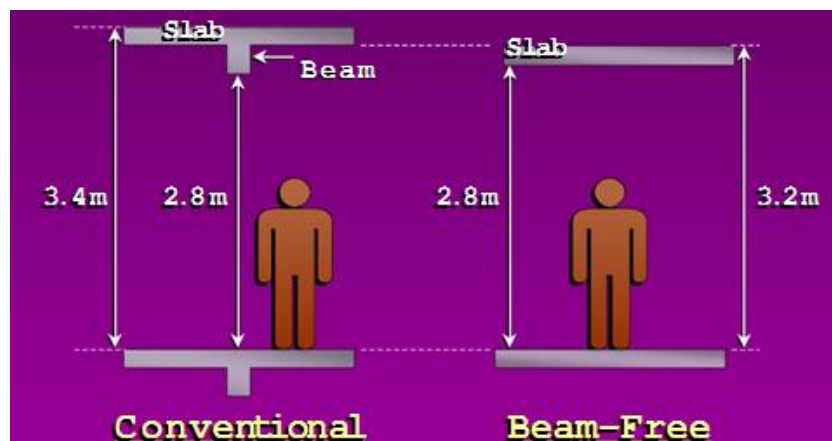
Flat-plate buildings consist of reinforced concrete slabs which are supported directly on reinforced concrete columns without the use of beams. These structural systems are mainly used in moderate or low seismic zones. Sometimes column heads, drop panels or both can be used with the objective of increasing the shear strength and decreasing the moment demands in the slab. In Figure 1.1 major types of flat plates are schematically shown.



**Figure 1.1 Major types of flat plates, (The Constructor Org)**

The major benefits of constructing flat plate systems are their architectural flexibility in room layout, savings in the floor height, less building height, shorter construction time and low workmanship costs due to ease of formwork. Possible gain in the story height is illustrated in Figure 1.2.

However if this system is constructed in high seismic zones, flat plate system should be combined with shear walls or moment resisting frames. When flat plate buildings are designed without strict drift deformation control in high seismic zones, slab column connections may sustain severe damage when subjected to lateral deformation demands in addition to gravity loads. The action of combined shear force and moment demands on the connections may cause- the so called punching shear failure. Punching failure, unlike the flexural failure, it is a catastrophic brittle failure mode describing the sudden movement of the slab towards the column due to a local failure.



**Figure 1.2 Change of the floor height by using flat plate, (The Constructor Org)**

Some of the well-known punching failure cases in the literature were listed below.

- **Sampoong Department Store (1995):**

Sampoong Department Store's collapse was accepted as a punching failure which occurred on June 29, 1995 in the Gangnam-gu district of Seoul, South Korea. In this building, 502 people died, 6 people missed and 937 people injured. This event was one of the most dramatic disaster of South Korea history. Initially the building was designed as an office building with four floors, but it was changed to a large department store during its construction. This involved cutting away a number of supporting columns in order to install escalators. Then a fifth floor was added and this floor was overloaded.

In April 1995, cracks began to appear in the ceiling of the south wing's fifth floor. On the June 29, the number of cracks in the area increased dramatically and at the end the building totally collapsed (Figure 1.3 and Figure 1.4). (Park T. W., 2011)



**Figure 1.3 Collapse moment of Sampoong Department Store, (McLean, et al.)**





**Figure 1.4 Sampoong Department Store after collapse, (Park T. W., 2011)**

- **Bullock's Department Store (1994):**

The Northridge earthquake occurred on January 17, 1994 in California USA. Bullock's department store was a flat plate building with shear walls. The combined effect of gravity shear and unbalanced moments resulted by earthquake caused distress in the slab column connections of the building. The investigations after earthquake showed that punching failures started at the interior bays and then continued with the partial collapse of building. The final view of the building could be seen in Figure 1.5, (Arnold, 1994; and USGS,1996).



**Figure 1.5 The view of the Bullock's Department Store after the collapse,  
(Dewey, 1994)**

- **J.C Penney Building (1964):**

This five stories tall flat plate building was in Anchorage, Alaska. It has almost  $9,300 \text{ m}^2$  floor plan area, slab thickness was 0.25 m and supported on shear walls and reinforced columns. The building was almost square in plan but shear walls was inserted unsymmetrically. Because of the eccentricity due to center of rigidity and center of the mass being at different locations, large torsional forces and deformations occurred in the building during the 1964 Alaska earthquake. In addition, due to the relatively poor workmanship and detailing, building partially collapsed, (Figure 1.6), (Bertero, June 1982).



**Figure 0.6 J.C Penney Building after Alaska Earthquake, (Bertero, 1982)**

- **Harbour Cay Condominium (1981):**

This was a five-story flat plate residential development project in Cocoa Beach (Brevard County, Florida, United States). It collapsed due to punching shear failure of the slab-column connections when workers were completing the framework by casting concrete for the roof on March 27, 1981. 11 workers were killed and 27 injured (see Figure 1.7). After the accident more serious enforcement of engineering and construction codes in Florida and elsewhere was begun to use.

The collapse was because of the miscellaneous errors in the design and construction. For example, although the concrete slabs should have been at least 280 mm thick to satisfy the American Concrete Institute's Building Code, instead of 200 mm used in the construction (Corley, 2010).



**Figure 1.7 Collapse of Harbour Cay Condominium, (Corley, 2010)**

- **Shopping Centre, Underground Car Parking Building :**

Three examples can be given about punching failure in Switzerland. First one was in late 70's, during slab construction punching failure occurred and large parts of the shopping centre destroyed (Figure 1.8a). During winter 1981 second case happened at Bluche, which an underground parking garage (Figure 1.8b). It resulted in the death of two children. Last one was the catastrophic one, at Gretzenbach in 2004, which occurred in an underground parking garage, causing the death of 7 firemen, who were interfered to a fire in that garage. The failure initiated at one slab-column connection and finished when large part of the structure collapsed (Figure 1.8c) (Mirzaei, 2010).





**Figure 1.8 Punching Failures in Switzerland, (Mirzaei, 2010)**

- **Jaya Supermarket (2009):**

Jaya Shopping Centre, better known as Jaya Supermarket, is a well-known landmark in Selangor, Malaysia. It collapsed while demonstration work was going on, killing two workers (see Figure 1.9). Despite the plans of the building was for four stories, a fifth story was added during construction and during rebuilding process this floor was overloaded by machinery, (Rashita, et al., 2009).



**Figure 1.9 Jaya Supermarket after the collapse, (Rashita, et al., 2009).**

- **Waffle-Slab Buildings (1985):**

During the 1985 Mexico City earthquake, 91 waffle-slab buildings collapsed and 44 building had severe damages.(see Figure1.10) Reason of these disasters was these buildings were not provided with shear walls against lateral loads hence interstory drifts were not controlled. Consequently, these structures could not resist the earthquake induced demands and brittle punching mechanism became an inevitable event (Rosenblueth & Meli, 1986).



**Figure 1.10 Example of collapse of waffle slab building failures in New Mexico  
(Rosenblueth, et al., 1986)**

## **1.2. Literature Survey**

In this section, some important studies, which were reviewed in the course of the study and contributed significantly to the development of design equations, are presented. Many other experimental results, which are not given below are also presented in Chapter 2.

Hognestad and Elstner (1956) worked on the methods and results of the experimental work on the shearing strength of slab-column connections subjected to concentrated

load. The behavior of the 34 specimens investigated by changing concrete strength, percentage of reinforcement, size of column, conditions of support and loading etc. Finally an ultimate strength theory was obtained, so the slab behavior under gravity load could be estimated. The testing consisted of nine series and thirty-four specimens. The slabs were 6 feet square and 6 inches thick. Supports were on the edges and loading was centrally located. Except the ninth series there was no shear reinforcement on specimens. The column sizes varied from 254 to 356 mm. The main conclusions of the report could be summarized as follows (Elstner & Hognestad, 1956):

- For the ultimate shearing strength of the slab-column connections, compression reinforcement was not effective.
- Failed slabs due to flexure had 10% to 20% greater ultimate capacity than predicted by the yield line theory, which was attributed to redistribution in the two way system and steel strain hardening.
- Shearing strength did not increased when the tension reinforcement was concentrated directly over a column.
- In most cases punching failure occurred after the initial yielding of reinforcement around the columns.

Zee and Moehle (1984) studied both interior and exterior slab-column connections under vertical and horizontal loads. The test specimen was three tenths scale of a prototype structure and designed to cover all requirements of ACI 318-82. Deflections and deformations were recorded during the loading and an analytical model for the prediction of load-deformation response was proposed. Key results from the study were as follows (Zee, et al., 1984):

- Standard moment curvature analysis assumes that plane sections remain plane in bending. This was found to be inapplicable for calculating the flexural capacity of the slab around the connection region since the moment distribution across the slab width was non-uniform.
- The flat plate subassemblies did not develop significant yielding until imposed lateral drifts approached 1.5%. If the drift ratios are limited to 1.5%

for high gravity shear situations, the structural damage may be minimized. However significant inelastic deformability should not be expected.

Pan and Moehle (1987) stated that the prevailing ductile design philosophy required that elements of a structural system could deform into the inelastic range during seismic events. In some conditions this requirement extended to elements which were not considered in design as part of lateral load resisting system. The aim of their experimental work was to develop new experimental data for major parameters which affected the lateral displacement capacity and ductility of reinforced concrete flat plates. In the tests, only interior, conventionally reinforced slabs without slab shear reinforcement were used. Obtained results can be summarized as follows

(Pan, et al., 1987):

- The magnitude of the gravity shear ratio carried by the slab was the primary variable that affects the lateral displacement capacity and ductility of slab-column connections.
- For a given level of gravity load, lateral stiffness, available ductility and punching strength is significantly reduced under biaxial lateral loading.
- Lateral interstory drifts under extreme earthquake loading should not exceed 1.5% of interstory height. Up to that level of deformation the flat plate connection will perform adequately.

Moehle et.al (1988) worked on a design methodology of slab column connections for punching shear strength and developed expressions for shear strength in the absence of moment transfer, in which they included modifications factors to take into account the influence of geometry, deformation levels and material strength. In addition, three alternate procedures to compute strength under combined shear and moment transfer were discussed and code expressions were proposed in light of their study (Moehle, et al., 1988). As a result of their benchmark paper;

- Eccentric shear stress model was recast in ACI 318-83 (1983).
- Further simplifications for design of edge and corner connections were proposed.



- New recommendations for the design of connections subjected to earthquake were presented.

Pan and Moehle (1992) tested four specimens under combined gravity and lateral loads. Specimens 1 and 3 were subjected to uniaxial, 2 and 4 were subjected to biaxial lateral loads. The aim of the study was to compare the effects of uniaxial versus biaxial lateral loading on the connection behavior. One of the biaxial loaded specimens (4) was repaired and tested again. Specimens were 60% scaled versions extracted from prototype structure. The main results from the study were as follows (Pan, et al., 1992):

- The lateral stiffness, strength and drift ratio capacities were less when biaxial lateral loading was present compared to the uniaxial lateral loading.
- Repaired specimen gained original drift capacity again but strength was not restored.
- The ACI eccentric shear stress model was found to be conservative enough for both uniaxial and biaxial loading.
- The stiffness of a flat plate consisting of single slab-column connection test specimen was found to be best modeled with the equivalent beam with proposed by Darwin and Pecknold (1974) along with a cracking reduction factor of 1/3. This conclusion is reevaluated in this study.

Robertson and Durrani (1992) studied the effect of superimposed slab loading on the behavior of interior slab column connections. Each specimen consisted of a subassembly made of two exterior connections and one interior connection. Three identical subassemblies were tested. Under different superimposed loading, specimens were subjected to the same cyclic lateral displacement excursions. As a result it is found that, when the gravity load was increased both unbalanced moment capacity and lateral drift capacity decreased. For interior connections a limiting shear stress was suggested, so that the drift capacity could be predicted. Finally the test results were compared with ACI 318 provisions and ACI Committee 352 recommendations for design of this type of connections (Robertson, et al.,1992).

Farhey et al. (1993) observed the resistance and final failure mechanism, the relative impact of cross sectional width of the column and the effect of shear force level on the occurrence of punching shear failure for connections subjected to combined shear and moment reversals. Four reinforced concrete  $\frac{3}{4}$  scaled flat slab interior column slab connections were tested. First and the second specimens had identical column strength, third one had different concrete strength and finally fourth specimen had different column size but same concrete strength with Specimen 3. At the final stage, all specimens failed because of the punching along one side of the connection. With the flexural failure of the connection, spalling of the concrete occurred at the front or back faces. These results showed that the failure mechanism and the final shape of the failure surfaces (Farhey, et al., 1993).

Durrani et al. (1995) studied the behavior of nonductile slab-column connections. Study provided a valuable insight of punching strength, moment transfer capacity and drift capacity of nonductile connections under earthquake loading. Four different specimens were tested. These slab column specimens were half scale models with identical longitudinal reinforcement ratio (0.59%). For subassemblies 1, 3 and 4, DL+0.3LL (DL: dead load, LL: live load) and for subassembly 2, DL+LL loading were applied. In addition each subassembly was subjected to 20 displacement cycles increasing in amplitude. Following conclusions can be deduced from this study (Durrani, et al., 1995):

- When applied gravity load was high, interior connections had a greater probability of failing in punching compared to the exterior columns.
- For gravity shear ratios ( $\frac{V_g}{\sqrt{f_{cb}}d}$ ) more than 0.125, interior connections are expected to fail due to punching, hence when this ratio is smaller than 0.083 the failure mode would be flexural.
- As gravity shear ratio increased, drift capacity decreased.
- Loss of stiffness in exterior connections during cyclic displacement excursions were more than those observed in interior connections

FIB (2001) published a comprehensive technical report on concentric punching shear strength of slab-column connections. The aim of the FIB technical was to summarize the developments in punching shear research. Furthermore, empirically derived code formulas and some of the mechanical models were discussed along with the concentric punching shear tests results presented in the report. There was no generally agreed design model for the design practice since punching problem is a complex one and codes prefer to give simple and empirically derived formulas. The bulletin gave a review of some of the most widely used codes (German Design Code DIN 1045(88); Eurocode-2; Model Code 90 & FIP-Recommendations 1996; British Standard 8110, Part 1, 1997 and ACI 318-95) their rules and definitions. The new developments for mechanical models were summarized and nonlinear finite element analyses applied to simulate the behavior of flat plate connections with and without shear reinforcement. A database without shear reinforcement consisted of 149 tests presented in the report. This database was used in Chapter 2 of this study. The test data were compared with some of the selected design codes, which were following key results were discussed as a result of this report (CEB/fib Task Group, 2001):

- Because of the important influence of the flexural reinforcement and the concrete compressive strength, coefficient of variation higher variation  $v$  ( $v = \frac{\sigma}{\xi_m}$  was indicated where  $\sigma$  was standard deviation and  $\xi_m$  was the mean was significantly large). Since the mean predictions were nearly 1 for Model Code 90 & FIP-Recommendations 1996 and DIN 1045(88), it could be said they gave good approximations.

Park and Choi (2006) worked on a numerical study of interior flat plate column connections subjected to unbalanced moments by using the finite element method. The findings were summarized as follows (Park, et al., 2006);

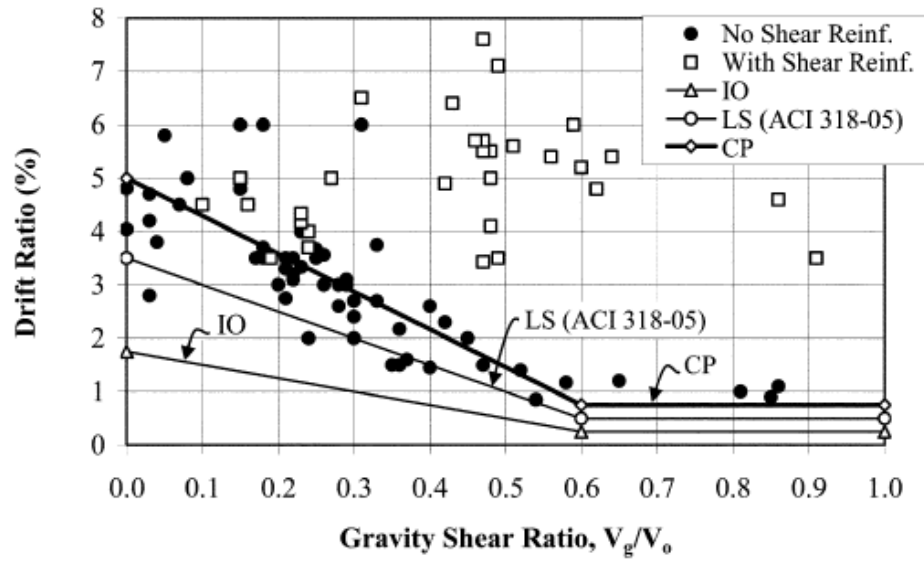
- Eccentric shear strength at the front back sides of columns is about  $v_c = 0.33(f_c)^{1/2}$ , which is similar to that recommended by same as ACI-318-11.

However, the shear strength at the sides providing by torsional resistance is more than three times the shear strength at the front/back faces.

- Although  $\gamma_v$  (ratio of the moment transferred by the eccentricity shear to total unbalanced moment) is calculated to be about 0.6-0.8 ranges, in ACI 318 it ( $\gamma_v$ ) is 0.4.
- For more accurate eccentric shear stress model, the interaction between the eccentricity shear strength and the flexural moment coexisting in the critical section must be considered.
- Strength and the distribution of the eccentric shear occurring at the slab column connection were different than assumed current design codes (ACI 318-02/318R-02).

Hueste et al. (2007) examined the previous relevant flat slab experiment data under gravity and lateral loading and evaluated the design code approaches. An equation that relates the inter-story drift ratio capacity (DR) to the gravity shear ratio at slab column connections to was proposed as  $DR = 5 - 7 \frac{V_g}{V_o} (\%)$ . In Figure 1.11 the Drift

Ratio versus Gravity Shear Ratio comparisons under the different design codes and approaches can be seen (Hueste, et al., 2007).



**Figure 1.11 Comparison of recommended performance based seismic design limits with slab-column connection test data, (Hueste, et al., 2007)**

Park and Choi (2007) worked on an improved model for exterior slab column connections. They claimed that the current design codes do not give accurate estimation for the punching shear strength of exterior slab column connections subjected to unbalanced moments. Nonlinear finite element analyses were performed to examine the magnitude and the distribution of eccentric shear and flexural moments developing at the critical sections of the exterior connections. Then the calculated strength values were compared with the current design codes. The results showed that the magnitude and distribution of eccentric shears were not constant along the edges of the column. In the improved model, to define the eccentric shear strength at the critical section; the effect of the flexural moment, depth of the compression zone of the cross-section, edge length of the column-section, and the slab thickness were taken into account. Finally, the validity of the improved model was verified by comparisons with existing test results (Park, et al., 2007).

Kang et al. (2009) proposed a limit state failure model, which was developed in order to model punching shear failure considering the gravity shear ratio and lateral interstory drift. Both analytical and experimental studies were employed to assess and improve the modeling techniques for interpreting the nonlinear behavior of flat plate connections. Shake table test resulted for two one third scale, two story reinforced concrete and post-tensioned concrete slab column frames were used for this purpose. Investigation onset of slab flexure yielding due to unbalanced moment transfer and loss of slab to column moment transfer capacity due to punching shear failure were the main objectives . According to their results, it could be said that gravity shear versus drift relations based on mean values gave the best estimate for the lateral drifts at punching. In conclusion, the model could be a valuable tool from a point of frame analysis for examining the existing slab column connections and design of new slab column connections (Kang, et al., 2009).

### 1.3. Design Approaches

The punching load carrying and the moment resisting capacity provisions of the three different building codes (ACI 318 2008, Eurocode-2 2011, TS500 2000) for both interior and exterior column connections with no shear reinforcement are presented in this section. In general, the punching shear strength without shear reinforcement is calculated as the product of nominal shear stress, critical perimeter and effective depth for all three codes (Equation 1.1) in the absence of any moment transfer. The main difference between the codes is the definition of the punching perimeter and the nominal shear stress. Punching load capacity,  $V_p$ , is calculated for all codes requirements as follows;

$$V_p = v u d \quad (1.1)$$

Where  $v$  is the nominal shear strength,  $u$  is the punching perimeter for without shear reinforcement slab and the  $d$  is the effective depth of the slab.

On the other hand, computing the punching shear strength in the presence of unbalanced moment for slabs without shear reinforcement differs between codes. The methods are explained below separately for each code approach considering the moment transfer.

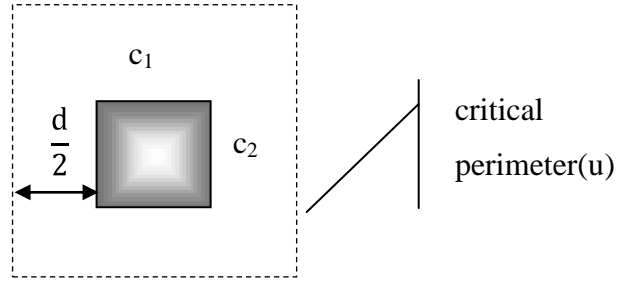
### 1.3.1. ACI 318-08

Nominal shear stress ( $v$ ) is defined as the minimum of three expressions given in Equation 1.2 in ACI 318-11. These three equations cover the effects of the column rectangularity, location of the connection and the loading area to effective thickness ratio on the nominal shear stress.

$$v = \text{minimum value of} \begin{cases} vc_1 = \frac{4}{12} \sqrt{f_c} \\ vc_2 = \frac{1}{12} \left( 2 + \frac{4}{\beta} \right) \sqrt{f_c} \\ vc_3 = \frac{1}{12} \left( \frac{\alpha d}{u} + 2 \right) \sqrt{f_c} \end{cases} \quad (\text{in SI units}) \quad (1.2)$$

$$u = 2(c_1 + c_2 + 2d) \quad (1.3)$$

where  $f_c$  is the concrete compressive strength,  $\beta$  (column aspect ratio) is the ratio of long side to short side of the column,  $\alpha$  (coefficient depending on the location of the connection) is 40 for interior columns, 30 for edge columns, 20 for corner columns,  $u$  (critical punching perimeter) is assumed  $d/2$  away from the column face and it is given in Equation 1.3.  $c_1$  is long side and  $c_2$  is the long side length of the column and  $d$  is the effective depth of the slab. ACI 318-11 punching perimeter definition is given in Figure 1.12.



**Figure 1.12 Location of critical punching perimeter in ACI 318.**

ACI-318-11 assumes a linear variation of stress distribution caused by vertical shear and unbalanced moment transfer along the critical perimeter. Therefore, the shear stress under action of gravity shear force and unbalanced moment can be calculated by using Equation 1.4 for a given gravity shear  $V_u$ .

$$v = \frac{V_u}{A_c} + \frac{\gamma_v M_{ACI} \left( \frac{(c_1 + d)}{2} \right)}{J_c} \quad (1.4)$$

$M_{ACI}$  is the factored unbalanced moment,  $A_c$  is the area of the assumed critical section (Equation 1.5),  $J_c$  is a property of the assumed critical section analogous to the polar moment of inertia (Equation 1.6),  $\gamma_f$  is a factor denoting the ratio of the moment carried in flexure (Equation 1.7), and  $\gamma_v$  is a factor denoting the ratio of the moment carried by the eccentricity of shear (Equation 1.8). For square columns,  $\gamma_v$  is equal to 0.4

$$A_c = 2d(c_1 + c_2 + 2d) \quad (1.5)$$

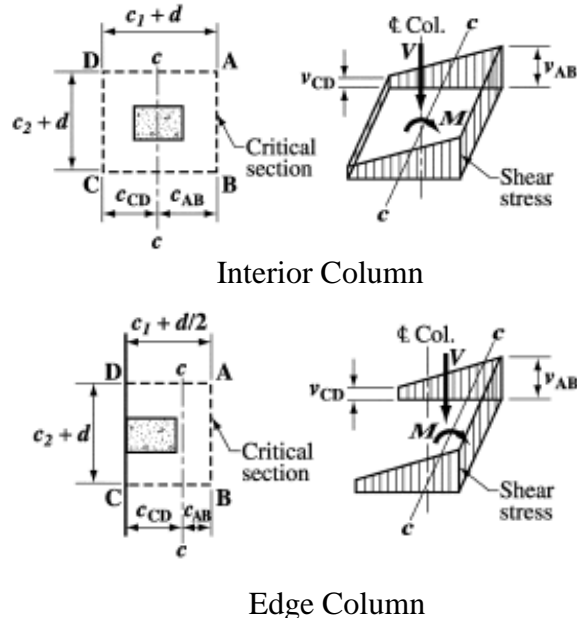
$$J_c = \left( \frac{d(c_1 + d)^3}{6} \right) + \left( \frac{(c_1 + d)d^3}{6} \right) + \left( \frac{d(c_2 + d)(c_1 + d)^2}{2} \right) \quad (1.6)$$

$$\gamma_f = \frac{1}{\left( 1 + \frac{2}{3} \right) * \left( \frac{b_2}{b_1} \right)^{0.5}} \quad (1.7)$$

$$\gamma_v = (1 - \gamma_f) \quad (1.8)$$



$$b_1=c_1+d \text{ \& } b_2=c_2+d \quad (1.9)$$



**Figure 1.13 Assumed distribution of shear stress in ACI 318(ACI Committee 318, 2011)**

In seismic design, the gravity shear acting on the flat-plate connections should be limited for safety purposes. The amount of gravity load acting on a flat-plate slab-column connection directly affects lateral load response of flat-plate structures. The lateral deformation capacity of flat-plate connection decreases when the ratio of  $V_g/V_o$  increases.

### 1.3.2. TS-500(2000)

The punching shear strength  $V_{TS500}$  according to TS-500 shall be calculated by using the Equation 1.10 given below:

$$V_p = \gamma^* f_{ct}^* u^* d \quad (1.10)$$

where  $f_{ct}$  is the tensile strength of concrete and is equal to  $0.35\sqrt{f_c}$ ,  $u$  is the critical perimeter and  $d$  is the effective depth of slab.

$\gamma$  is a coefficient reflecting the effects of unbalanced moment. Unless the effect of unbalanced column moments transferred to the slab has been obtained by carrying out more reliable calculations, the shear due to bending moments should be considered in calculations by using the coefficients  $\gamma$  given below (Equation 1.11).

In case of axial loading,  $\gamma = 1.0$ , while in case of eccentric loading the following formula is used,

$$\gamma = \frac{1}{1 + \eta \frac{e}{W_m} * u * d} \quad (1.11)$$

$$\eta = \frac{1}{1 + \sqrt{b_2 / b_1}} \quad (1.12)$$

The Equation 1.12 is only valid if  $b_2 \geq 0.7 * b_1$ .

When columns are not near edges or corners of the slabs,  $\gamma$  can be calculated by simpler equations (Equations 1.13 and 1.14).

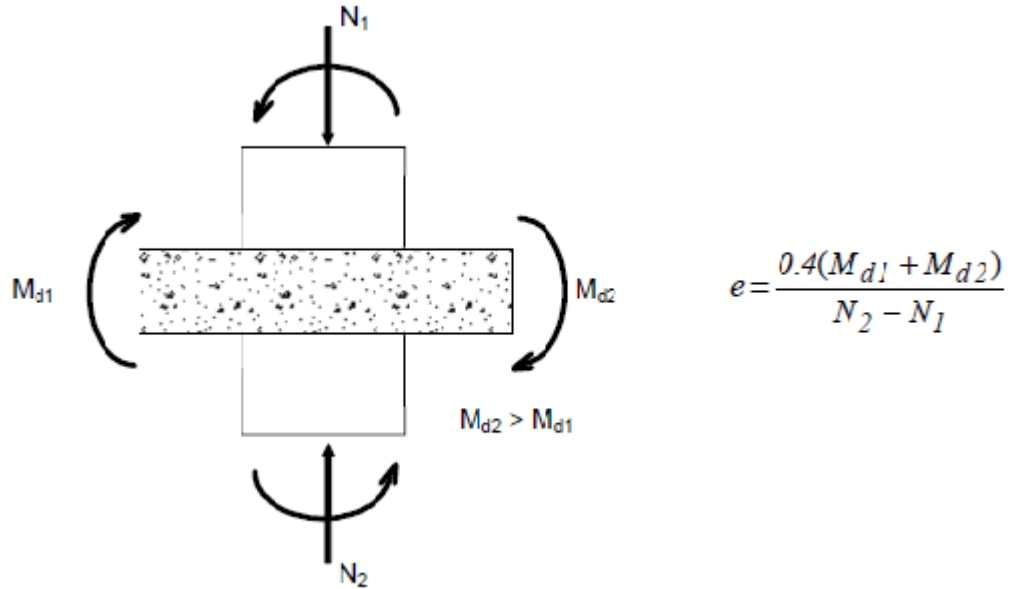
For rectangular loading areas or rectangular columns,

$$\gamma = \frac{1}{1 + 1.5 \frac{e_x + e_y}{\sqrt{b_x * b_y}}} \quad (1.13)$$

For circular loading areas or circular columns,

$$\gamma = \frac{1}{1 + \frac{2e}{d + d_0}} \quad (1.14)$$

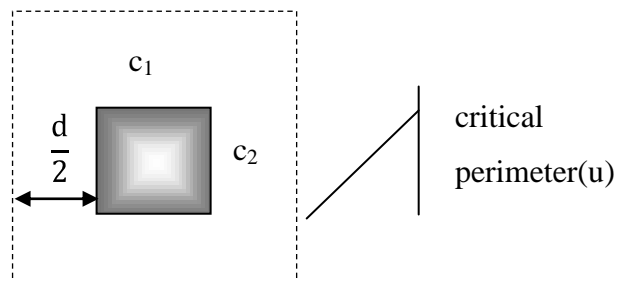
The eccentricity calculation can be seen in Figure 1.15.



**Figure 1.14 Eccentricity calculation in TS500, (Turkish Standards Institutes, 2000)**

As it can be seen in Figure 1.15, critical punching perimeter is calculated by using the same equation as in ACI-318 (Equation 1.15).

$$u = 2 * (c_1 + c_2 + 2 * d) \quad (1.15)$$



**Figure 1.15 Location of critical punching perimeter in TS500**

The design recommendation of TS-500 and ACI 318-11 are very similar. In fact one may obtain Equation 1.10 from Equation 1.4 upon organizing Equation 1.4 by taking into V parenthesis. The final equation can be seen in Equation 1.16.

$$V = v \left( \frac{1}{ud + \frac{\gamma_v M / V}{J / c}} \right) = \left( \frac{1}{1 + \frac{\gamma_v e}{J / c} ud} \right) udv \quad (1.16)$$

It can be observed that the first term of the right hand side is analogous to  $\gamma$  of TS-500 given in Equation 1.11, when  $\gamma_v$  and  $J/c$  are replaced by  $\eta$  and  $W_m$ . Since  $W_m$  is not given in TS-500 as explicit expressions for exterior columns, one may choose to use the  $J/c$  from ACI 318-08 for  $\gamma$  calculation of TS-500.

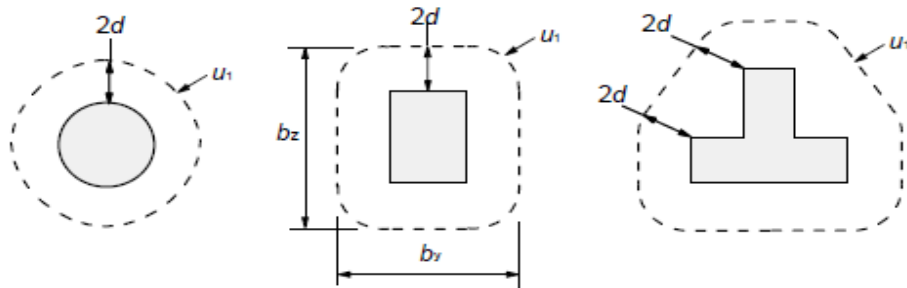
### 1.3.3. Eurocode-2(2003)

Nominal shear stress ( $v_E$ ) is defined as given in Equation 1.17 in Eurocode-2.

$$v_u = \frac{V_u}{u * d} \beta \quad (1.17)$$

where  $v_u$  is the shear stress,  $u$  is the control perimeter (see Figure 1.16),  $d$  is effective depth of the slab and finally  $\beta$  is given as (Equation 1.18):

$$\beta = 1 + k * \frac{M_{Eurocode}}{V_u} * \frac{u}{W_1} \quad (1.18)$$

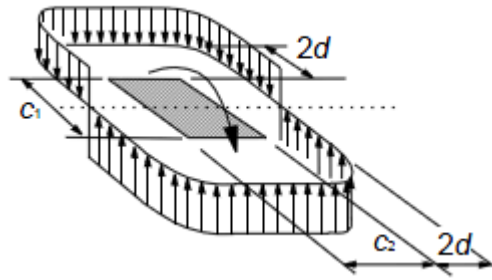


**Figure 1.16 Typical control parameters, (Eurocode 2-2003, 2003)**

$k$  is a coefficient dependent on the ratio of the column dimensions  $c_1$  and  $c_2$  and its value is a function of the proportions of the unbalanced moment transmitted by uneven shear and by bending and torsion (see Table 1.1).  $W_1$  corresponds to shear distribution as illustrated in Figure 1.17 and is a function of the basic control perimeter  $u_1$ :

**Table 1.1 Values of  $k$  for rectangular loaded areas(Eurocode 2-2003, 2003)**

$c_1/c_2$	$\leq 0,5$	1,0	2,0	$\geq 3,0$
$k$	0,45	0,60	0,70	0,80



**Figure 1.17 Shear distribution due to unbalanced moment at a slab-internal column connection, (Eurocode 2-2003, 2003)**

$W_1$  value for rectangular columns (Equation 1.19):

$$W = \frac{c_1^2}{2} + c_1 c_2 + 4c_2 d + 16d^2 + 2\pi d c_1 \quad (1.19)$$

where  $c_1$  is the column dimension parallel to the eccentricity of the load and  $c_2$  is the column dimension perpendicular to the eccentricity of the load. For internal circular columns  $\beta$  follows from (Equation 1.20):

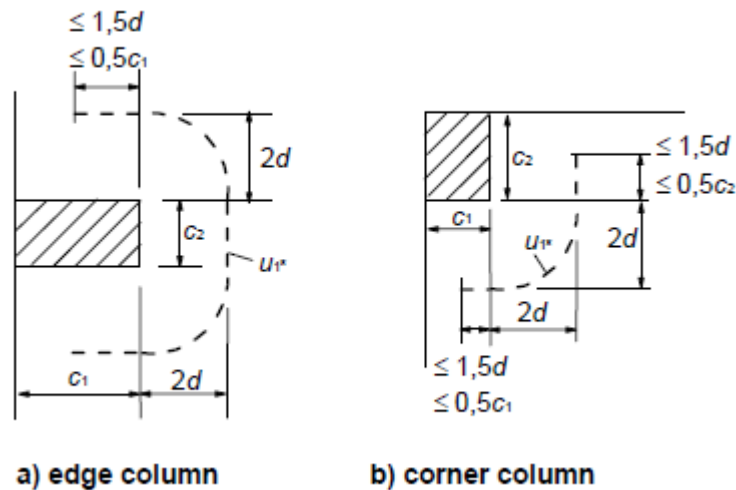
$$\beta = 1 + 0.6\pi \frac{e}{D + 4d} \quad (1.20)$$

For an internal rectangular column where the loading is eccentric to both axes, the following approximate expression for  $\beta$  may be used (Equation 1.21):

$$\beta = 1 + 1.18 \sqrt{\left(\frac{e_y}{b_z}\right)^2 + \left(\frac{e_z}{b_y}\right)^2} \quad (1.21)$$

where  $e_y$  and  $e_z$  are the eccentricities  $M_E/V_E$  along y and z axes respectively,  $b_y$  and  $b_z$  is the dimensions of the control perimeter and  $D$  is the diameter of the circular column.

For edge column connections, where the eccentricity perpendicular to the slab edge (resulting from a moment about an axis parallel to the slab edge) is toward the interior and there is no eccentricity parallel to the edge, the punching force may be considered to be uniformly distributed along the control perimeter  $u_1^*$  as shown in Figures 1.18a and 1.18b.



**Figure 1.181 Equivalent control perimeter  $u_1^*$  (Eurocode 2-2003, 2003)**

When there are eccentricities in both orthogonal directions,  $\beta$  may be determined using the following expression (Equation 1.22).

$$\beta = \frac{u_1}{u_{1*}} + k \frac{u_1}{W_1} e_{par} \quad (1.22)$$

Where  $u_1$  is the basic control perimeter,  $u_{1*}$  is the reduced basic control perimeter,  $e_{par}$  is the eccentricity parallel to the slab edge resulting from a moment about an axis perpendicular to the slab edge.  $k$  may be explained from Table 1.1 with the ratio  $c_1/c_2$  replaced by  $c_1/2c_2$ .  $W_1$  is calculated for the basic control perimeter  $u$ .

Punching shear resistance can be determined as follows (Equation 1.23).

$$v_{eurocode} = 0.18 * k * (100 \rho_f c)^{1/3} \geq v_{min} \quad (1.23)$$

In Equations 1.24, 1.25 and 1.26 the values which are in above equation are explained as it can be seen:

$$k = 1 + \sqrt{\frac{200}{d}} \leq 2.00 \quad d \text{ in mm} \quad (1.24)$$

$$\rho_1 = \sqrt{\rho_{ly} * \rho_{lz}} \leq 0.02 \quad (1.25)$$

$\rho_{ly}$ ,  $\rho_{lz}$  relate to the bonded tension steel in y- and z- directions respectively. The values  $\rho_{ly}$  and  $\rho_{lz}$  should be found as mean values taking into consideration a slab width.

$$\sigma_{cp} = (\sigma_{cy} + \sigma_{cz})/2 \quad (1.26)$$

For unbalanced moment calculation Equation 1.27 can be used:

$$v_{eurocode} = \frac{V_{exp}}{u * d} \left[ 1 + k \frac{M_{eurocode} * u}{V_{exp} * W} \right] \quad (1.27)$$

$k$  is a coefficient dependent on the ratio between the column dimensions  $c_1$  and  $c_2$  which was given in Table 1.1.

#### **1.4. Objectives and Scope:**

The key objectives of this thesis are as follows:

- To examine the punching shear strength prediction equations of current design codes for both exterior and interior slab-column connections under the action of concentric and eccentric type of loading.
- To compare the experimental results of load deflection behavior of flat plates under gravity loads to those obtained by using typical shell and beam models.
- To simulate the behavior of a flat plate type of building and examine the effect of a punching failure on one slab-column connection and redistribution of stresses that may lead to progressive collapse of the structure.

With these objectives, this thesis is composed of 5 chapters.



## **CHAPTER 2**

### **EVALUATION OF DESIGN GUIDELINES IN LIGHT OF EXPERIMENTAL RESULTS**

#### **2.1. Introduction:**

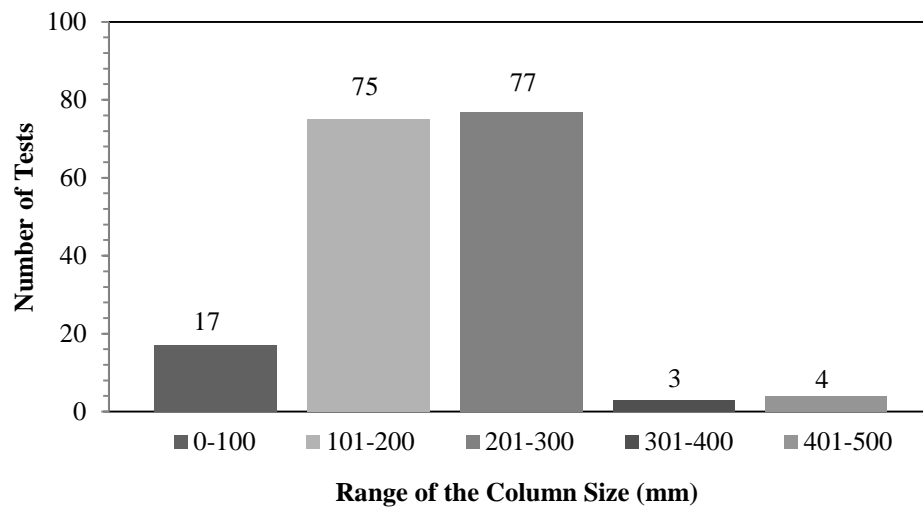
There are several experimental studies focused on the behavior of flat plate slab column connections under eccentric and concentric loadings. In the light of experimental results, a database was compiled for each loading case (i.e. concentric and eccentric shear) in this chapter. The accuracy of the design guidelines given in the codes presented in Chapter 1 are critically examined by using these databases.

The gathered databases consist of mainly two parts: Concentric and eccentric load cases. Eccentric load case is further separated into two parts, exterior and interior slab-column connections. The design equations were expressed in Chapter 1.3 in detail previously. For concentric loading, 176 experiments were compiled. Moreover, 103 test specimen data were collected for the eccentric loading databases, 54 of them were interior slab column connection and the rest of them were exterior slab column connection tests.

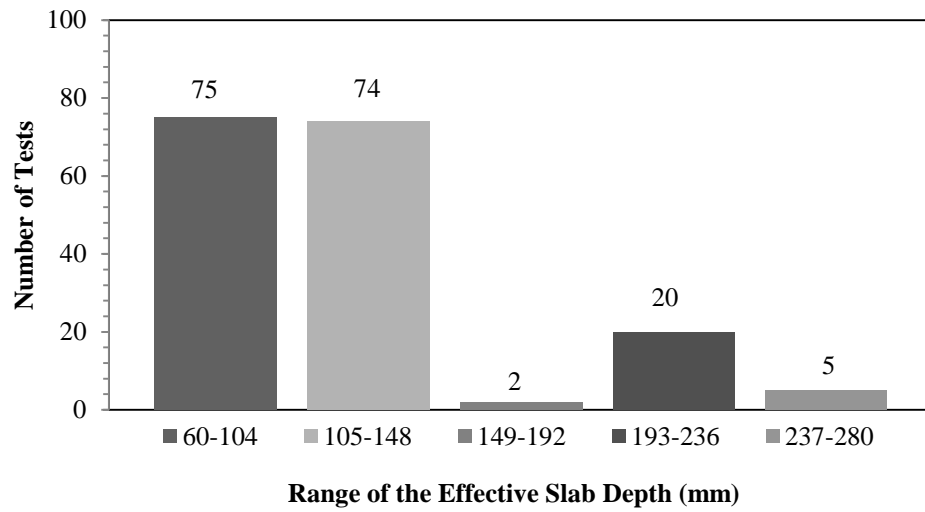
#### **2.2. Concentric Loading:**

After collecting the data, shear force that would cause punching failure was computed according to code equations and results were compared with the test results for concentrically loaded specimen. This database mainly compiled using the CEB-FIP document (CEB/fib Task Group, 2001). In Table 2.1 results are presented.

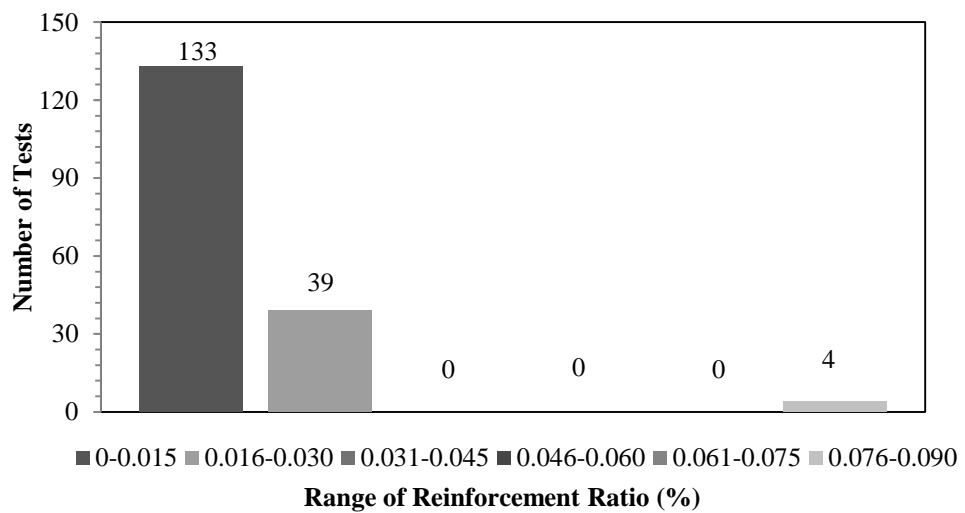
A total of 176 test specimens were used for comparison purposes. Distribution of the test parameters such as column size, the slab depth, reinforcement ratio and concrete compressive strength were presented in Figure 2.1, Figure 2.2, Figure 2.3 and Figure 2.4 respectively. Minimum column size was 54 mm and maximum of it was 500 mm and effective depth values are changing between 64 and 275 mm. Moreover, the reinforcement ratio varied from 0.001 to 0.085 and compressive strength of the concrete ( $f_c$ ) alters from 9.86 to 127 MPa.



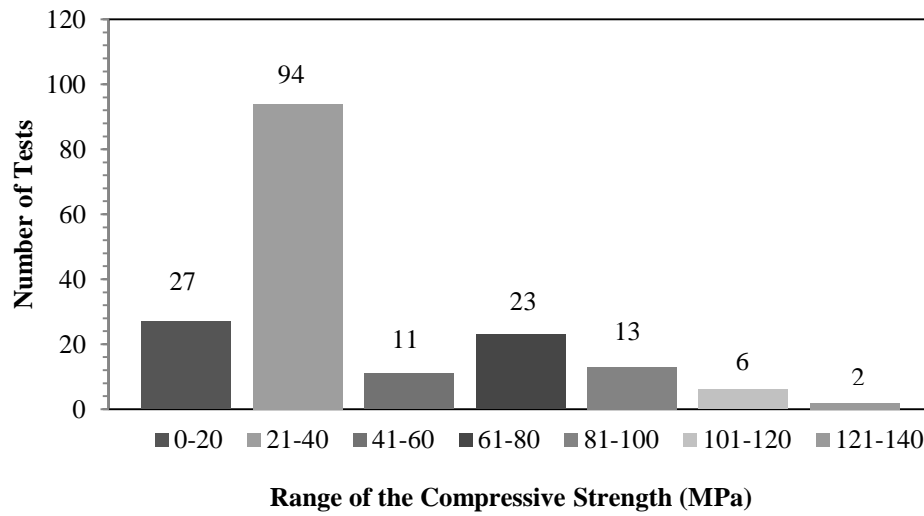
**Figure 2.1 Distribution of the Column Size for Slab-Column Connections in the Concentric Loading Database**



**Figure 2.2 Distribution of the Effective Depth of the Slabs in the Concentric Loading Database**



**Figure 2.3 Distribution of the Reinforcement Ratio for Slab-Column Connections in the Concentric Loading Database**



**Figure 2.4 Distribution of the Compressive Strength of the Concrete for Slab-Column Connections in the Concentric Loading Database**

Table 2.1 Comparison of punching loads according to ACI-318, Eurocode-2 and TS-500 on concentric loading

running number	serial no	slab no (n)	author	radius/size(r/s)	radius/size(r/s)	effective depth(d)	reinf. Ratio( $\rho$ )	effective perimeter(u)	comp.strength(cyl)(fc)	failure load (V <sub>exp</sub> )	failure load(VACI)	failure load(VEurocode)	failure load(VTS500)	VACI/V <sub>exp</sub>	VEurocode/V <sub>exp</sub>	VTS500/V <sub>exp</sub>
unit	-	-	A	mm	mm	mm	-	mm	Mpa	kN	kN	kN	kN			
1	1-1	HSC 0	Hallgreen	250	250	200	0.008	2199.11	95.97	965	1422	1250	1508	1.47	1.30	1.56
2	1-2	HSC 1	Hallgreen	250	250	200	0.008	2199.11	91.30	1021	1387	1229	1471	1.36	1.20	1.44
3	1-3	HSC 2	Hallgreen	250	250	194	0.008	2180.27	85.70	889	1292	1155	1370	1.45	1.30	1.54
4	1-4	HSC 4	Hallgreen	250	250	200	0.001	2199.11	91.60	1041	1389	654	1473	1.33	0.63	1.42
5	1-5	HSC 6	Hallgreen	250	250	201	0.006	2202.26	108.80	960	1524	1192	1616	1.59	1.24	1.68
6	1-6	HSC 8	Hallgreen	250	250	198	0.008	2192.83	94.90	944	1396	1228	1480	1.48	1.30	1.57
7	1-7	HSC 9	Hallgreen	250	250	202	0.003	2205.40	84.10	565	1348	874	1430	2.39	1.55	2.53
8	2-1	ND65-1-1	Tomas.	200	200	275	0.015	1900.00	64.30	2050	1383	1790	1466	0.67	0.87	0.72
9	2-2	ND65-1-2	Tomas.	150	150	200	0.017	1400.00	70.20	1200	774	1104	821	0.65	0.92	0.68
10	2-3	ND95-1-1	Tomas.	200	200	275	0.015	1900.00	83.70	2250	1577	1954	1673	0.70	0.87	0.74
11	2-4	ND95-1-3	Tomas.	200	200	275	0.025	1900.00	89.90	2400	1635	2373	1734	0.68	0.99	0.72
12	2-5	ND95-2-1	Tomas.	150	150	200	0.017	1400.00	88.20	1100	868	1191	920	0.79	1.08	0.84
13	2-6	ND95-2-1D	Tomas.	150	150	200	0.017	1400.00	86.70	1300	860	1184	913	0.66	0.91	0.70
14	2-7	ND95-2-3	Tomas.	150	150	200	0.026	1400.00	89.50	1450	874	1379	927	0.60	0.95	0.64
15	2-8	ND95-2-3D	Tomas.	150	150	200	0.026	1400.00	80.30	1250	828	1330	878	0.66	1.06	0.70
16	2-9	ND95-2-3D+	Tomas.	150	150	200	0.026	1400.00	98.00	1450	915	1421	970	0.63	0.98	0.67
17	2-10	ND95-3-1	Tomas.	100	100	88	0.018	752.00	85.10	330	201	320	214	0.61	0.97	0.65
18	2-11	ND115-1-1	Tomas.	200	200	275	0.015	1900.00	112.00	2450	1825	2154	1935	0.74	0.88	0.79
19	2-12	ND115-2-1	Tomas.	150	150	200	0.017	1400.00	119.00	1400	1008	1316	1069	0.72	0.94	0.76
20	2-13	ND115-2-3	Tomas.	150	150	200	0.026	1400.00	108.10	1550	961	1.468	1019	0.62	0.95	0.66

Table 2.1 continued

running number	serial no	slab no (n)	author	radius/size(r/s)	radius/size(r/s)	effective depth(d)	reinf. Ratio( $\rho$ )	effective perimeter(u)	comp.strength(cyl)( $f_c$ )	failure load ( $V_{exp}$ )	failure load(VACI)	failure load(VEurocode)	failure load(VTS500)	VACI/ $V_{exp}$	VEurocode/ $V_{exp}$	VTS500/ $V_{exp}$
unit	-	-	A	mm	mm	mm	-	mm	Mpa	kN	kN	kN	kN			
21	3-1	1	Ramdane	150	150	98	0.006	2120.58	110.30	224	697	377	764	3.11	1.68	3.41
22	3-2	2	Ramdane	150	150	98	0.006	1570.80	70.20	212	426	324	451	2.01	1.53	2.13
23	3-3	3	Ramdane	150	150	98	0.006	1570.80	33.60	169	294	253	312	1.74	1.50	1.85
24	3-4	4	Ramdane	150	150	98	0.006	1250.35	73.40	233	346	329	367	1.49	1.41	1.58
25	3-5	6	Ramdane	150	150	98	0.006	1250.35	127.00	233	456	395	483	1.96	1.69	2.07
26	3-6	12	Ramdane	150	150	98	0.013	1250.35	75.50	319	351	430	373	1.10	1.35	1.17
27	3-7	13	Ramdane	150	150	98	0.013	1250.35	54.50	297	299	385	317	1.01	1.30	1.07
28	3-8	14	Ramdane	150	150	98	0.013	1250.35	76.00	341	353	431	374	1.03	1.26	1.10
29	3-9	16	Ramdane	150	150	98	0.013	1250.35	123.00	362	448	506	476	1.24	1.40	1.31
30	3-10	21	Ramdane	150	150	98	0.013	1250.35	52.40	286	293	380	310	1.02	1.33	1.09
31	3-11	22	Ramdane	150	150	98	0.013	1250.35	105.30	405	415	480	440	1.02	1.19	1.09
32	3-12	23	Ramdane	150	150	100	0.009	1250.35	70.50	341	346	381	367	1.02	1.12	1.08
33	3-13	25	Ramdane	150	150	100	0.012	1250.35	41.10	244	265	350	281	1.08	1.44	1.15
34	3-14	26	Ramdane	150	150	100	0.012	1250.35	47.00	294	283	366	300	0.96	1.25	1.02
35	3-15	27	Ramdane	150	150	102	0.010	1256.64	42.10	227	274	341	291	1.21	1.50	1.28

Table 2.1 continued

running number	serial no	slab no (n)	author	radius/size(r/s)	radius/size(r/s)	effective depth(d)	reinf. Ratio( $\rho$ )	effective perimeter(u)	comp.strength(cyl)(fc)	failure load (V <sub>exp</sub> )	failure load(VACI)	failure load (VEurocode)	failure load(VTS500)	VACI/V <sub>exp</sub>	VEurocode/V <sub>exp</sub>	VTS500/V <sub>exp</sub>
unit	-	-	A	mm	mm	mm	-	mm	Mpa	kN	kN	kN	kN			
36	4-1	I.HS1	Marz./Hus.	150	150	95	0.004	980.00	67.00	178	251	225	267	1.41	1.26	1.50
37	4-2	I.HS2	Marz./Hus.	150	150	95	0.007	980.00	70.00	249	257	275	273	1.03	1.10	1.09
38	4-3	I.HS3	Marz./Hus.	150	150	95	0.012	980.00	69.00	356	255	328	271	0.72	0.92	0.76
39	4-4	I.HS4	Marz./Hus.	150	150	90	0.021	960.00	66.00	418	232	361	246	0.55	0.86	0.59
40	4-5	I.HS7	Marz./Hus.	150	150	95	0.009	980.00	74.00	356	264	305	280	0.74	0.86	0.79
41	4-6	II.HS5	Marz./Hus.	150	150	125	0.005	1100.00	68.00	365	374	358	397	1.03	0.98	1.09
42	4-7	II.HS6	Marz./Hus.	150	150	120	0.005	1080.00	70.00	489	358	341	380	0.73	0.70	0.78
43	4-8	II.HS8	Marz./Hus.	150	150	120	0.010	1080.00	69.00	436	355	428	377	0.81	0.98	0.86
44	4-9	II.HS9	Marz./Hus.	150	150	120	0.015	1080.00	74.00	543	368	501	390	0.68	0.92	0.72
45	4-10	II.HS10	Marz./Hus.	150	150	120	0.021	1080.00	80.00	645	383	576	406	0.59	0.89	0.63
46	4-11	III.HS11	Marz./Hus.	150	150	70	0.007	880.00	70.00	196	170	184	180	0.87	0.94	0.92
47	4-12	III.HS12	Marz./Hus.	150	150	70	0.012	880.00	75.00	258	176	225	187	0.68	0.87	0.72
48	4-13	III.HS13	Marz./Hus.	150	150	70	0.016	880.00	68.00	267	168	239	178	0.63	0.90	0.67
49	4-14	IV.HS14	Marz./Hus.	220	220	95	0.012	1260.00	72.00	498	335	384	355	0.67	0.77	0.71
50	4-15	IV.HS15	Marz./Hus.	300	300	95	0.012	1580.00	71.00	560	417	441	443	0.75	0.79	0.79
51	4-16	I.NS1	Marz./Hus.	150	150	95	0.012	980.00	42.00	320	199	278	211	0.62	0.87	0.66
52	4-17	II.NS2	Marz./Hus.	150	150	120	0.005	1080.00	30.00	396	234	257	248	0.59	0.65	0.63
53	5-1	F1	Lov./McL.	100	100	83	0.017	889.07	39.30	480	153	259	162	0.32	0.54	0.34
54	5-2	F2	Lov./McL.	100	100	83	0.017	889.07	39.30	204	153	259	162	0.75	1.27	0.79
55	5-3	F3	Lov./McL.	100	100	83	0.017	889.07	39.30	149	153	259	162	1.02	1.74	1.09
56	5-4	F4	Lov./McL.	100	100	83	0.017	889.07	39.30	129	153	259	162	1.18	2.00	1.26
57	5-5	F5	Lov./McL.	100	100	83	0.017	889.07	39.30	139	153	259	162	1.10	1.86	1.16

Table 2.1 continued

running number	serial no	slab no (n)	author	radius/size(r/s)	radius/size(r/s)	effective depth(d)	reinf. Ratio( $\rho$ )	effective perimeter(u)	comp.strength( $c_y$ l)( $f_c$ )	failure load ( $V_{exp}$ )	failure load(VACI)	failure load(VEurocode)	failure load(VTS500)	VACI/ $V_{exp}$	VEurocode/ $V_{exp}$	VTS500/ $V_{exp}$
unit	-	-	A	mm	mm	mm	-	mm	Mpa	kN	kN	kN	kN			
58	6-1	S2.1	Tolf	250	250	200	0.008	2199.11	25.76	603	737	806	781	1.22	1.34	1.30
59	6-2	S2.2	Tolf	250	250	199	0.008	2195.97	24.31	600	711	785	754	1.19	1.31	1.26
60	6-3	S2.3	Tolf	250	250	200	0.005	2199.11	26.95	489	753	700	799	1.54	1.43	1.63
61	6-4	S2.4	Tolf	250	250	197	0.005	2189.69	25.67	444	721	674	765	1.62	1.52	1.72
62	6-5	S1.1	Tolf	125	125	100	0.008	1099.56	30.35	216	200	257	212	0.93	1.19	0.98
63	6-6	S1.2	Tolf	125	125	99	0.008	1096.42	24.31	194	177	235	187	0.91	1.21	0.97
64	6-7	S1.3	Tolf	125	125	98	0.004	1093.27	28.31	145	188	194	200	1.30	1.34	1.38
65	6-8	S1.4	Tolf	125	125	99	0.004	1096.42	26.69	148	185	193	196	1.25	1.30	1.33



Table 2.1 continued

running number	serial no	slab no (n)	author	radius/size(r/s)	radius/size(r/s)	effective depth(d)	reinf. Ratio( $\rho$ )	effective perimeter(u)	comp.strength(cyl)( $f_c$ )	failure load ( $V_{exp}$ )	failure load(VACI)	failure load (VEurocode)	failure load(VTS500)	VACI/ $V_{exp}$	VEurocode/ $V_{exp}$	VTS500/ $V_{exp}$
unit	-	-	A	mm	mm	mm	-	mm	Mpa	kN	kN	kN	kN			
66	7-1	I/1	Regan	200	200	77	0.024	1108.00	27.37	194	147	258	156	0.76	1.33	0.81
67	7-2	I/2	Regan	200	200	77	0.012	1108.00	24.91	176	141	199	149	0.80	1.13	0.85
68	7-3	I/3	Regan	200	200	77	0.014	1108.00	29.16	194	152	220	161	0.78	1.14	0.83
69	7-4	I/4	Regan	200	200	77	0.012	1108.00	34.34	194	165	221	175	0.85	1.14	0.90
70	7-5	I/5	Regan	200	200	79	0.015	1116.00	29.92	165	159	235	169	0.96	1.42	1.02
71	7-6	I/6	Regan	200	200	79	0.008	1116.00	23.29	165	140	175	149	0.85	1.06	0.90
72	7-7	I/7	Regan	200	200	79	0.008	1116.00	32.30	186	165	195	175	0.89	1.05	0.94
73	7-8	II/1	Regan	250	250	200	0.010	1800.00	37.06	825	723	843	767	0.88	1.02	0.93
74	7-9	II/2	Regan	160	160	128	0.010	1152.00	35.36	390	289	383	307	0.74	0.98	0.79
75	7-10	II/3	Regan	160	160	128	0.010	1152.00	36.47	365	294	387	312	0.81	1.06	0.85
76	7-11	II/4	Regan	80	80	64	0.010	576.00	35.36	117	72	118	77	0.62	1.01	0.66
77	7-12	II/5	Regan	80	80	64	0.010	576.00	36.47	105	73	119	78	0.70	1.13	0.74
78	7-13	II/6	Regan	80	80	64	0.010	576.00	38.42	105	75	121	80	0.72	1.15	0.76
79	7-14	III/1	Regan	150	150	95	0.080	980.00	24.65	197	153	438	162	0.77	2.22	0.82
80	7-15	III/2	Regan	150	150	95	0.080	980.00	10.12	123	98	325	104	0.79	2.64	0.84
81	7-16	III/3	Regan	150	150	95	0.080	980.00	40.21	214	195	515	207	0.91	2.41	0.97
82	7-17	III/4	Regan	150	150	93	0.015	972.00	12.67	154	106	195	113	0.69	1.27	0.73
83	7-18	III/5	Regan	150	150	93	0.015	972.00	28.48	214	159	255	169	0.74	1.19	0.79
84	7-19	III/6	Regan	150	150	93	0.015	972.00	45.31	248	201	298	213	0.81	1.20	0.86
85	7-20	V/1	Regan	54	54	118	0.008	688.00	36.47	170	162	256	172	0.95	1.50	1.01
86	7-21	V/2	Regan	170	170	118	0.008	1152.00	34.17	280	262	319	278	0.94	1.14	0.99
87	7-22	V/3	Regan	110	110	118	0.008	912.00	40.50	265	226	300	240	0.85	1.13	0.90
88	7-23	V/4	Regan	102	102	118	0.008	880.00	45.30	285	231	306	245	0.81	1.07	0.86

Table 2.1 continued

running number	serial no	slab no (n)	author	radius/size(r/s)	radius/size(r/s)	effective depth(d)	reinf. Ratio( $\rho$ )	effective perimeter(u)	comp.strength(cyl)( $f_c$ )	failure load (V <sub>exp</sub> )	failure load(VACI)	failure load(VEurocode)	failure load(VTS500)	VACI/V <sub>exp</sub>	VEurocode/V <sub>exp</sub>	VTS500/V <sub>exp</sub>
unit	-	-	A	mm	mm	mm	-	mm	Mpa	kN	kN	kN	kN			
89	8-1	S1	Swamy/Ali	150	150	100	0.006	1000.00	40.10	198	209	233	222	1.06	1.18	1.12
90	8-2	S7	Swamy/Ali	150	150	100	0.007	1000.00	37.40	222	202	240	214	0.91	1.08	0.96
91	9-1	P2	ETH	300	300	143	0.015	2334.20	36.72	628	667	787	708	1.06	1.25	1.13
92	9-2	P5	ETH	300	300	171	0.012	2422.17	27.88	626	722	833	765	1.15	1.33	1.22
93	10-1	0	Schaefers	210	210	113	0.008	1674.47	23.10	280	300	343	318	1.07	1.23	1.14
94	10-2	3	Schaefers	210	210	170	0.006	1853.54	23.30	460	502	531	532	1.09	1.15	1.16
95	11-1	DA6	Ladner	100	100	80	0.018	720.00	31.88	183	107	201	114	0.59	1.10	0.62
96	11-2	DA7	Ladner	200	200	80	0.018	1120.00	35.62	288	176	269	187	0.61	0.93	0.65
97	11-3	DA10	Ladner	240	240	80	0.018	1280.00	34.00	281	197	288	209	0.70	1.02	0.74
98	11-4	DA11	Ladner	320	320	80	0.018	1600.00	32.30	324	240	329	255	0.74	1.02	0.79
99	12-1	P1	Ladner	500	500	240	0.013	3895.57	29.67	1662	1680	1719	1782	1.01	1.03	1.07
100	12-2	M1	Ladner	226	226	109	0.012	1762.43	33.75	362	368	443	391	1.02	1.22	1.08
101	13-1	AN-1	Corl./Hawk	254	254	111	0.015	1460.00	44.40	334	356	457	378	1.07	1.37	1.13
102	13-2	AN-2	Corl./Hawk	203	203	111	0.010	1256.00	44.40	266	307	366	325	1.15	1.37	1.22

Table 2.1 continued

running number	serial no	slab no (n)	author	radius/size(r/s)	radius/size(r/s)	effective depth(d)	reinf. Ratio( $\rho$ )	effective perimeter(u)	comp.strength(cyl)(fc)	failure load (V <sub>exp</sub> )	failure load(V <sub>ACI</sub> )	failure load (VEurocode)	failure load(V <sub>TS500</sub> )	V <sub>ACI</sub> /V <sub>exp</sub>	V <sub>Eurocode</sub> /V <sub>exp</sub>	V <sub>TS500</sub> /V <sub>exp</sub>
unit	-	-	A	mm	mm	mm	-	mm	Mpa	kN	kN	kN	kN			
103	14-1	A1/M1	Base	203	203	114	0.011	1268.00	16.30	322	193	280	204	0.60	0.87	0.63
104	14-2	A1/M2	Base	203	203	117	0.015	1280.00	15.50	346	195	317	206	0.56	0.91	0.60
105	14-3	A1/M3	Base	203	203	121	0.019	1296.00	14.20	307	195	348	207	0.64	1.13	0.67
106	14-4	A1/M4	Base	203	203	124	0.010	1308.00	14.00	259	200	289	212	0.77	1.12	0.82
107	14-5	A1/M5	Base	203	203	117	0.012	1280.00	21.00	346	226	325	240	0.65	0.94	0.69
108	14-6	A2/M1	Base	203	203	124	0.010	1308.00	35.40	409	318	394	338	0.78	0.96	0.83
109	14-7	A2/M2	Base	203	203	117	0.015	1280.00	32.80	419	283	406	300	0.68	0.97	0.72
110	14-8	A2/M3	Base	203	203	121	0.019	1296.00	32.50	430	295	459	313	0.69	1.07	0.73
111	14-9	A2/T1	Base	203	203	124	0.010	1308.00	39.30	419	336	408	356	0.80	0.97	0.85
112	14-10	A2/T2	Base	203	203	124	0.017	1308.00	41.40	439	344	496	365	0.78	1.13	0.83
113	14-11	A3/M1	Base	203	203	124	0.010	1308.00	18.80	247	232	319	246	0.94	1.29	1.00
114	14-12	A3/M2	Base	203	203	102	0.017	1220.00	19.30	336	180	295	191	0.54	0.88	0.57
115	14-13	A3/M3	Base	203	203	117	0.019	1280.00	27.30	298	258	414	274	0.87	1.39	0.92
116	14-14	A3/T1	Base	203	203	121	0.010	1296.00	20.60	328	235	318	249	0.72	0.97	0.76
117	14-15	A3/T2	Base	203	203	119	0.012	1288.00	16.00	298	202	304	215	0.68	1.02	0.72
118	14-16	A4/M1	Base	203	203	114	0.011	1268.00	38.30	259	295	373	313	1.14	1.44	1.21
119	14-17	A4/M2	Base	203	203	119	0.015	1288.00	29.20	341	273	400	290	0.80	1.17	0.85
120	14-18	A4/M3	Base	203	203	117	0.019	1280.00	32.20	541	280	437	297	0.52	0.81	0.55
121	14-19	A4/T1	Base	203	203	114	0.011	1268.00	32.80	384	273	354	290	0.71	0.92	0.75
122	14-20	A4/T2	Base	203	203	117	0.012	1280.00	29.30	402	268	363	284	0.67	0.90	0.71

Table 2.1 continued

running number	serial no	slab no (n)	author	radius/size(r/s)	radius/size(r/s)	effective depth(d)	reinf. Ratio( $\rho$ )	effective perimeter(u)	comp.strength(cyl)(fc)	failure load (Vexp)	failure load(VACI)	failure load(VEurocode)	failure load(VTS500)	VACI/Vexp	VEurocode/Vexp	VTS500/Vexp
unit	-	-	A	mm	mm	mm	-	mm	Mpa	kN	kN	kN	kN			
123	15-1	P1-S1	Manterola	100	100	107	0.011	828.00	25.60	216	148	242	157	0.68	1.12	0.73
124	15-2	P2-S1	Manterola	250	250	107	0.011	1428.00	33.80	257	293	357	311	1.14	1.39	1.21
125	15-3	P3-S1	Manterola	450	450	107	0.011	2228.00	29.70	301	423	458	455	1.40	1.52	1.51
126	15-4	P1-S2	Manterola	100	100	107	0.011	828.00	24.20	196	144	237	153	0.73	1.21	0.78
127	15-5	P2-S2	Manterola	250	250	107	0.011	1428.00	33.10	283	290	354	308	1.03	1.25	1.09
128	15-6	P3-S2	Manterola	450	450	107	0.011	2228.00	31.90	397	438	469	471	1.10	1.18	1.19
129	15-7	P1-S3	Manterola	100	100	107	0.011	828.00	39.70	184	184	280	195	1.00	1.52	1.06
130	15-8	P2-S3	Manterola	100	100	107	0.014	828.00	35.80	211	175	293	186	0.83	1.39	0.88
131	15-9	P3-S3	Manterola	100	100	107	0.005	828.00	39.20	165	183	214	194	1.11	1.30	1.18
132	15-10	P1-S4	Manterola	100	100	107	0.005	828.00	26.40	175	150	188	159	0.86	1.07	0.91
133	15-11	P2-S4	Manterola	250	250	107	0.005	1428.00	31.30	246	282	267	299	1.15	1.09	1.22
134	15-12	P3-S4	Manterola	450	450	107	0.005	2228.00	24.20	294	382	329	410	1.30	1.12	1.40

Table 2.1 continued

running number	serial no	slab no (n)	author	radius/size(r/s)	radius/size(r/s)	effective depth(d)	reinf. Ratio( $\rho$ )	effective perimeter(u)	comp.strength(cyl)(fc)	failure load ( $V_{exp}$ )	failure load(VACI)	failure load (VEurocode)	failure load(VTS500)	VACI/ $V_{exp}$	VEurocode/ $V_{exp}$	VTS500/ $V_{exp}$
unit	-	-	A	mm	mm	mm	-	mm	Mpa	kN	kN	kN	kN			
135	16-1	II-5	Yitzhaki	221	221	82	0.005	1646.19	18.28	152	190	191	202	1.25	1.26	1.33
136	16-2	II-8	Yitzhaki	333	333	82	0.006	2349.91	19.89	218	242	270	301	1.11	1.24	1.38
137	16-3	IIS20-1	Yitzhaki	201	201	78	0.007	1116.00	11.65	128	98	131	104	0.77	1.02	0.81
138	16-4	II-1	Yitzhaki	221	221	82	0.012	1646.19	11.14	181	149	217	158	0.82	1.20	0.87
139	16-5	II-4a	Yitzhaki	221	221	82	0.009	1646.19	19.04	245	194	236	206	0.79	0.96	0.84
140	16-6	II-4b	Yitzhaki	201	201	82	0.009	1132.00	10.46	162	99	146	105	0.61	0.90	0.65
141	16-7	II-4c	Yitzhaki	201	201	82	0.009	1132.00	14.79	215	118	164	125	0.55	0.76	0.58
142	16-8	IIR20-2	Yitzhaki	201	201	83	0.009	1523.67	15.90	307	166	213	176	0.54	0.70	0.57
143	16-9	IIR30-1	Yitzhaki	300	300	80	0.020	2136.28	18.70	239	215	359	259	0.90	1.50	1.08
144	16-10	II-2	Yitzhaki	221	221	82	0.013	1646.19	10.37	152	143	218	152	0.94	1.43	1.00
145	16-11	II-3	Yitzhaki	201	402	82	0.013	1534.00	14.37	244	157	224	167	0.64	0.92	0.68
146	16-12	II-6	Yitzhaki	221	221	82	0.013	1646.19	22.95	240	213	284	226	0.89	1.18	0.94
147	16-13	II-9	Yitzhaki	201	201	79	0.085	1120.00	9.86	157	92	290	97	0.58	1.85	0.62
148	16-14	III-3	Yitzhaki	221	221	82	0.012	1646.19	19.21	201	195	260	207	0.97	1.30	1.03
149	16-15	7	Yitzhaki	119	119	82	0.007	1005.31	10.63	117	89	131	94	0.76	1.12	0.80
150	16-16	II-10	Yitzhaki	119	119	82	0.010	1005.31	12.41	98	96	156	102	0.98	1.59	1.04

Table 2.1 continued

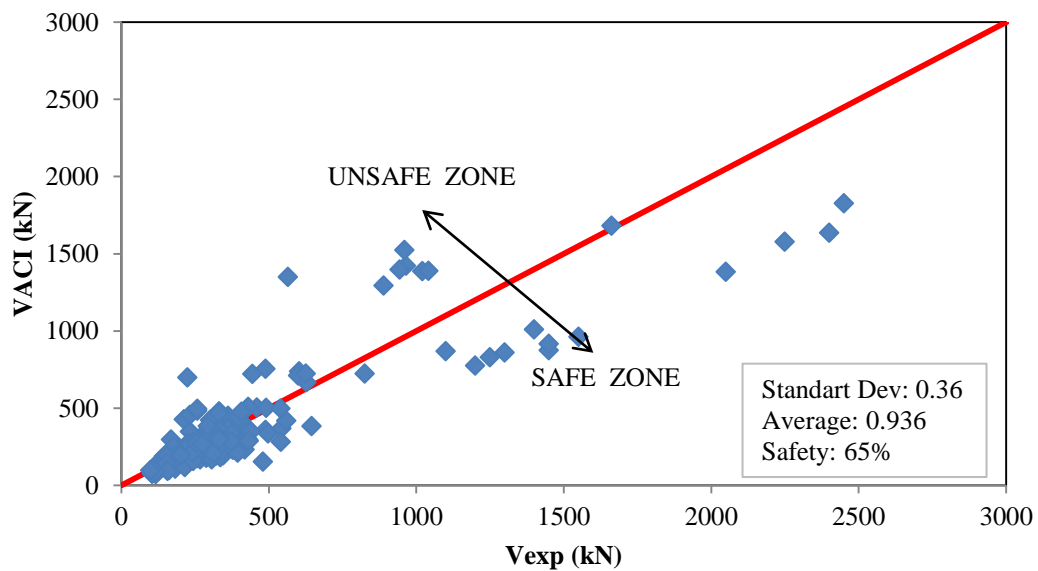
running number	serial no	slab no (n)	author	radius/size(r/s)	radius/size(r/s)	effective depth(d)	reinf. Ratio( $\rho$ )	effective perimeter(u)	comp.strength(cyl)(fc)	failure load (V <sub>exp</sub> )	failure load(V <sub>ACI</sub> )	failure load(V <sub>Eurocode</sub> )	failure load(V <sub>TS500</sub> )	V <sub>ACI</sub> /V <sub>exp</sub>	V <sub>Eurocode</sub> /V <sub>exp</sub>	V <sub>TS500</sub> /V <sub>exp</sub>
unit	-	-	A	mm	mm	mm	-	mm	Mpa	kN	kN	kN	kN			
151	17-1	S1-60	Moe	254	254	114	0.011	1472.00	23.30	389	267	344	284	0.69	0.89	0.73
152	17-2	S2-60	Moe	254	254	114	0.015	1472.00	22.10	356	260	375	276	0.73	1.05	0.78
153	17-3	S3-60	Moe	254	254	114	0.020	1472.00	22.60	364	263	416	279	0.72	1.14	0.77
154	17-4	S4-60	Moe	254	254	114	0.026	1472.00	23.80	334	270	462	287	0.81	1.38	0.86
155	17-5	S1-70	Moe	254	254	114	0.011	1472.00	24.50	393	274	350	291	0.70	0.89	0.74
156	17-6	S3-70	Moe	254	254	114	0.020	1472.00	25.40	378	279	433	296	0.74	1.14	0.78
157	17-7	S4-70	Moe	254	254	114	0.026	1472.00	35.20	374	329	526	348	0.88	1.41	0.93
158	17-8	S4-70A	Moe	254	254	114	0.026	1472.00	20.50	312	251	440	266	0.80	1.41	0.85
159	17-9	S5-60	Moe	203	203	114	0.011	1268.00	22.20	343	225	311	238	0.66	0.91	0.69
160	17-10	S5-70	Moe	203	203	114	0.011	1268.00	23.00	378	229	314	243	0.61	0.83	0.64
161	17-11	R1	Moe	152	152	114	0.014	1064.00	26.60	312	206	325	219	0.66	1.04	0.70
162	17-12	R2	Moe	152	152	114	0.014	1064.00	27.60	394	210	329	223	0.53	0.84	0.57
163	17-13	H1	Moe	254	254	114	0.011	1472.00	26.10	372	283	358	300	0.76	0.96	0.81
164	17-14	M1A	Moe	305	305	114	0.015	1676.00	20.80	433	288	398	305	0.66	0.92	0.70

Table 2.1 continued

running number	serial no	slab no (n)	author	radius/size(r/s)	radius/size(r/s)	effective depth(d)	reinf. Ratio( $\rho$ )	effective perimeter(u)	comp.strength(cyl)(fc)	failure load (Vexp)	failure load(VACI)	failure load(VEurocode)	failure load(VTS500)	VACI/Vexp	VEurocode/Vexp	VTS500/Vexp
unit	-	-	A	mm	mm	mm	-	mm	Mpa	kN	kN	kN	kN			
165	18-1	IAI5a-5	Kinn./Nyl.	150	150	117	0.008	1310.04	29.67	255	275	337	292	1.08	1.32	1.15
166	18-2	IAI5a-6	Kinn./Nyl.	150	150	118	0.008	1313.19	27.37	275	268	332	284	0.97	1.21	1.03
167	18-3	IAI5c-11	Kinn./Nyl.	150	150	121	0.018	1322.61	33.41	334	305	480	324	0.91	1.44	0.97
171	18-7	IA30c-30	Kinn./Nyl.	300	300	120	0.021	2261.95	31.37	491	502	678	532	1.02	1.38	1.08
172	18-8	IA30c-31	Kinn./Nyl.	300	300	119	0.021	2258.81	31.37	540	497	672	527	0.92	1.24	0.98
173	18-9	IA30d-32	Kinn./Nyl.	300	300	123	0.005	2271.37	27.46	258	483	414	512	1.87	1.60	1.99
174	18-10	IA30d-33	Kinn./Nyl.	300	300	125	0.005	2277.65	27.80	258	495	423	525	1.92	1.64	2.04
175	18-11	IA30e-34	Kinn./Nyl.	300	300	120	0.010	2261.95	28.56	332	479	513	508	1.44	1.55	1.53
176	18-12	IA30e-35	Kinn./Nyl.	300	300	122	0.010	2268.23	26.10	332	466	508	495	1.41	1.53	1.49
										Average=				0.936	1.185	0.996
										Standart Deviation=				0.36	0.30	0.39

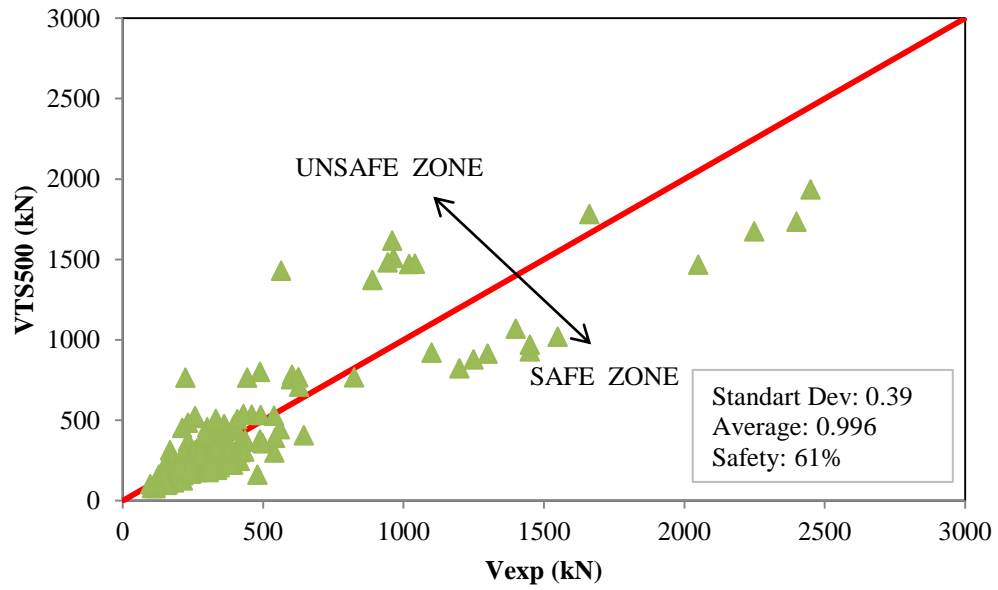
For regions where  $V_{exp}$  (punching load obtained by the tests) was greater than the  $V_{code}$  (punching load obtained by the codes) ‘*safe zone*’ was marked, otherwise ‘*unsafe zone*’ statement was used. Standart deviation, average and % of data points that were estimated safely were also noted on the figures. Unsafe and safe zones are labeled excluding material safety factors, which are used to consider other uncertainties other than those inherent in the estimations of prediction equations.

Table 2.1 shows that, Eurocode-2 seems the most unsafe code for analysis purposes. Standard deviation value of Eurocode-2 estimations is 0.3, but it is 0.36 for ACI-318 and 0.39 for TS500. This shows that the least amount of scatter is inherent in the Eurocode-2 approach, which considers reinforcement ratio and size effect. However, for  $V_{exp}/V_{code}$  average values, the closest value to the 1 is obtained by TS500, whereas this value is 0.936 for ACI-318 and 1.185 for Eurocode-2. The summary of the Table 2.1 can be seen in Figure 2.5, Figure 2.6 and Figure 2.7.

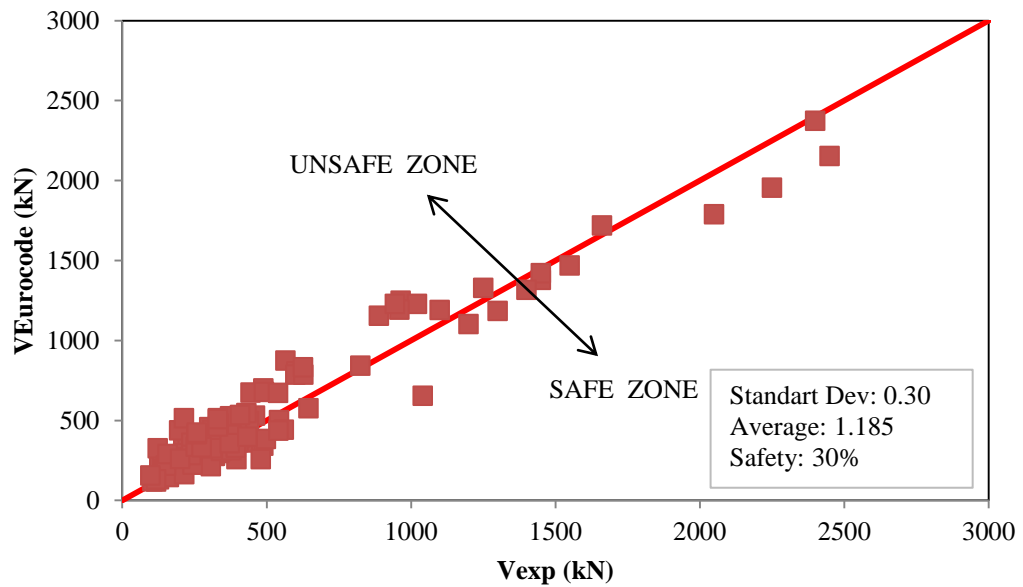


**Figure 2.5 Comparison of punching loads between ACI-318 and experimental values**





**Figure 2.6 Comparison of punching loads between TS500 and experimental values**



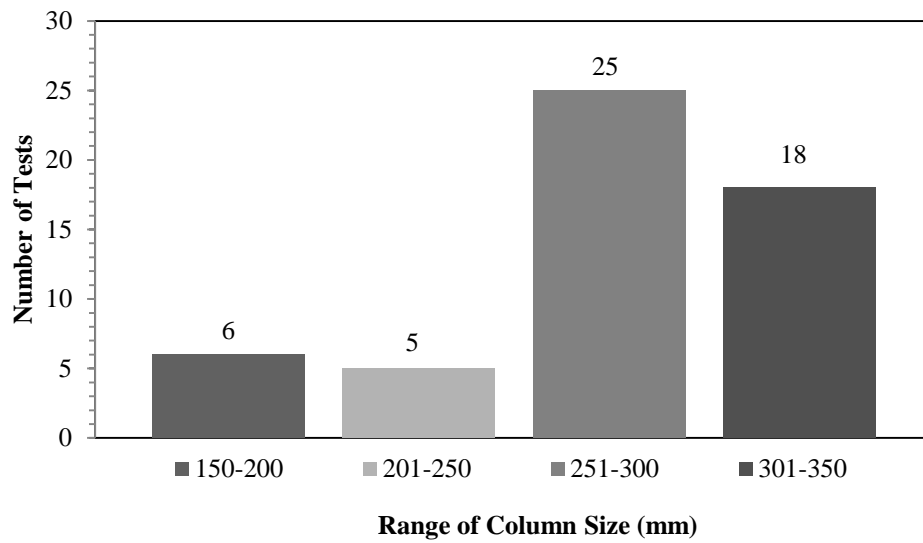
**Figure 2.7 Comparison of unbalanced moments between Eurocode-2 and experimental**

### **2.3. Eccentric Loading:**

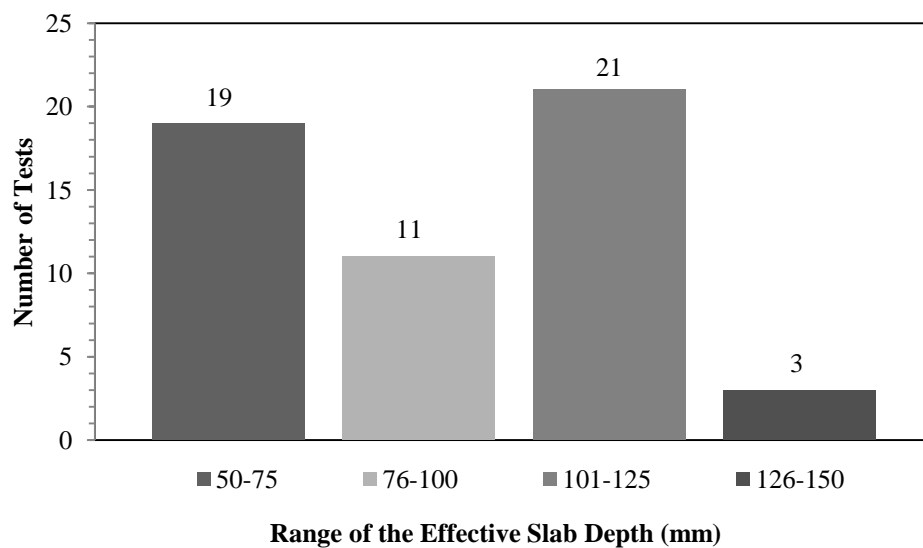
In the presence of lateral loads on a flat plate structure (i.e. earthquake, wind etc.) eccentric shear occurs. In addition, eccentric shear may occur due to unbalanced vertical loads on adjacent spans. The major reason of the punching shear failure in such loadings is the combined effect of shear force and bending moment acting together on the slab-column connections. In this chapter, moment values corresponding to punching failure in the presence of a shear force was computed for the test specimens both for interior and exterior connections by using the current design codes ACI-318, Eurocode-2 and TS500. Afterwards, computed moments were compared with the measured moments from experiments to assess the accuracy of design equations.

#### **2.3.1. Interior Slab-Column Connections:**

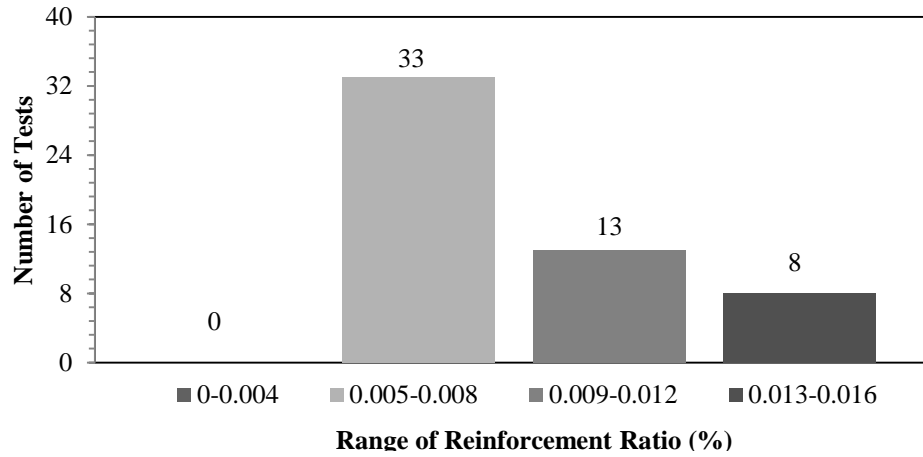
There are 54 interior slab-column connections under eccentric loading data obtained from the literature survey. Column size, concrete strength, slab effective depth, applied vertical load and reinforcement ratio were the key parameters that affect the unbalanced moment which cause the punching failure. The column dimensions were between 137 to 325 mm as can be seen in Figure 2.8 and the effective depth of the slab varied 51 to 142.4 mm and their distribution is given in Figure 2.9. Moreover, the distribution of the reinforcement ratios and concrete compressive strengths can be seen in Figure 2.10 and Figure 2.11.



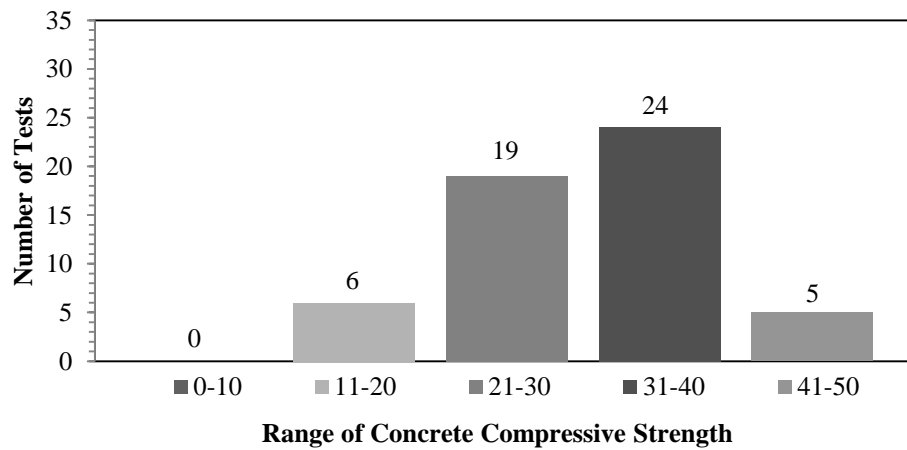
**Figure 2.8 Distribution of the Column Size for Interior Slab-Column Connections for the Database**



**Figure 2.9 Distribution of the Effective Depth of the Slab for Interior Slab-Column Connections for the Database**



**Figure 2.10 Distribution of the Reinforcement Ratio for Interior Slab-Column Connections for the Database**



**Figure 2.11 Distribution of the Compressive Strength of Concrete ( $f_c$ ) for Interior Slab-Column Connections for the Database**

In Table 2.2 the experimental unbalanced moments for interior connection values were compared with the moment estimations of design equations given by ACI-318, TS500 and Eurocode-2 respectively. The calculation steps were followed according to the given equations in current codes as described in Chapter 1.

**Table 2.2 Unbalanced moments from ACI-318, Eurocode-2 and TS500 for interior slab-column connections on eccentric loading**

running number notation	serial no	slab no (n)	author(A)	column size(c1)	radius/size(c2)	b1	b2	effective depth(d)	reinf. Ratio( $\rho$ )	effective perimeter(u)	comp.strength( $c_y$ )(fc)	yield strength( $f_y$ )	failure load(V exp)	failure moment(Mexp)	failure moment(MACI)	failure moment(MEurocode)	failure moment(MTS500)	MACI/Mexp	MEurocode/Mexp	MTS500/Mexp
unit	-	-	-	mm	mm	mm	mm	mm	-	mm	MPa	MPa	N	kNm	kNm	kNm	kNm			
1	1-1	II	Luo/Durrani/Conte	250	250	352	352	102	1.56	1408.00	20.7	379.0	15544.00	38.1	60.58	93.02	51.07	1.59	2.44	1.34
2	1-2	DNY_1	Luo/Durrani/Conte	254	254	350.8	350.8	96.8	0.59	1403.20	35.3	372.1	53801.08	45.52	64.11	58.02	54.49	1.41	1.27	1.20
3	1-3	DNY_2	Luo/Durrani/Conte	254	254	350.8	350.8	96.8	0.59	1403.20	25.7	372.1	68859.12	31.59	47.86	44.89	41.03	1.52	1.42	1.30
4	1-4	DNY_3	Luo/Durrani/Conte	254	254	350.8	350.8	96.8	0.59	1403.20	24.6	372.1	53895.50	46.27	50.84	49.23	43.35	1.10	1.06	0.94
5	1-5	DNY_4	Luo/Durrani/Conte	254	254	350.8	350.8	96.8	0.59	1403.20	19.1	372.1	55404.93	41.59	42.44	43.15	36.31	1.02	1.04	0.87
6	2-1	1	Long/Clealand/Kirk	150	150	201.5	201.5	51.5	0.97	806.00	34.3	316.0	61000.00	2.72	3.42	2.68	3.29	1.26	0.99	1.21
7	2-2	2	Long/Clealand/Kirk	150	150	201.5	201.5	51.5	0.97	806.00	32	316.0	66500.00	2.15	2.01	1.24	2.14	0.93	0.58	1.00
8	2-3	3	Long/Clealand/Kirk	150	150	201.5	201.5	51.5	0.97	806.00	26.5	316.0	64300.00	3.54	1.18	0.79	1.43	0.33	0.22	0.40
9	3-1	S1	Mor./Hir./Sozen	305	305	371.2	371.2	66.2	0.65	1484.80	45.7	322.5	6285.02	39.28	63.36	46.47	56.44	1.61	1.18	1.44
10	3-2	S2	Mor./Hir./Sozen	305	305	371.2	371.2	66.2	0.98	1484.80	35.1	330.0	5508.11	44.98	55.53	49.14	49.47	1.23	1.09	1.10
11	3-3	S3	Mor./Hir./Sozen	305	305	371.2	371.2	66.2	1.31	1484.80	33.9	334.9	5413.13	47.48	54.57	53.70	48.61	1.15	1.13	1.02
12	3-4	S4	Mor./Hir./Sozen	305	305	371.2	371.2	66.2	0.98	1484.80	34.9	319.7	12815.58	40.88	53.09	46.72	47.50	1.30	1.14	1.16
13	3-5	S5	Mor./Hir./Sozen	305	305	371.2	371.2	66.2	0.98	1484.80	35.1	339.7	27540.54	42.33	48.66	42.12	43.97	1.15	0.99	1.04
14	4-1	1	Islam/Park	229	229	307.9	307.9	78.9	1.07	1231.60	27.3	355.5	42310.36	36.74	33.10	38.32	28.25	0.90	1.04	0.77
15	4-2	2	Islam/Park	229	229	307.9	307.9	78.9	1.07	1231.60	31.9	373.4	42077.37	45.55	36.74	41.12	31.30	0.81	0.90	0.69
16	4-3	3C	Islam/Park	229	229	307.9	307.9	78.9	1.07	1231.60	29.7	315.6	42365.75	43.38	34.99	39.76	29.83	0.81	0.92	0.69

Table 2.2 continued

running number notation unit	serial no	slab no (n)	author(A)	column size(c1)	radius/size(c2)	b1	b2	effective depth(d)	reinf. Ratio( $\rho$ )	effective perimeter(u)	comp.strength(cyl)(fc)	yield strength(fy)	failure load(Vexp)	failure moment(Mexp)	failure moment(MA CI)	failure moment(MEurocode)	failure moment(MTS500)	MA CI/Mexp	MEurocode/Mexp	MTS500/Mexp
mm	mm	mm	mm	mm	mm	mm	mm	mm	-	mm	MPa	MPa	N	kNm	kNm	kNm	kNm			
17	5-1	81	Robertson	254	254	358.3	358.3	104.3	0.83	1433.20	39.3	524.3	56226.19	82.00	78.10	84.38	66.29	0.95	1.03	0.81
18	6-1	II	Luo/Durrani	254	254	358.3	358.3	104.3	0.59	1433.20	20.7	380.3	18136.15	44.52	63.59	69.19	53.64	1.43	1.55	1.20
19	6-2	INT 1	Luo/Durrani	254	254	358.3	358.3	104.3	0.55	1433.20	30.9	417.5	119101.59	56.80	48.14	40.29	41.89	0.85	0.71	0.74
20	6-3	INT 2	Luo/Durrani	254	254	358.3	358.3	104.3	0.55	1433.20	30.7	417.5	138041.30	49.67	42.09	33.03	37.04	0.85	0.66	0.75
21	7-1	A12	Hanson/Hanson	152	152	218.2	218.2	66.2	1.5	872.80	33.2	372.1	32182.41	17.73	14.66	22.12	12.55	0.83	1.25	0.71
22	7-2	A13L	Hanson/Hanson	152	152	218.2	218.2	66.2	1.5	872.80	32.8	370.0	31987.95	17.34	14.57	22.05	12.48	0.84	1.27	0.72
23	7-3	B16	Hanson/Hanson	305	152	371.2	218.2	66.2	1.5	1178.80	30.4	340.4	41523.99	22.62	23.81	26.96	20.99	1.05	1.19	0.93
24	7-4	C17	Hanson/Hanson	305	152	371.2	218.2	66.2	1.5	1178.80	36	341.1	37396.14	27.45	27.73	30.15	24.34	1.01	1.10	0.89
25	8-1	INT	Zee/Moehle	137	137	188	188	51	0.65	752.00	26.2	434.8	15704.66	10.30	7.93	7.80	6.77	0.77	0.76	0.66
26	9-1	1	Pan/Moehle	274	274	385.9	385.9	111.9	0.72	1543.60	33.3	471.3	116287.70	87.93	70.91	71.26	61.09	0.81	0.81	0.69
27	9-2	3	Pan/Moehle	274	274	385.9	385.9	111.9	0.72	1543.60	31.3	471.3	70866.09	112.20	82.50	87.10	70.23	0.74	0.78	0.63
28	10-1	S1	Hawkings	305	305	447.4	447.4	142.4	1.18	1789.60	23.4	458.9	139711.31	170.03	103.67	161.18	89.22	0.61	0.95	0.52
29	10-2	S2	Hawkings	305	305	447.4	447.4	142.4	0.79	1789.60	23.2	459.6	184120.10	118.72	86.03	110.31	75.08	0.72	0.93	0.63
30	10-3	S3	Hawkings	305	305	447.4	447.4	142.4	1.18	1789.60	26.5	458.9	179288.11	163.72	98.63	151.63	85.59	0.60	0.93	0.52
31	11-1	3	Farhey	300	200	370	270	70	0.58	1280.00	15	456.8	30075.01	22.00	22.45	19.31	19.48	1.02	0.88	0.89
32	11-2	4	Farhey	300	120	370	190	70	0.58	1120.00	15	456.8	27327.77	15.69	13.89	14.52	14.23	0.88	0.93	0.91

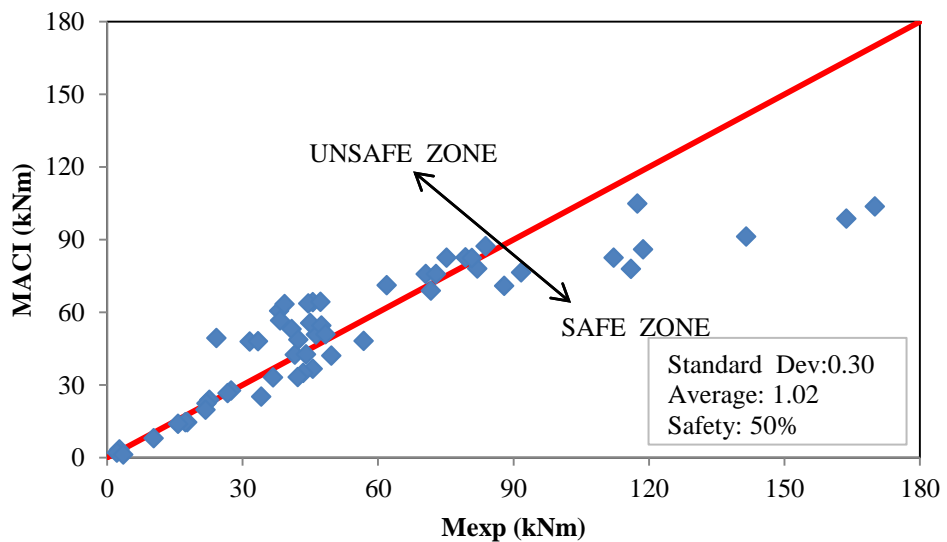
Table 2.2 continued

running number notation	serial no	slab no (n)	author(A)	column size(c1)	radius/size(c2)	b1	b2	effective depth(d)	reinf. Ratio( $\rho$ )	effective perimeter(u)	comp.strength(cyl)(fc)	yield strength(fy)	failure load(V <sub>exp</sub> )	failure moment(M <sub>exp</sub> )	failure moment(MACI)	failure moment (MEurocode)	failure moment(MTS500)	MACI/M <sub>exp</sub>	MEurocode/M <sub>exp</sub>	MTS500/M <sub>exp</sub>
unit	-	-	-	mm	mm	mm	mm	mm	-	mm	MPa	MPa	N	kNm	kNm	kNm	kNm			
33	12-1	1	Robertson/Durrani	254	254	358.3	358.3	104.3	0.83	1433.20	38	500.2	58360.00	70.55	75.86	82.41	64.43	1.08	1.17	0.91
34	12-2	2C	Robertson/Durrani	254	254	358.3	358.3	104.3	0.83	1433.20	33	500.2	60109.92	71.71	68.95	76.97	58.65	0.96	1.07	0.82
35	12-3	3SE	Robertson/Durrani	254	254	358.3	358.3	104.3	0.83	1433.20	44	500.2	59493.39	79.33	82.64	87.20	70.14	1.04	1.10	0.88
36	12-4	4S	Robertson/Durrani	254	254	358.3	358.3	104.3	0.83	1433.20	43.8	500.2	59358.02	80.80	82.45	87.09	69.98	1.02	1.08	0.87
37	12-5	5SO	Robertson/Durrani	254	254	358.3	358.3	104.3	0.83	1433.20	38	500.2	58360.00	72.83	75.86	82.41	64.43	1.04	1.13	0.88
38	13-1	SM0,5	Ghali	305	305	409.3	409.3	104.3	0.5	1637.20	36.8	470.0	107041.06	75.15	82.58	58.92	70.85	1.10	0.78	0.94
39	13-2	SM1,0	Ghali	305	305	409.3	409.3	104.3	1	1637.20	33.4	470.0	108555.53	91.67	76.40	80.74	65.68	0.83	0.88	0.72
40	13-3	SM1,5	Ghali	305	305	409.3	409.3	104.3	1.5	1637.20	40	470.0	107998.08	83.85	87.35	107.79	74.87	1.04	1.29	0.89
41	13-4	DM0,5	Ghali	305	305	409.3	409.3	104.3	0.5	1637.20	44.1	470.0	75598.66	117.39	104.82	77.92	89.09	0.89	0.66	0.76
42	13-5	DM1,0	Ghali	305	305	409.3	409.3	104.3	1	1637.20	32.7	470.0	100902.14	115.99	77.85	82.94	66.79	0.67	0.72	0.58
43	13-6	DM1,5	Ghali	305	305	409.3	409.3	104.3	1.5	1637.20	42.5	470.0	107611.15	141.55	91.32	111.04	78.20	0.65	0.78	0.55
44	14-1	b2	Hwang/Moehle	244	244	315	315	71	0.64	1260.00	21.8	456.0	38984.67	26.65	26.65	22.70	22.80	1.00	0.85	0.86
45	14-2	b3	Hwang/Moehle	244	163	315	234	71	0.74	1098.00	21.8	456.0	33972.36	21.76	19.79	20.06	17.18	0.91	0.92	0.79
46	14-3	c2	Hwang/Moehle	325	244	396	315	71	0.66	1422.00	21.8	456.0	43966.05	42.18	33.21	25.76	28.77	0.79	0.61	0.68
47	14-4	c3	Hwang/Moehle	325	163	396	234	71	0.77	1260.00	21.8	456.0	38984.67	34.16	25.12	22.50	22.06	0.74	0.66	0.65
48	15-1	A	Robertson/Durrani	254	254	358.3	358.3	104.3	0.83	1433.20	33.03	500.6	52931.20	61.92	71.17	79.48	60.43	1.15	1.28	0.98
49	15-2	B	Robertson/Durrani	254	254	358.3	358.3	104.3	0.83	1433.20	30.75	524.7	90739.20	38.31	56.58	62.86	48.64	1.48	1.64	1.27
50	15-3	C	Robertson/Durrani	254	254	358.3	358.3	104.3	0.83	1433.20	32.20	524.7	120985.60	24.18	49.32	52.94	42.91	2.04	2.19	1.77
51	16-1	DNY_1	Luo/Durrani/Du	254	254	350.8	350.8	96.8	0.59	1403.20	35.27	372.3	53263.07	47.23	64.23	58.00	54.59	1.36	1.23	1.16
52	16-2	DNY_2	Luo/Durrani/Du	254	254	350.8	350.8	96.8	0.59	1403.20	25.73	372.3	68170.53	33.45	48.10	44.91	41.22	1.44	1.34	1.23
53	16-3	DNY_3	Luo/Durrani/Du	254	254	350.8	350.8	96.8	0.59	1403.20	24.59	372.3	53356.54	48.36	50.99	49.22	43.46	1.05	1.02	0.90
54	16-4	DNY_4	Luo/Durrani/Du	254	254	350.8	350.8	96.8	0.59	1403.20	19.11	372.3	54850.88	44.07	42.63	43.16	36.46	0.97	0.98	0.83

The results presented in Table 2.2 were summarized in Figures 2.12, 2.13 and 2.14. In these figures calculated moment value that would cause punching failure under the applied shear force was computed for each code and results were plotted against the experimental moment values at punching failure observed.

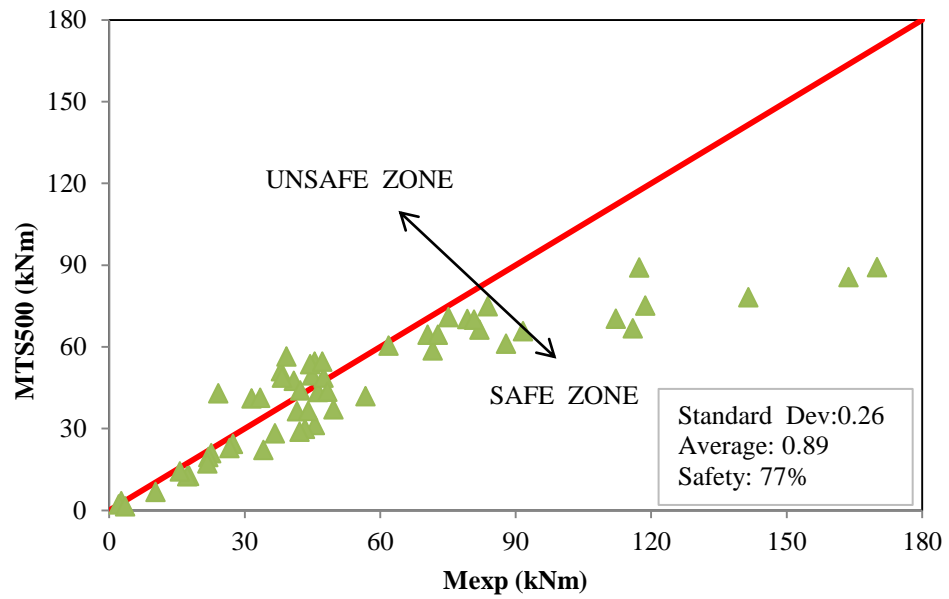
For regions where  $M_{exp}$  (unbalanced moment obtained by the tests) was greater than the  $M_{code}$  (unbalanced moment obtained by the codes) ‘*safe zone*’ was marked, otherwise ‘*unsafe zone*’ statement was used. On the figures, standart deviation, average and % of data points that were estimated safely were also noted. Unsafe and safe zones are labeled excluding material safety factors, which are used to consider other uncertainties than the estimations of prediction equations.

It can be observed that ACI-318 is the most accurate in the average sense, however TS500 is the safest among the three codes for interior slab column connections. The highest standart deviation is in the Eurocode-2 predictions. ACI-318 estimations are similar to TS500, perhaps being slightly on the unsafe side.

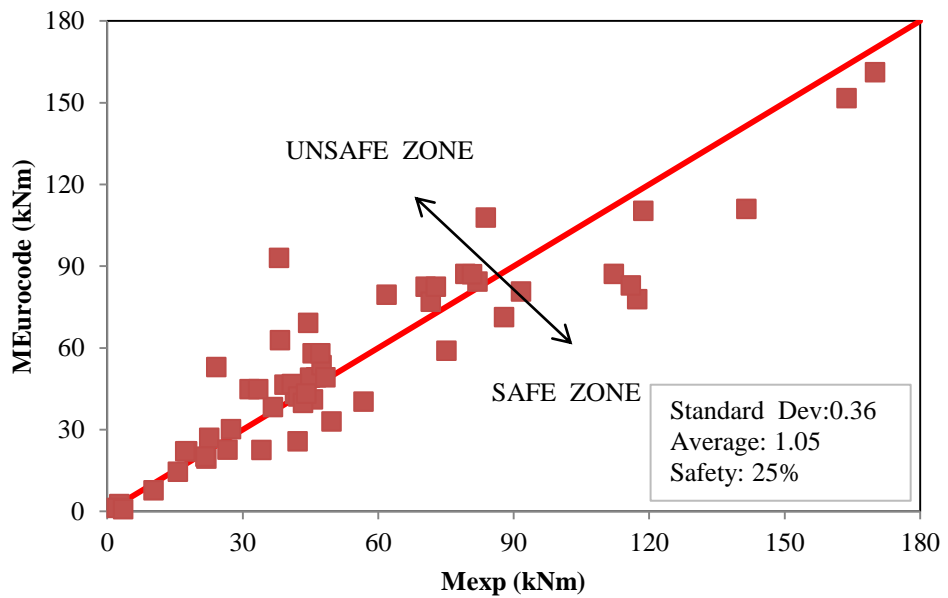


**Figure 2.12 Comparison of Unbalanced Moments between ACI-318 and Experimental Values**





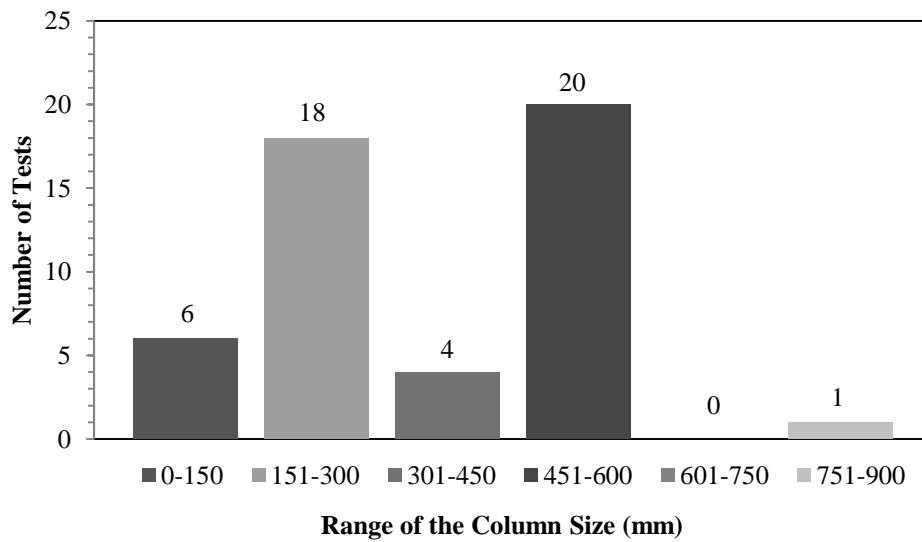
**Figure 2.13 Comparison of Unbalanced Moments between TS500 and Experimental Values**



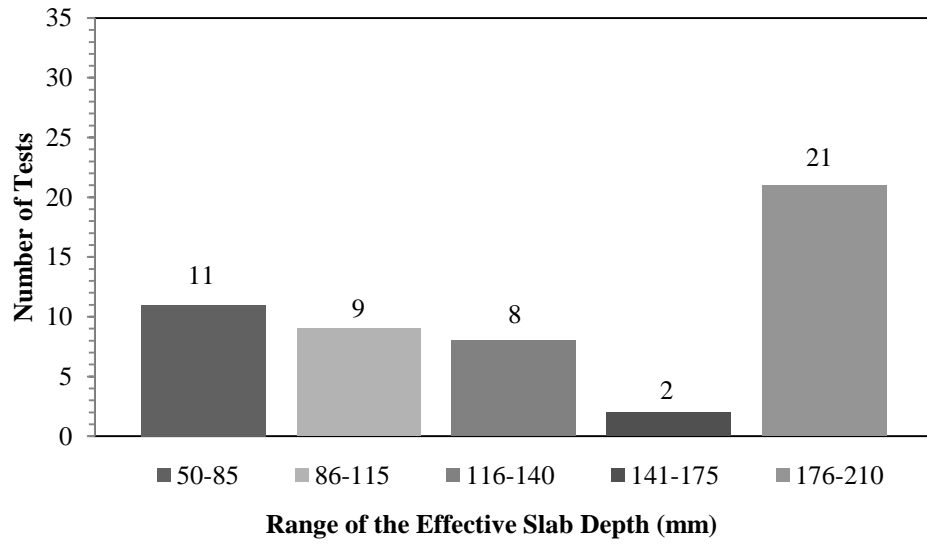
**Figure 2.14 Comparison of Unbalanced Moments between Eurocode-2 and Experimental Values**

### 2.3.2. Exterior Slab-Column Connections

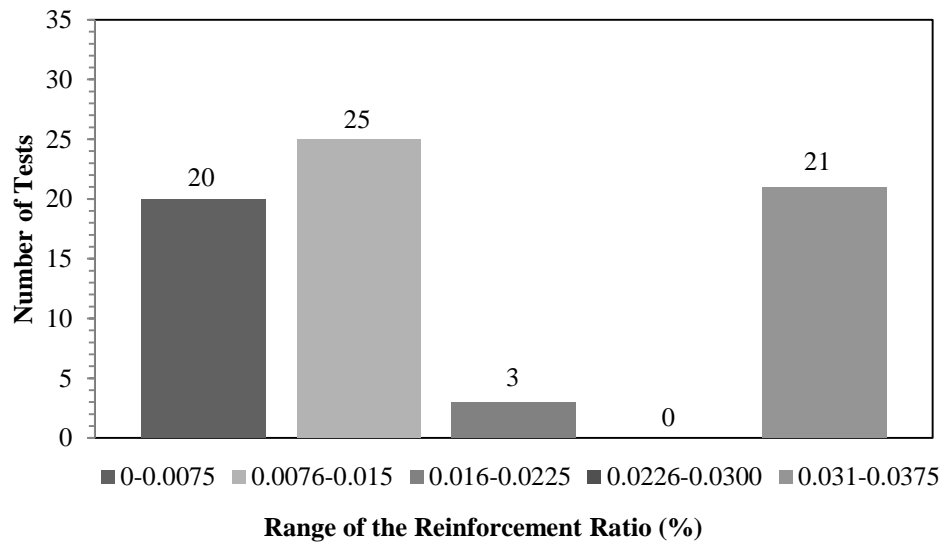
49 exterior slab-column connections under eccentric loading data collected. The column dimensions change between 100 to 900 mm and the slab effective depth vary between 41 to 210 mm. The distributions of the column size, effective depth of the slab, reinforcement ratio and compressive strength of concrete can be seen in Figures 2.15, 2.16, 2.17 and 2.18.



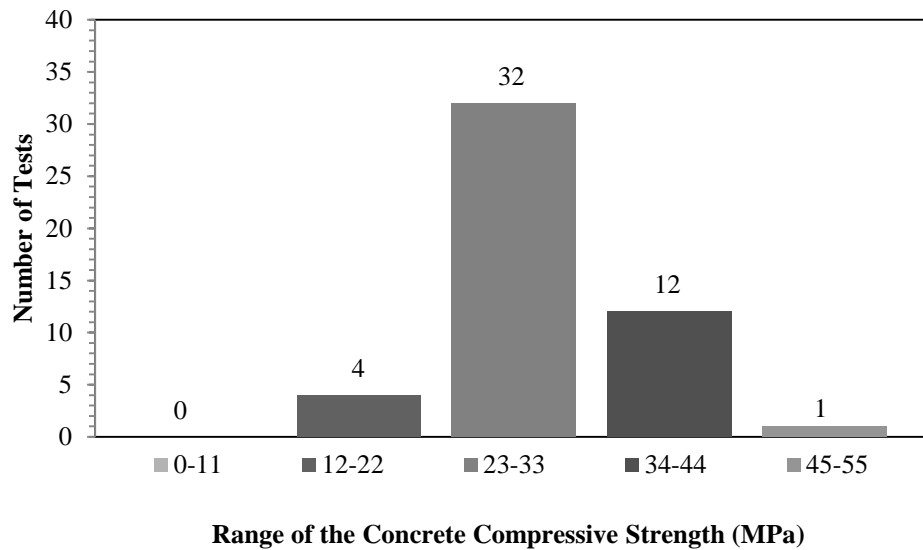
**Figure 2.15 Distribution of the Column Size for Exterior Slab-Column Connections**



**Figure 2.16 Distribution of the Effective Depth of the Slab for Exterior Slab-Column Connections**



**Figure 2.17 Distribution of the Reinforcement Ratio of the Slab for Exterior Slab-Column Connections**



**Figure 2.18 Distribution of the Compressive Concrete Strength ( $f_c$ ) for Exterior Slab-Column Connections**

In Table 2.3 the experimental unbalanced moments for exterior connection values were compared with the moment estimations of design equations given by ACI-318, TS500 and Eurocode-2 respectively. The calculation steps were followed according to the given equations in current codes as described in Chapter 1.

**Table 2.3 Comparison of unbalanced moments with ACI-318, Eurocode-2 and TS500 for exterior slab-column connections on eccentric loading**

running number	notation	serial no	slab no (n)	author(A)	column size(c1)	radius/size(c2)	effective depth(d)	reinf. Ratio( $\rho$ )	effective perimeter(u)	comp.strength( $cyl$ )( $f_c$ )	yield strength( $f_y$ )	failure moment( $M_{exp}$ )	failure moment(MACI)	failure moment (Meurocode)	failure moment(MTS500)	MACI/ $M_{exp}$	MEurocode/ $M_{exp}$	MTS500/ $M_{exp}$
unit		-	-	-	mm	mm	mm	-	mm	MPa	MPa	kNm	kNm	kNm	kNm			
1		1-1	E1	Hawkings	305	305	138	0.8	1191.00	22.5	463	67.7	76.98	84.37	66.33	1.14	1.25	0.98
2		1-2	E2	Hawkings	406	406	149	1.1	1516.00	29.5	425	150.50	142.84	149.68	123.47	0.95	0.99	0.82
3		1-3	E3	Hawkings	495	203	149	1.3	1491.00	22.6	447	126.10	72.09	113.59	73.93	0.57	0.90	0.59
4		2-1	D15	Hanson/Hanson	152	152	62	1.5	580.00	31.1	365	10.5	10.70	13.99	9.15	1.02	1.33	0.87
5		3-1	SE1	Regan	300	200	104	1.1	1008.00	35.5	480	39.6	2.77	0.00 <sup>(*)</sup>	4.69	0.07	0.00	0.12
6		3-2	SE4	Regan	300	200	104	1.1	1008.00	26.6	480	30.5	3.27	0.00	4.77	0.11	0.00	0.16
7		3-3	SE7	Regan	300	200	103	0.9	1006.00	39.8	490	31.80	21.01	11.70	19.74	0.66	0.37	0.62
8		3-4	SE9	Regan	250	250	104	0.5	958.00	41.9	480	35.70	29.55	11.01	26.63	0.83	0.31	0.75
9		3-5	SE10	Regan	250	250	104	0.5	958.00	41.1	480	36.00	31.88	14.43	28.48	0.89	0.40	0.79
10		3-6	SE11	Regan	250	250	104	0.5	958.00	51.5	480	39.60	32.15	9.10	29.03	0.81	0.23	0.73
11		4-1	W5_B	Falamaki/Loo	200	200	83	0.6	766.00	26.8	500	16.60	9.88	5.07	9.11	0.60	0.31	0.55
12		4-2	M5_B	Falamaki/Loo	400	300	84	1.5	1268.00	34	614	41.10	40.50	35.55	36.26	0.99	0.87	0.88

<sup>(\*)</sup> 0 kNm load carrying capacity means that the specimen is calculated to reach its punching capacity under pure shear force without any moment.

Table 2.3 continued

running number notation	serial no	slab no (n)	author (A)	column size(c1)	radius/size(c2)	effective depth(d)	reinf. Ratio( $\rho$ )	effective perimeter(u)	comp.strength(cyl)(fc)	yield strength(fy)	failure moment(Mexp)	failure moment(MA CI)	failure moment (Meurocode)	failure moment(MTS500)	MA CI/Mexp	MEurocode/Mexp	MTS500/Mexp
unit	-	-	-	mm	mm	mm	-	mm	MPa	MPa	kNm	kNm	kNm	kNm			
13	5-1	C/E/1	Stamenkovic/Chapman	127	127	60	1.1	501.00	31.5	448	5.60	0.00	0.00	0.00	0.00	0.00	0.00
14	5-2	C/E/2	Stamenkovic/Chapman	127	127	60	1.1	501.00	33	496	9.20	0.43	0.00	0.74	0.05	0.00	0.08
15	5-3	C/E/3	Stamenkovic/Chapman	127	127	60	1.1	501.00	34	496	10.10	5.67	6.72	4.97	0.56	0.67	0.49
16	5-4	C/E/4	Stamenkovic/Chapman	127	127	60	1.1	501.00	27.8	496	8.80	7.10	9.10	6.09	0.81	1.03	0.69
17	6-1	K1	Kane	100	68	44	1	356.00	30.2	480	2.40	0.47	0.69	0.50	0.20	0.29	0.21
18	6-2	K3	Kane	114	75	41	1.1	385.00	41.2	480	2.50	0.94	1.01	0.92	0.38	0.41	0.37
19	7-1	ZIV(1)	Zaghlool	178	178	127	1.8	788.00	27.4	476	45.00	14.07	41.98	13.31	0.31	0.93	0.30
20	7-2	ZIV(1)	Zaghlool	267	267	127	1.4	1055.00	34.3	474	84.60	16.26	24.13	16.89	0.19	0.29	0.20
21	7-3	ZIV(2)	Zaghlool	267	267	127	1.6	1055.00	40.5	474	93.60	12.90	23.00	14.51	0.14	0.25	0.15
22	7-4	ZIV(3)	Zaghlool	267	267	125	1.8	1051.00	38.7	475	103.60	0.87	10.51	4.61	0.01	0.10	0.04
23	7-5	ZIV(6)	Zaghlool	267	267	127	1.4	1055.00	31.3	476	88.10	47.31	67.61	41.79	0.54	0.77	0.47
24	7-6	ZIV(1)	Zaghlool	356	356	127	1.2	1322.00	26	476	106.90	8.47	0.00	11.91	0.08	0.00	0.11
25	8-1	S1	Scavuzzo	152	102	52	0.7	510.00	38.1	379	4.70	3.25	2.17	2.98	0.69	0.46	0.63

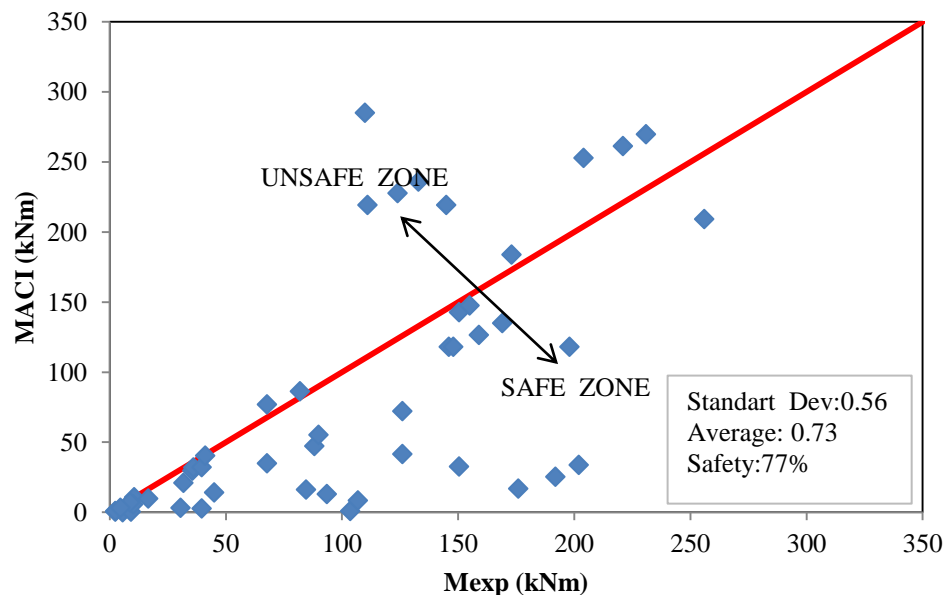
Table 2.3 continued

running number notation	serial no	slab no (n)	author(A)	column size(c1)	radius/size(c2)	effective depth(d)	reinf. Ratio( $\rho$ )	effective perimeter(u)	comp.strength(cyl)(fc)	yield strength(fy)	failure moment(Mexp)	failure moment(MACI)	failure moment (Meurocode)	failure moment(MTS500)	MACI/Mexp	MEurocode/Mexp	MTS500/Mexp
unit	-	-	-	mm	mm	mm	-	mm	MPa	MPa	kNm	kNm	kNm	kNm			
26	9-1	1	Park/Choi	500	500	180	0.3	1860.00	23.5	379	133.00	236.07	126.63	203.79	1.77	0.95	1.53
27	9-2	2	Park/Choi	500	500	180	0.6	1860.00	23.5	379	169.00	134.90	67.14	122.27	0.80	0.40	0.72
28	9-3	3	Park/Choi	500	500	180	0.9	1860.00	23.5	379	202.00	33.72	0.00	40.76	0.17	0.00	0.20
29	9-4	4	Park/Choi	500	500	180	1.2	1860.00	23.5	379	231.00	269.79	317.09	230.96	1.17	1.37	1.00
30	9-5	5	Park/Choi	500	500	180	0.3	1860.00	23.5	379	124.00	227.64	116.23	197.00	1.84	0.94	1.59
31	9-6	6	Park/Choi	500	500	180	0.6	1860.00	23.5	379	159.00	126.46	56.74	115.48	0.80	0.36	0.73
32	9-7	7	Park/Choi	500	500	180	0.9	1860.00	23.5	379	192.00	25.29	0.00	33.96	0.13	0.00	0.18
33	9-8	8	Park/Choi	500	500	180	1.2	1860.00	23.5	379	221.00	261.36	306.68	224.17	1.18	1.39	1.01
34	9-9	9	Park/Choi	500	500	180	0.3	1860.00	23.5	379	111.00	219.21	105.82	190.20	1.97	0.95	1.71
35	9-10	10	Park/Choi	500	500	180	0.6	1860.00	23.5	379	146.00	118.03	46.33	108.69	0.81	0.32	0.74
36	9-11	11	Park/Choi	500	500	180	0.9	1860.00	23.5	379	176.00	16.86	0.00	27.17	0.10	0.00	0.15
37	9-12	12	Park/Choi	500	500	180	1.2	1860.00	23.5	379	204.00	252.93	296.28	217.38	1.24	1.45	1.07
38	9-13	13	Park/Choi	500	500	180	0.3	1860.00	23.5	379	110.00	284.97	186.98	243.19	2.59	1.70	2.21
39	9-14	14	Park/Choi	500	500	180	0.6	1860.00	23.5	379	145.00	219.21	171.19	190.20	1.51	1.18	1.31
40	9-15	15	Park/Choi	500	500	180	0.9	1860.00	23.5	379	173.00	183.80	173.35	161.67	1.06	1.00	0.93
41	9-16	16	Park/Choi	500	500	180	1.2	1860.00	23.5	379	198.00	118.03	128.69	108.69	0.60	0.65	0.55
42	9-17	17	Park/Choi	600	300	180	0.6	1860.00	23.5	379	82.00	86.22	67.52	81.63	1.05	0.82	1.00
43	9-18	18	Park/Choi	300	300	180	0.6	1260.00	23.5	379	90.00	55.31	49.55	51.10	0.61	0.55	0.57
44	9-19	19	Park/Choi	900	600	180	0.6	2760.00	23.5	379	256.00	209.25	71.69	201.32	0.82	0.28	0.79
45	9-20	20	Park/Choi	500	500	210	0.6	1920.00	23.5	379	155.00	147.53	76.50	135.98	0.95	0.49	0.88
46	9-21	21	Park/Choi	500	500	180	0.6	1860.00	23.5	379	148.00	118.03	46.33	108.69	0.80	0.31	0.73
47	10-1	EI	Luo/Durrani/Conte	250	250	102	1.38	954.00	20.7	379	67.70	34.88	48.23	30.03	0.52	0.71	0.44
48	10-2	II	Luo/Durrani/Conte	250	250	102	0.00	954.00	20.7	379	150.50	32.56	0.00	28.16	0.22	0.00	0.19
49	10-3	DNY_1	Luo/Durrani/Conte	250	250	102	3.11	954.00	35.3	372	126.10	41.59	74.58	36.03	0.33	0.59	0.29

The results mentioned in Table 2.3 were summarized in Figures 2.19, 2.20 and 2.21. In these figures calculated moment value that would cause punching failure under the applied shear force was computed for each code and results were plotted against the experimental moment values at punching failure observed.

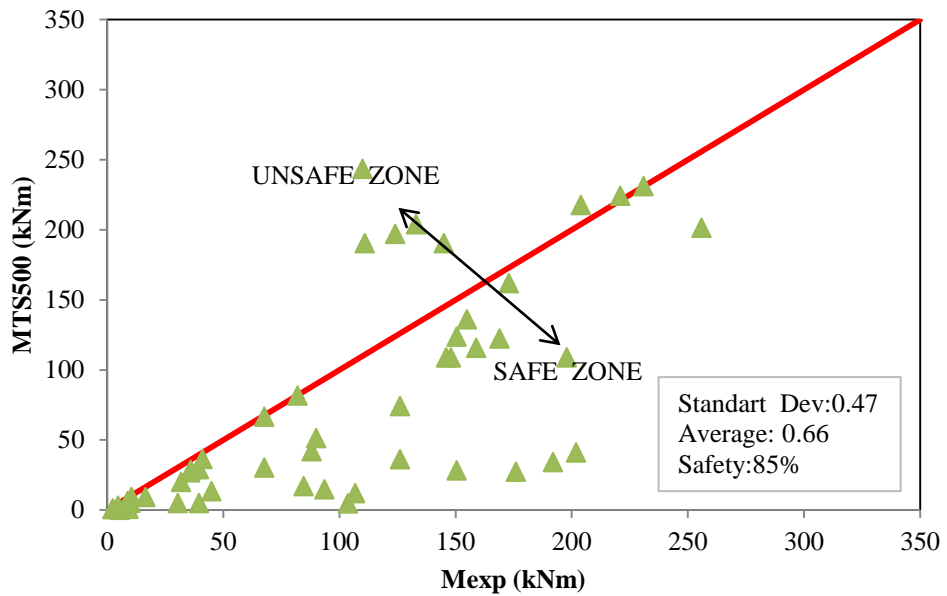
For regions where  $M_{exp}$  (unbalanced moment obtained by the tests) was greater than the  $M_{code}$  (unbalanced moment obtained by the codes) ‘*safe zone*’ was marked, otherwise ‘*unsafe zone*’ statement was used. On the figures, standart deviation, average and % of data points that were estimated safely were also noted.

It can be concluded that ACI-318 is the most accurate in the average sense, however TS500 is the safest among the three codes for exterior slab column connections. The highest standart deviation is in the ACI-318 predictions. Although Eurocode-2 and TS500 predictions seem similar, TS500 is more safe side. Compared to the other type of loadings, the accuracy of strength predictions for exterior slab column connections are less accurate and shows wider scatter.



**Figure 2.19 Comparison of unbalanced moments between ACI and experimental values**

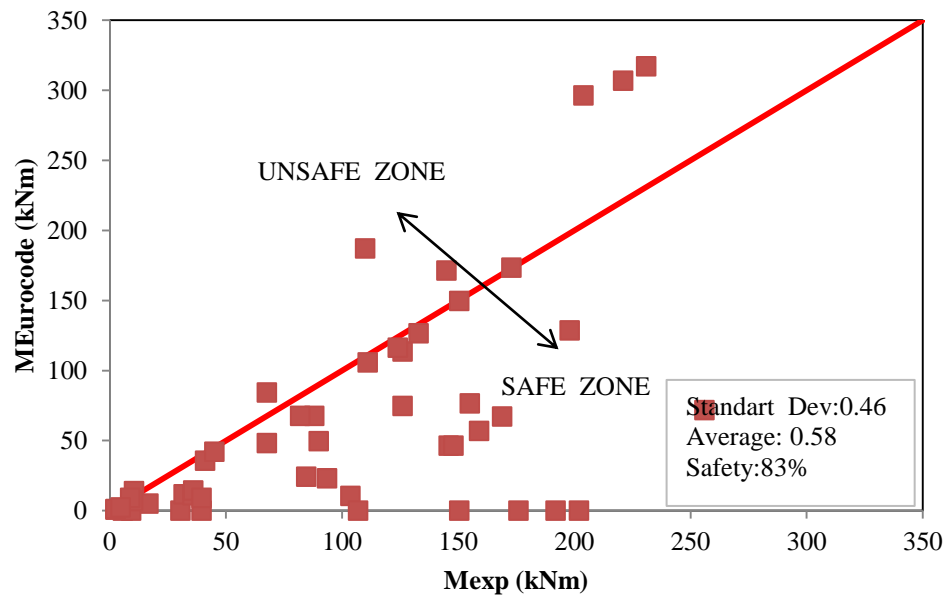




**Figure 2.20 Comparison of unbalanced moments between TS500 and experimental values**

Following observations can be made from the analysis of test data presented in this chapter.

- Eurocode-2 provides the most unsafe estimation among the codes.
- TS500 provides acceptable estimation for concentric interior slab-column connection and eccentric interior slab-column connection, whereas it lacks sufficient information for exterior slab-column connection.
- None of the codes provides a uniform level of safety for different loading cases, despite the failure mode being same.



**Figure 2.21 Comparison of unbalanced moments between Eurocode and experimental values**

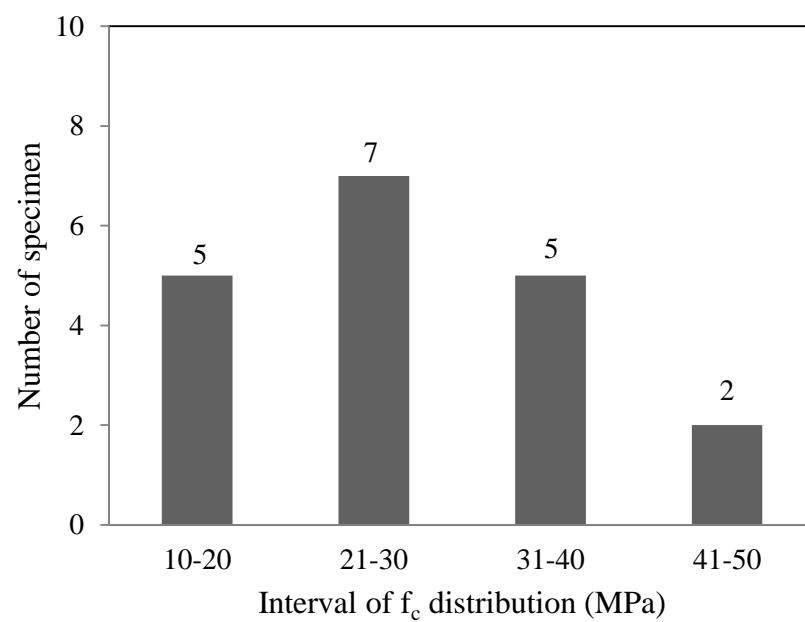
## **CHAPTER 3**

### **ANALYSIS OF PUNCHING FAILURE EXPERIMENTS FOR FLAT PLATES**

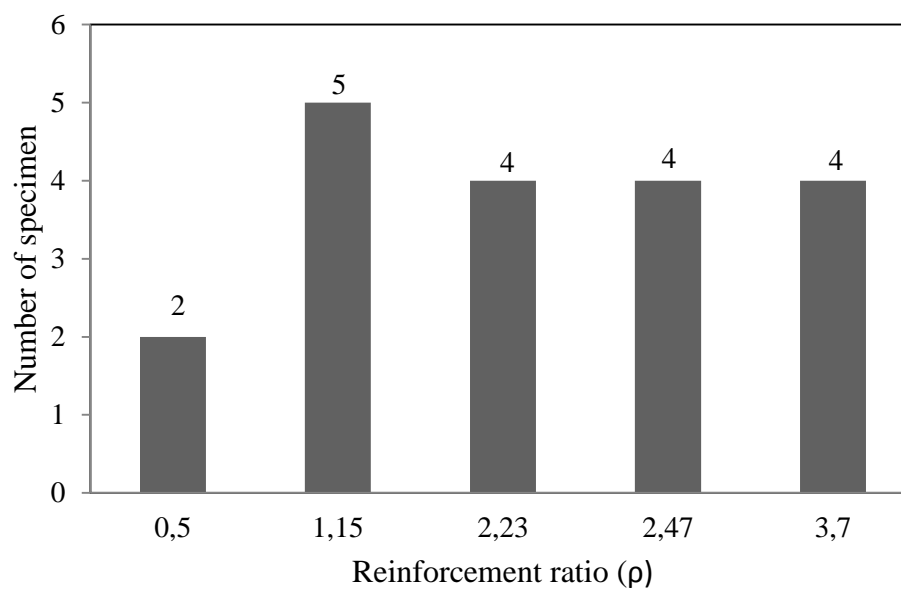
#### **3.1.General:**

To analyze the consequences of punching failure on slab column connections for a whole building (Chapter 4), failure mechanism for one column slab connection should be simulated with simple and reliable models. For this purpose, the load deformation behavior of a slab-column connection was simulated by using a subset of the database described in Chapter 2.

15 specimens taken from the experiments of Hognestad(Elstner & Hognestad, 1956). All specimens had a slab area of 1829x1829 mm. The column sizes varied from 200 to 254 mm and the effective depth of the slabs was changed from 114,3 to 120 mm. Except the column sizes and slab effective depths, the concrete strength, so modulus of elasticity and reinforcement ratios were different. The general properties of the experiments can be seen in Table 3.1 below. The distribution of these variables are shown in Figure 3.1, Figure 3.2.



**Figure 3.1 Distribution of  $f_c$**



**Figure 3.2 Distribution of reinforcement ratio ( $\rho$ )**

**Table 3.1 General properties of used experiment**

Specimen Name	c <sub>1</sub> (mm)	c <sub>2</sub> (mm)	h (mm)	d (mm)	ρ (reinf. ratio)	f <sub>c</sub> '(MPa)	E(ACI) (MPa)	E <sub>cr</sub> =E/3
A-1a	254	254	155.7	117.6	1.15	14.07	17814	5938.09
A-1b	254	254	155.7	117.6	1.15	25.23	23861	7953.76
A-1c	254	254	155.7	117.6	1.15	29.03	25591	8530.47
A-1d	254	254	155.7	117.6	1.15	36.82	28822	9607.33
A-1e	254	254	155.7	117.6	1.15	20.27	21386	7128.62
A-2a	254	254	152.4	114.3	2.47	13.65	17550	5850.12
A-2b	254	254	152.4	114.3	2.47	19.51	20982	6993.99
A-2c	254	254	152.4	114.3	2.47	37.44	29064	9687.95
A-7b	254	254	152.4	114.3	2.47	27.92	25100	8366.80
A-3a	254	254	152.4	114.3	3.70	12.76	16964	5654.81
A-3b	254	254	152.4	114.3	3.70	22.61	22589	7529.55
A-3c	254	254	152.4	114.3	3.70	26.54	24473	8157.60
A-3d	254	254	152.4	114.3	3.70	34.54	27917	9305.74
B-1	254	254	152.4	114.3	0.50	14.20	17901	5967.13
B-2	254	254	152.4	114.3	0.50	47.57	32763	10920.5

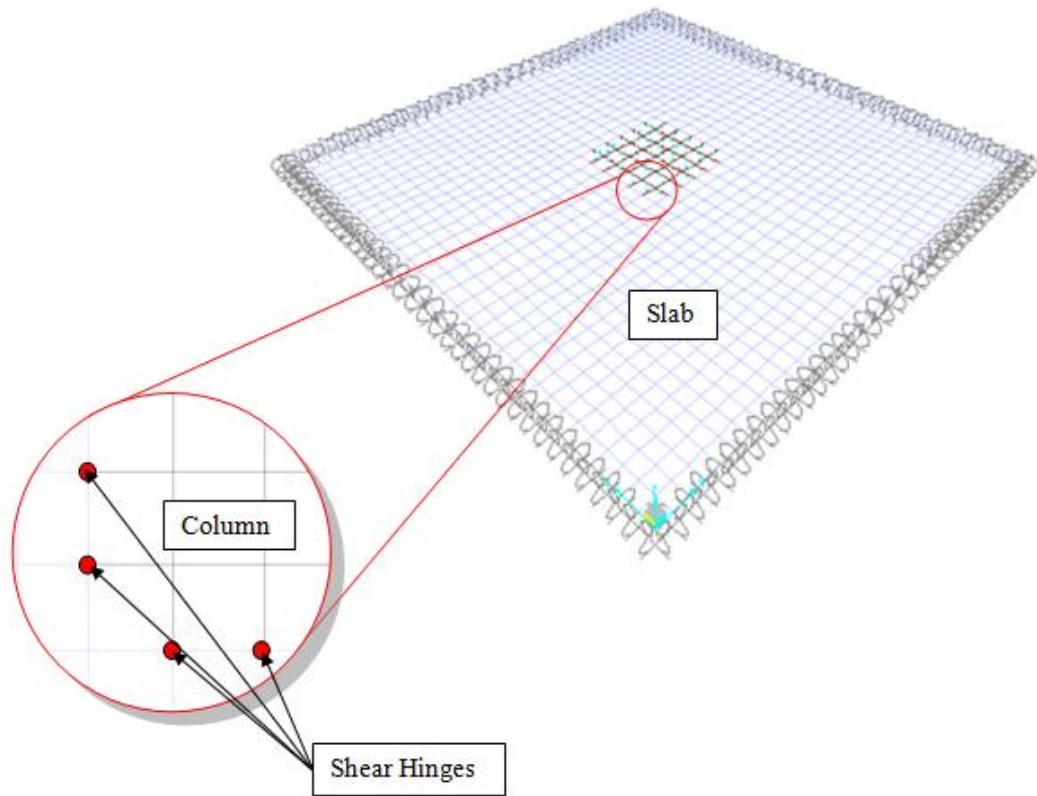
In order to simulate the ductility prior to punching, values obtained from actual experiments were collected, and then load deformation curves corresponding to these values were plotted for each specimen.

After this step each specimen was simulated using two different approaches. One of the models employed shell elements to model the slab along with shear hinges whereas the second model used beam elements used for analyzing the connections. These models will be explained next.

### 3.2. Approach1: Shell Method

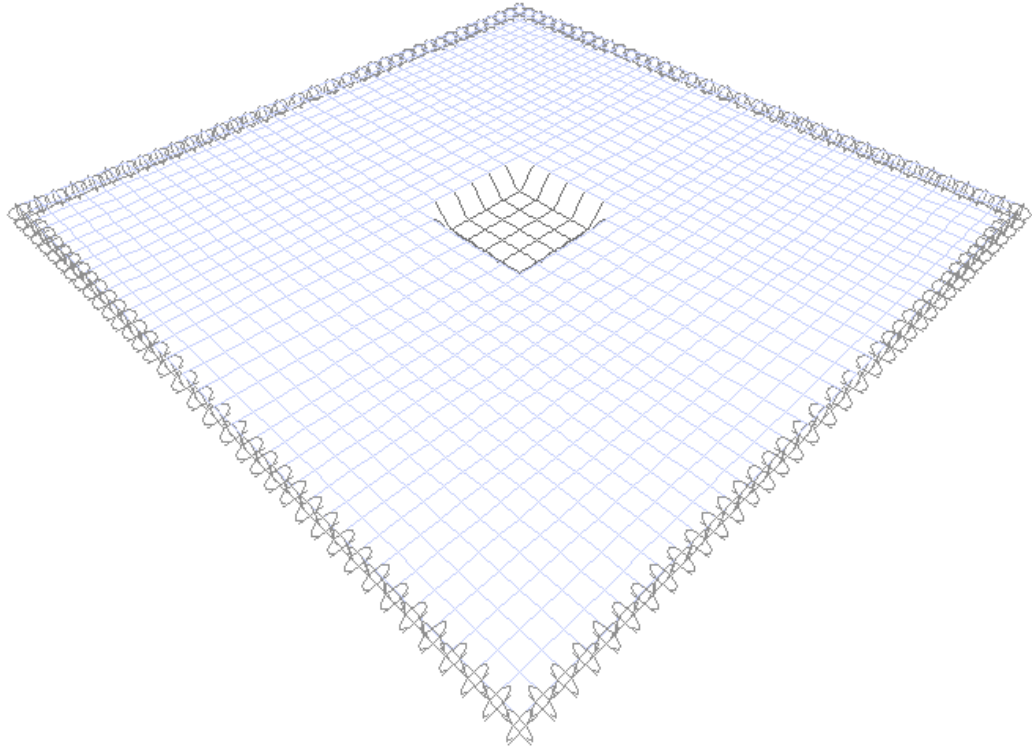
In the shell method, slab was modeled with shell elements and divided into a fine enough mesh. The column was modeled by defining a central rigid zone with high modulus of elasticity (E). Shear hinges were inserted between rows of shell elements d/2 distance away the column face,. Total of the carrying capacity of shear hinges was equal to the punching load of the slab column connection. Along the edges of

the slab, simply supported and roller type of restraints were defined. The thickness of the shells were defined same as the thickness of the slab. For all specimens central displacement was defined. Until the slab-column connection punched, static pushover analysis continued with the same increment of load. The general view of the analyzed test specimen could be seen in Figure 3.3.



**Figure 3.3 General view of the test specimen**

In the first part of analysis, slabs were assumed as cracked sections, for this reason modulus of elasticity for them were taken as  $E_c/3$  (Pan & Moehle, 1992), where  $E_c$  is the modulus of elasticity of the slab according to ACI-318. When all hinges failed, this situation showed that punching type of failure occurred. In Figure 3.4, the final stage of the analysis after punching is shown.



**Figure 3.4 Punching stage of the specimen**

The load deformation curves of the simulations for each specimen is shown in Figures 3.5, 3.6 and 3.7. It can be observed that, the use of  $E_c/3$  to simulate slab cracking provided a good match for the initial stiffness. However, when such a stiff initial loading branch was used, the ductility could be grossly overestimated.

In order to provide a better estimation of the experimental load deformation response, 75% of the exact punching load value was marked on the experimental load deformation graphs and a straight line was drawn from the zero point to the 75% of the maximum load ( $K_{75\%}$ :stiffness of the load deformation graph) and the line was extended until it reached the actual load deformation curve with the same slope. In this way a better representation of cracked stiffness was found.

In the second part of the analysis, the effective stiffness of the slab that would give the  $K_{75\%}$  was back calculated. Then an  $\alpha$  value was found for each experiment where  $\alpha = \frac{E_{75\%}}{E_{ACI}}$ . By using this  $\alpha$  value a new stiffness definition was obtained. When this new stiffness was used instead of  $EI/3$ , obtained stiffness was exactly equal to  $K_{75\%}$ , so it gave more reliable and proper results for deformability estimations. The summary of the results were given in Figures 3.5, 3.6 and 3.7. The back-calculated  $\alpha$  and  $\mu_{\Delta}$  (displacement ductility  $\Delta_u/\Delta_y$ , where  $\Delta_u$  is the ultimate ductility and  $\Delta_y$  is yielding ductility) values by matching the  $K_{75\%}$  were plotted in Figures 3.8 and 3.9. It can be observed that  $\alpha$  is directly proportional with  $\rho$ , whereas  $\mu_{\Delta}$  is inversely proportional with  $\rho$ . The following best fit expressions can be used to estimate  $\mu_{\Delta}$  and  $\alpha$  as a function of  $\rho$  based on the database of Hognestad:

$$\checkmark \quad \mu_{\Delta} = 5.2 \rho^{-1.4} \quad (3.1)$$

$$\checkmark \quad \alpha = 0.025\rho^2 - 0.05\rho + 0.16 \quad (3.2)$$



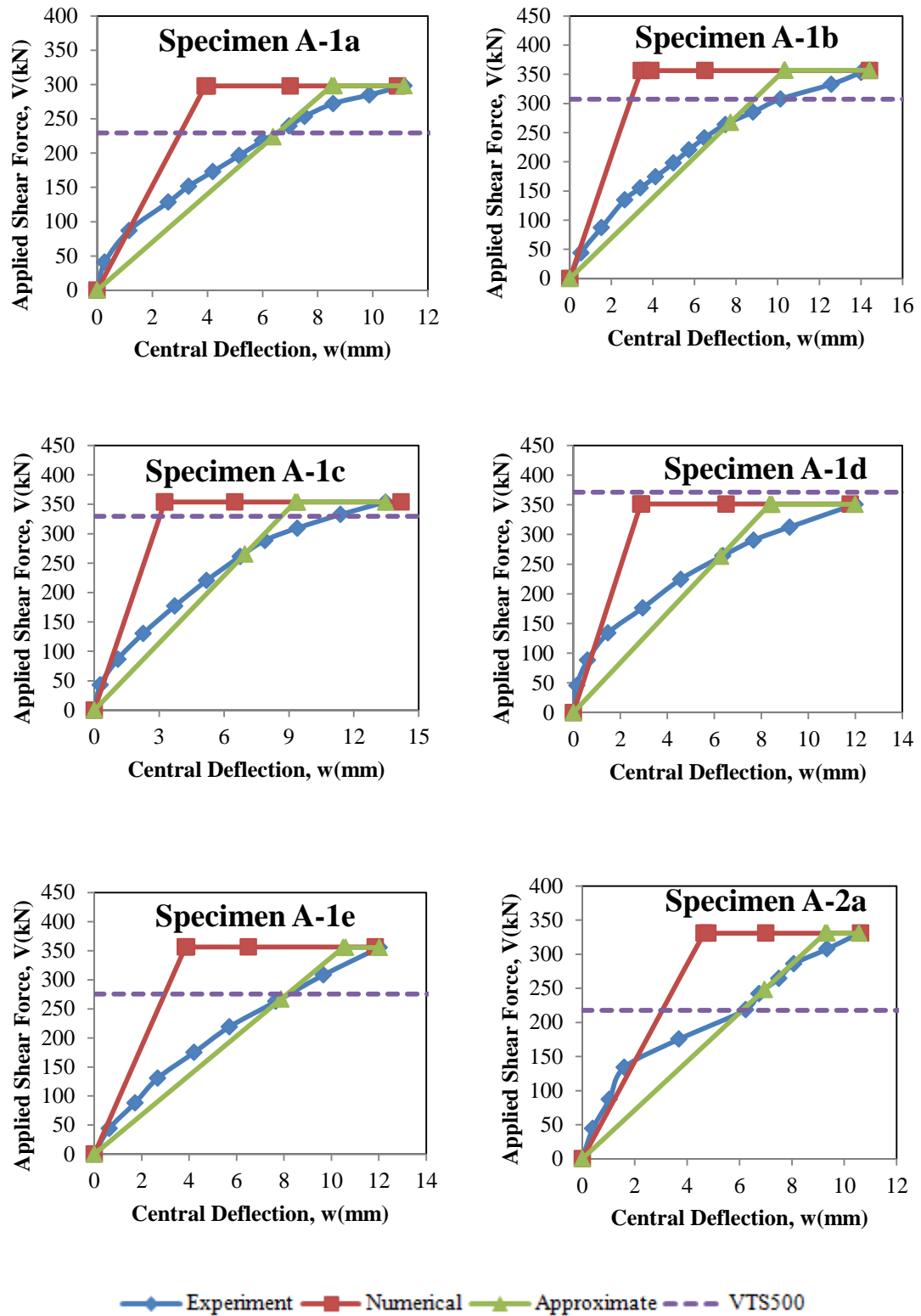


Figure 3.5 Summary of the load deformation curves for shell method

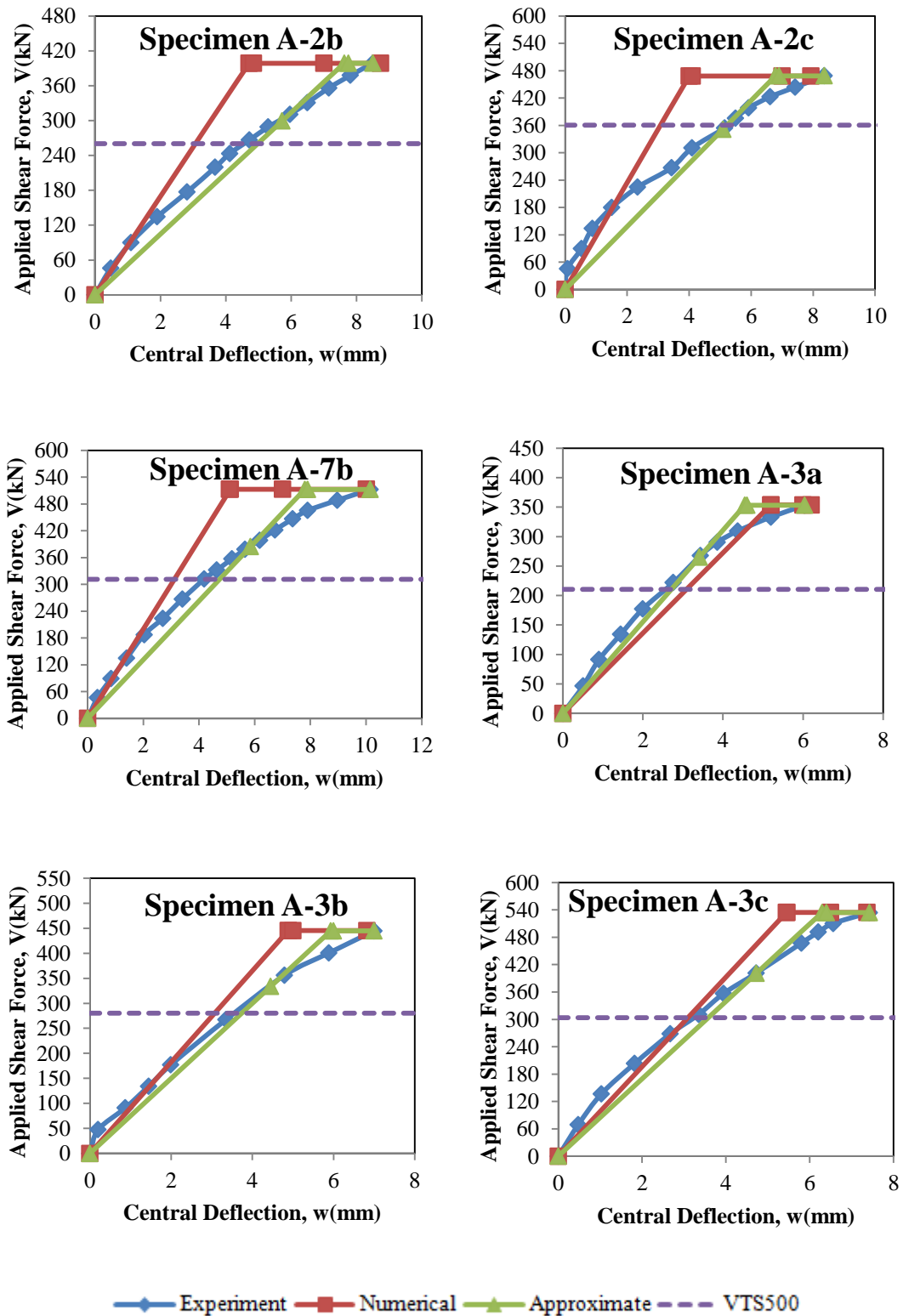


Figure 3.6 Summary of the load deformation curves for shell method

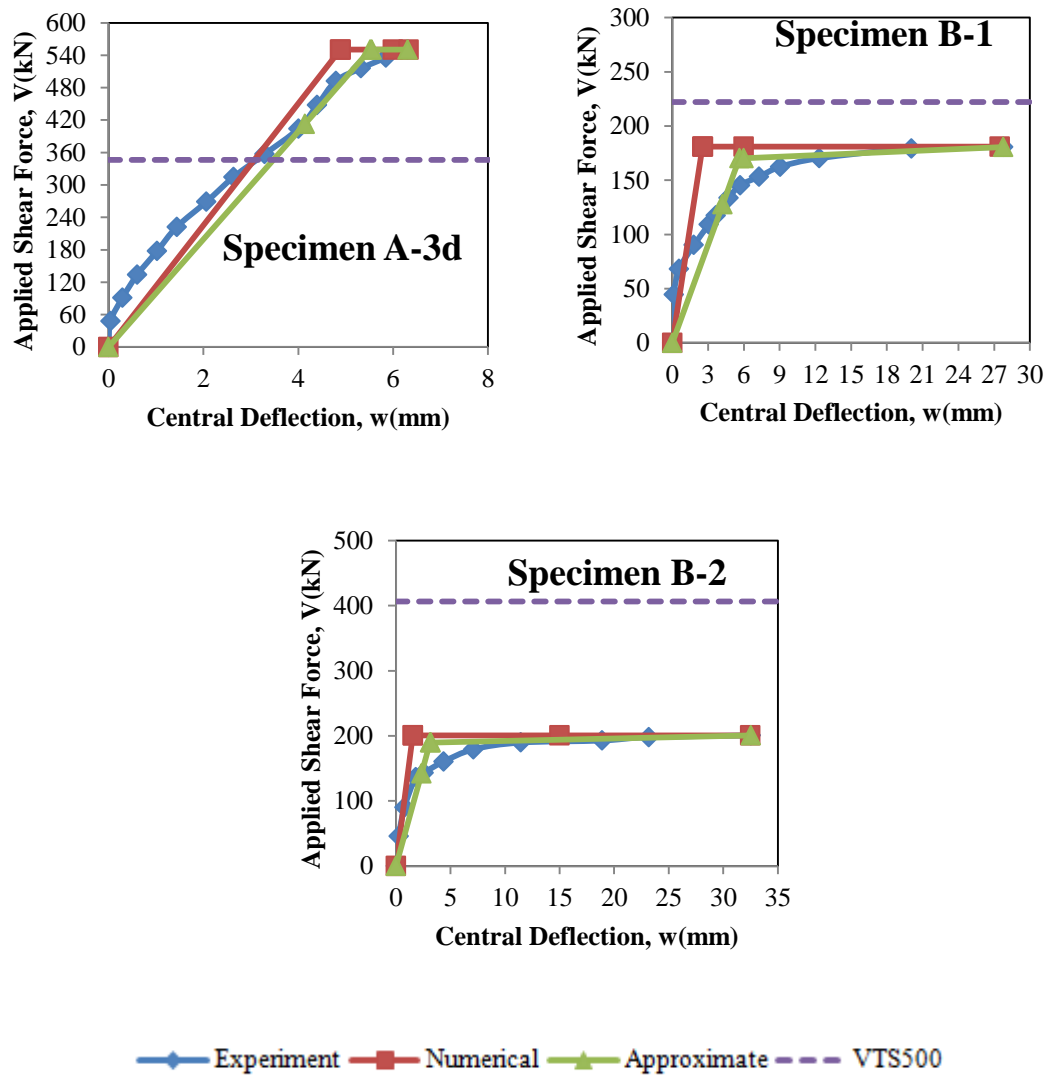
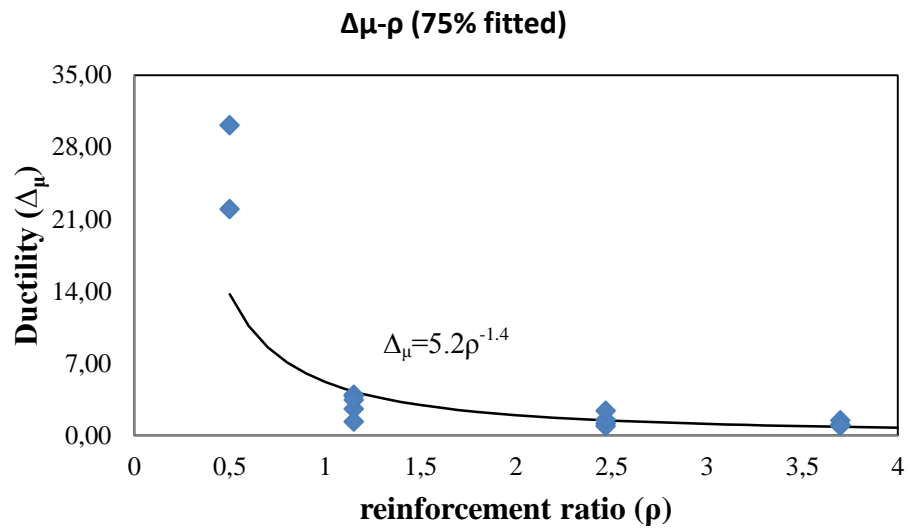
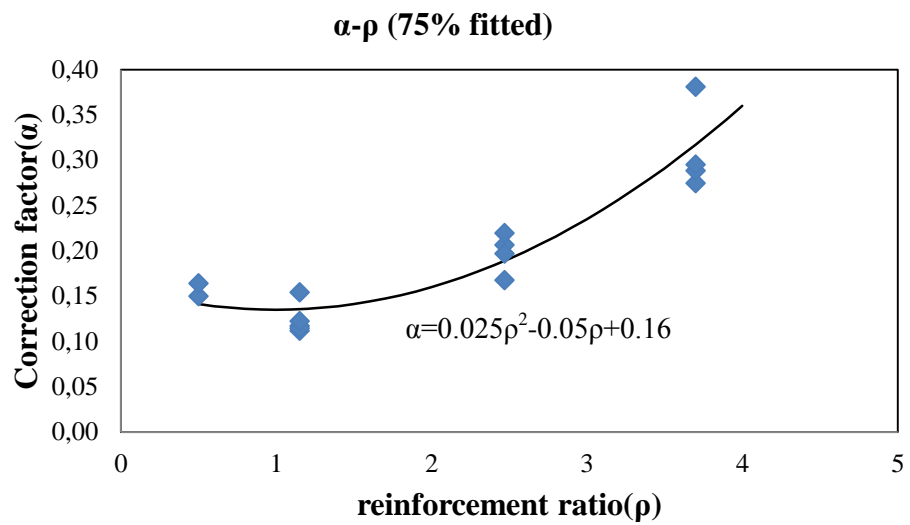


Figure 3.7 Summary of the load deformation curves for shell method



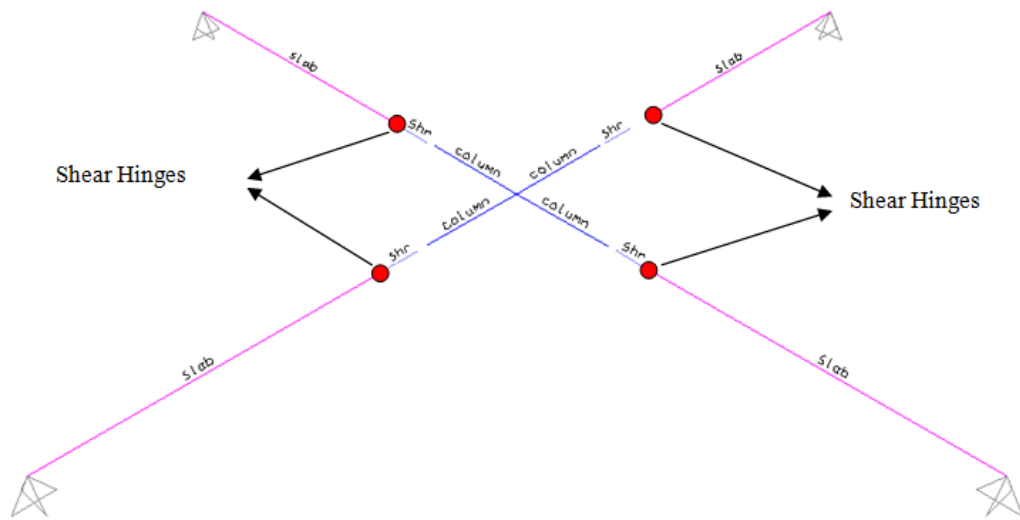
**Figure 3.8 Ductility versus reinforcement ratio curve**



**Figure 3.9 Correction factor versus reinforcement ratio curve**

### 3.3. Approach 2: Beam Method

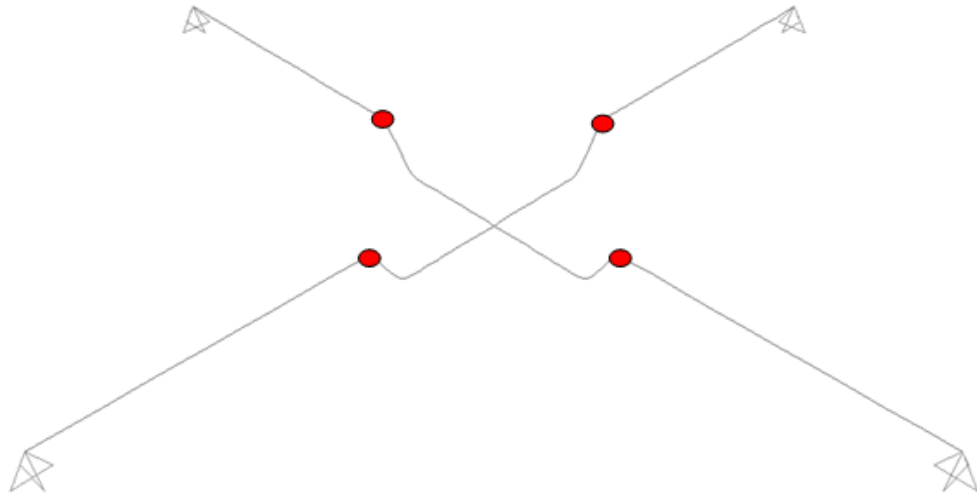
This approach is usually preferred in the lateral load analysis of flat plate buildings due to the ease of model definition and run time (Hueste, Browning, Lepage, & Wallace, 2007). The major difference between shell and beam method was in the beam method all members were defined as beam elements. Similar to the shell method, connection regions were defined as infinitely rigid zones and shear hinges were employed at a distance of  $d/2$  from the column face. The general model for beam method was shown in Figure 3.10.



**Figure 3.10 The General Model for Beam Method**

There were 4 shear hinges at each specimen model and every hinges had a carrying capacity, which was equal to  $V_u/4$ , where  $V_u$  is punching load capacity of slab-column connection. The thickness of the slab assigned beams were defined same as the depth of the slab. Displacement increments were imposed at the center of the columns. Until the punching failure of the slab-column connection, static pushover analysis was conducted. The final state of the connection was shown in Figure 3.11.

The procedure of the analysis was same as the shell method. In the first part of the analysis, to define the cracked sections, the stiffness of the slab was taken as  $E_c I/3$ .



**Figure 3.11 The Final Stage of Shear Hinges**

It can be discovered that, when stiffness was taken as  $E_c I/3$  to simulate slab cracking, a good match was obtained for the initial stiffness but by using that stiff initial loading brunch, the ductility could be grossly overestimated.

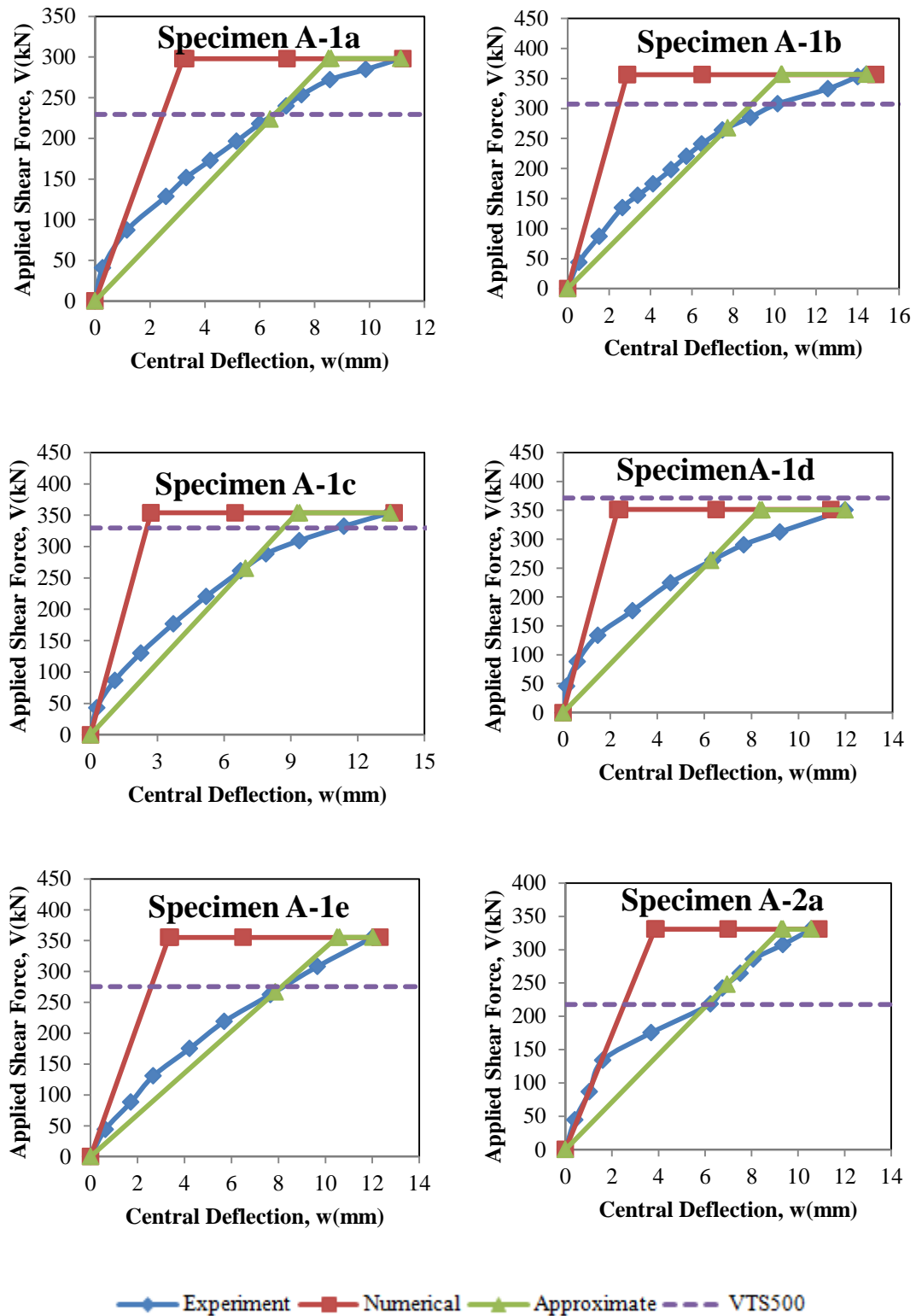
On the experimental load deformation graphs 75% of the exact punching load value was marked and a straight line was drawn from the zero point to the 75% of the maximum load ( $K_{75\%}$  :stiffness of the load deformation graph) for supplying a better estimation of the experimental load deformation response, and the line was extended until it reached the actual load deformation curve with the same slope, so better representation of cracked stiffness was obtained.

In the following part of the analysis, the effective stiffness of the slab that would give the  $K_{75\%}$  was back calculated. Then an  $\alpha$  value was found for each experiment

where  $\alpha = \frac{E_{75\%}}{E_{ACI}}$  and by the use of this  $\alpha$  value a new stiffness definition was obtained. By using this new stiffness instead of  $EI/3$ , found stiffness was exactly equal to  $K_{75\%}$ , so it gave more reliable and proper results for deformability estimations. The summary of the results were given in Figures 3.12, 3.13 and 3.14. The back-calculated  $\alpha$  and  $\mu_{\Delta}$  (displacement ductility  $\Delta_u/\Delta_y$ ) values by matching the  $K_{75\%}$  were plotted in Figures 3.15 and 3.16. It can be found that, although  $\mu_{\Delta}$  is inversely proportional with  $\rho$ ,  $\alpha$  is directly proportional with  $\rho$ . The following best fit expressions can be used to estimate  $\mu_{\Delta}$  and  $\alpha$  as a function of  $\rho$  based on the database of Hognestad:

$$\checkmark \quad \mu_{\Delta} = 5.4\rho^{-1.4} \quad (3.3)$$

$$\checkmark \quad \alpha = 0.02\rho^2 - 0.04\rho + 0.13 \quad (3.4)$$



**Figure 3.12 Summary of the load deformation curves for beam method**



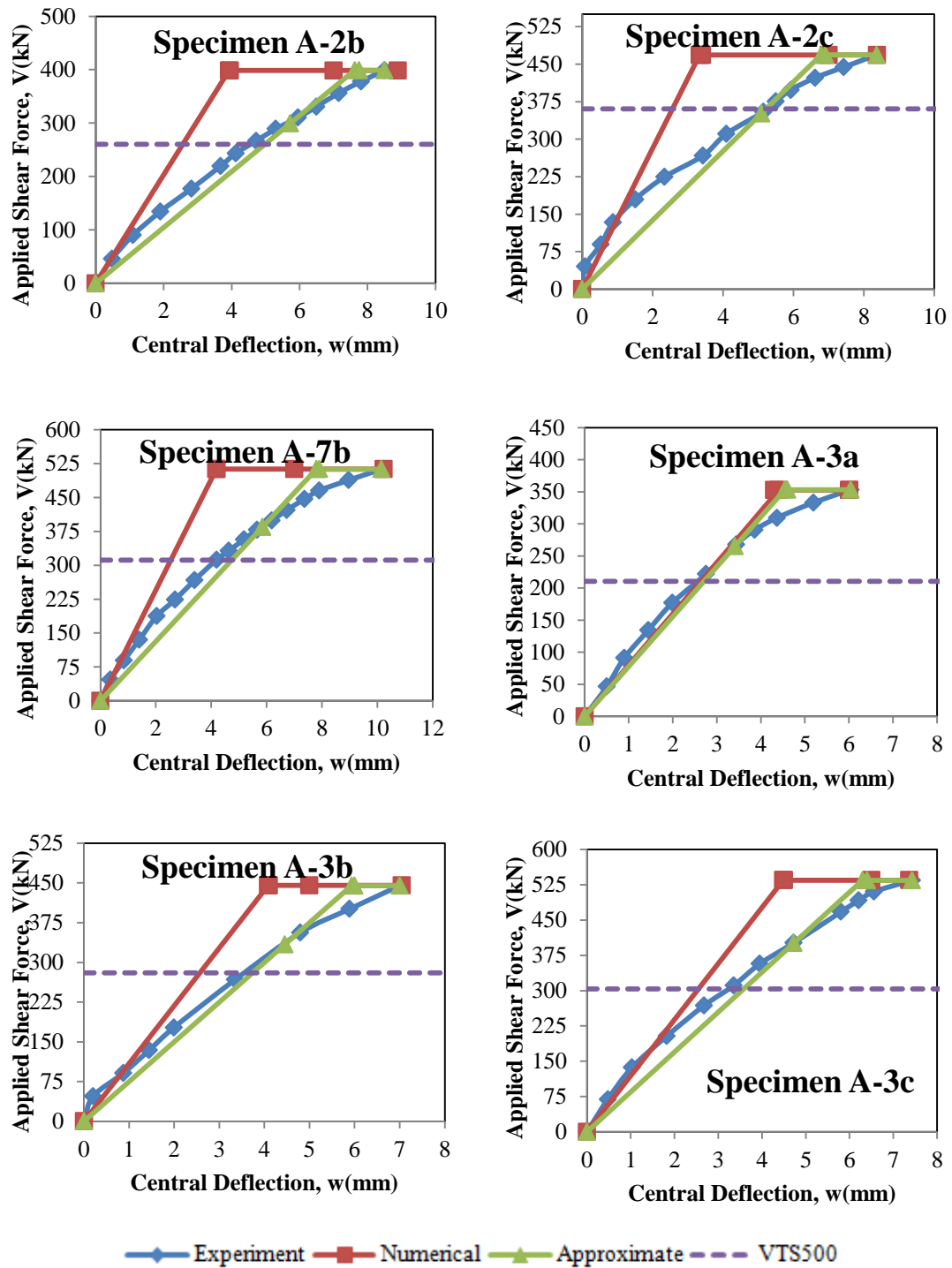


Figure 3.13 Summary of the load deformation curves for beam method

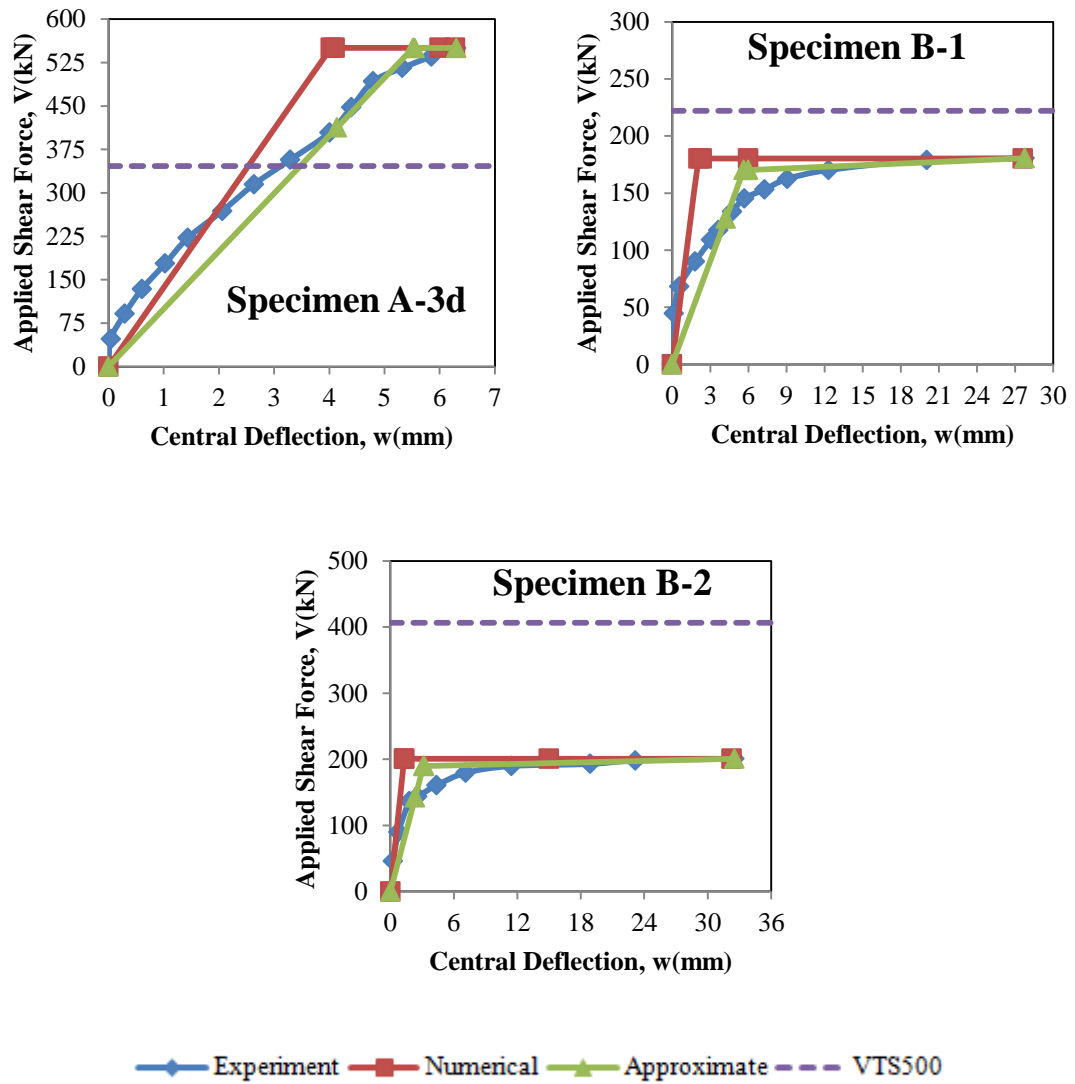
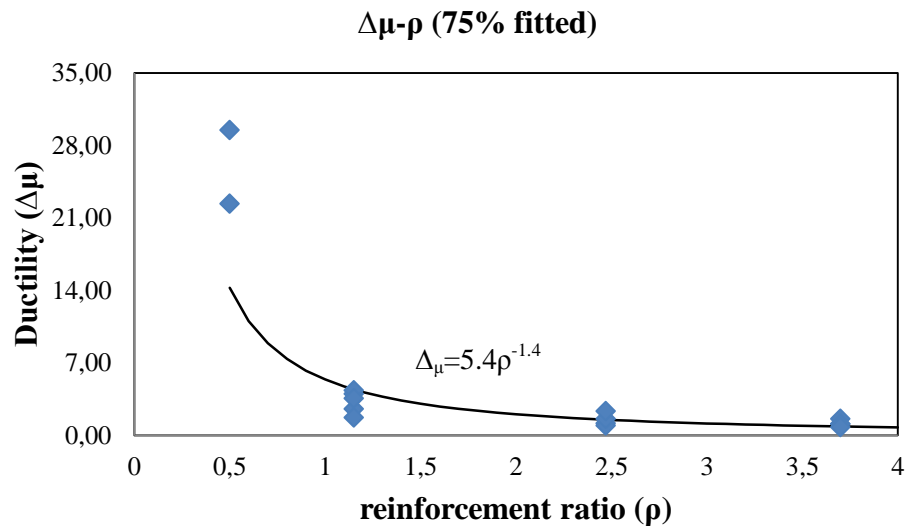
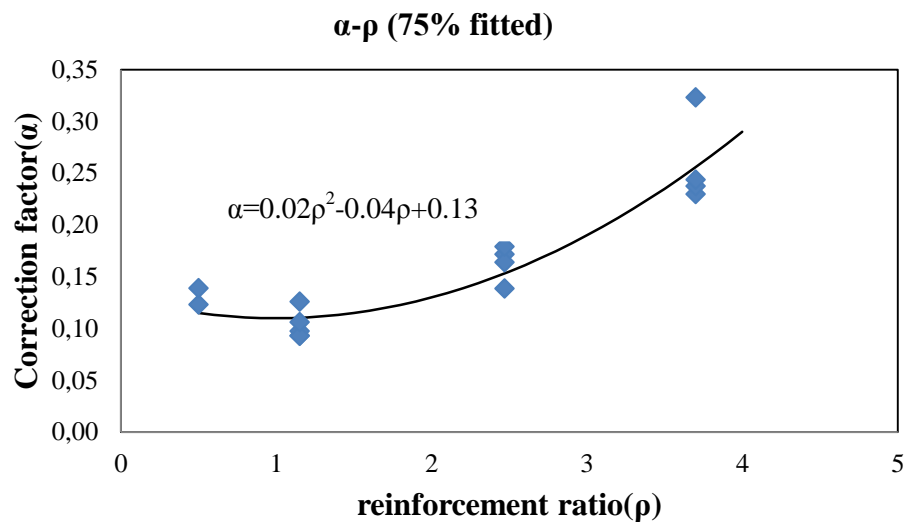


Figure 3.14 Summary of the load deformation curves for beam method



**Figure 3.15 Ductility versus reinforcement ratio curve**



**Figure 3.16 Correction factor versus reinforcement ratio curve**

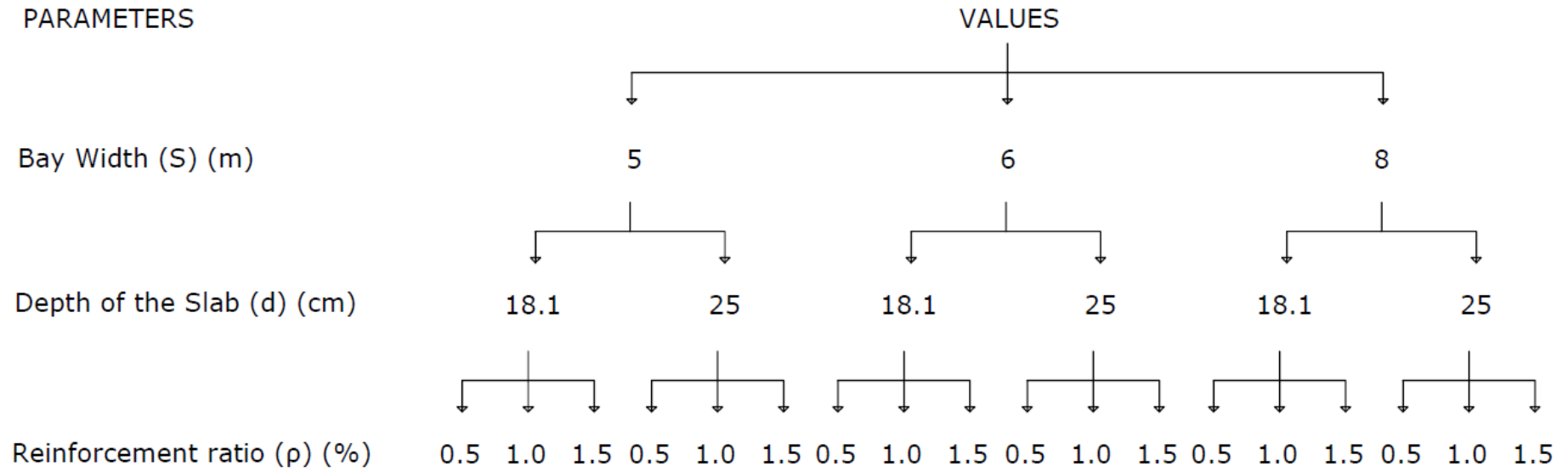
## CHAPTER 4

### A NUMERICAL STUDY TO EXAMINE THE POST-PUNCHING CAPACITY REQUIRED TO AVOID PROGRESSIVE PUNCHING

#### 4.1. Introduction:

The aim of this chapter is to demonstrate the minimum post-punching capacity required to avoid progressive punching failure in a flat plate system. For this purpose typical floor plans of a flat plate system were selected. The effective depth of the slab ( $d$ ), the bay width ( $S$ ) and the reinforcement ratio ( $\rho$ ) were the major model parameters. Three different bay widths were chosen, which were 5, 6 and 8 meters. For each bay widths, both 180 and 250 mm slab effective depths were examined. Finally each slab effective depth was investigated by using 3 different reinforcement ratios (0.5%, 1.0% and 1.5%). The strength of concrete was chosen as 27 MPa. The analysis matrix is presented in Figure 4.1.

The difference in reinforcement ratio affected mainly two parameters, which are the effective stiffness to incorporate cracking and the ductility. Both parameters were taken into account to understand the behavior. By using  *$\alpha$  versus reinforcement ratio* and *ductility versus reinforcement ratio* equations proposed in Chapter 3, these parameters were calculated.

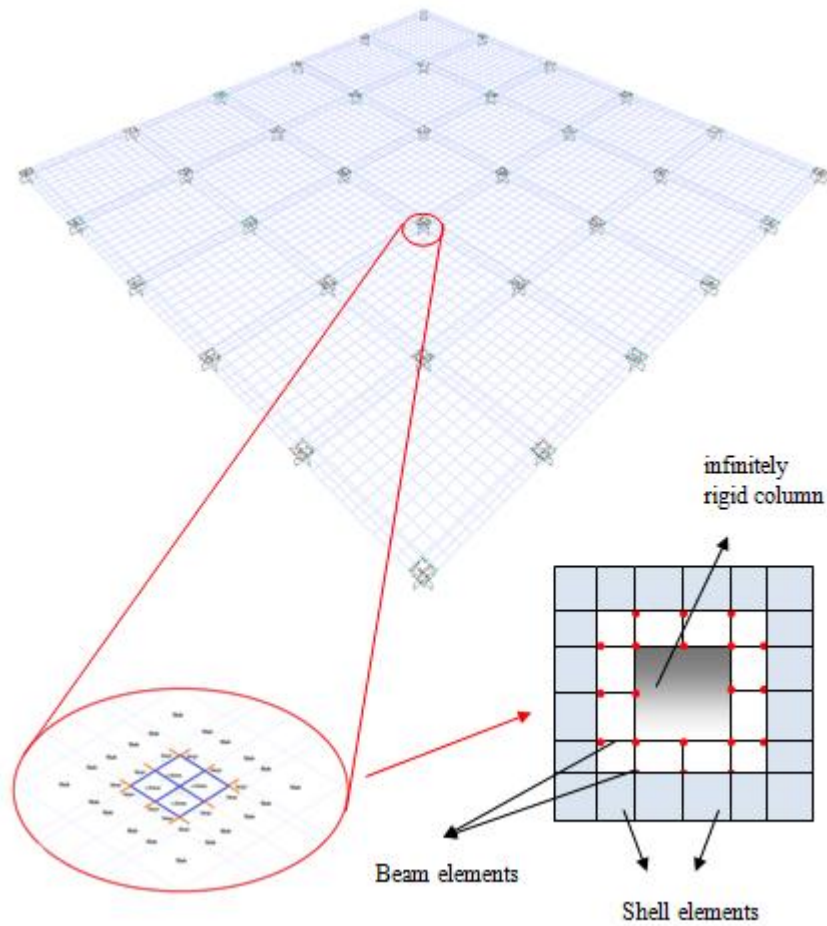


**Figure 4.1 Analysis procedure of slab column connections**

The general properties of the slab-column connection system and how they were used in SAP 2000 has to be elaborated.

The flat plate model used in the study consisted of 36 columns, with cross section dimensions of 450x450 mm. The connection regions were defined with infinitely rigid members. Moreover, fixed ended restraints were assigned to the bottom of each column to simulate the column supports. Beam members were defined from the column face to a distance of  $d/2$  from this location to read the shear force around the connection region. Punching shear strength was calculated according to TS500 design equations. The slab elements were modelled with shell elements. For each analysis the slab was divided into a fine enough mesh (73x73 elements for each bay). This mesh size was found to be optimum for the system, since beyond that number the analysis process was taking very long time without any change in the displacements. The general view of the system and its members is shown in Figure 4.2. Figures 4.3, 4.4 and 4.5 demonstrate the models in each step and Figure 4.6 shows the complete process of analysis.

Because of the eccentricity in the neighboring connections, the side of the slab-column connection (S2) closest to the loaded column (S1) was considered as the critical side. The average shear force on this side was taken as the critical shear in the neighboring connection (average of  $x_1$ ,  $x_2$  and  $x_3$ ).



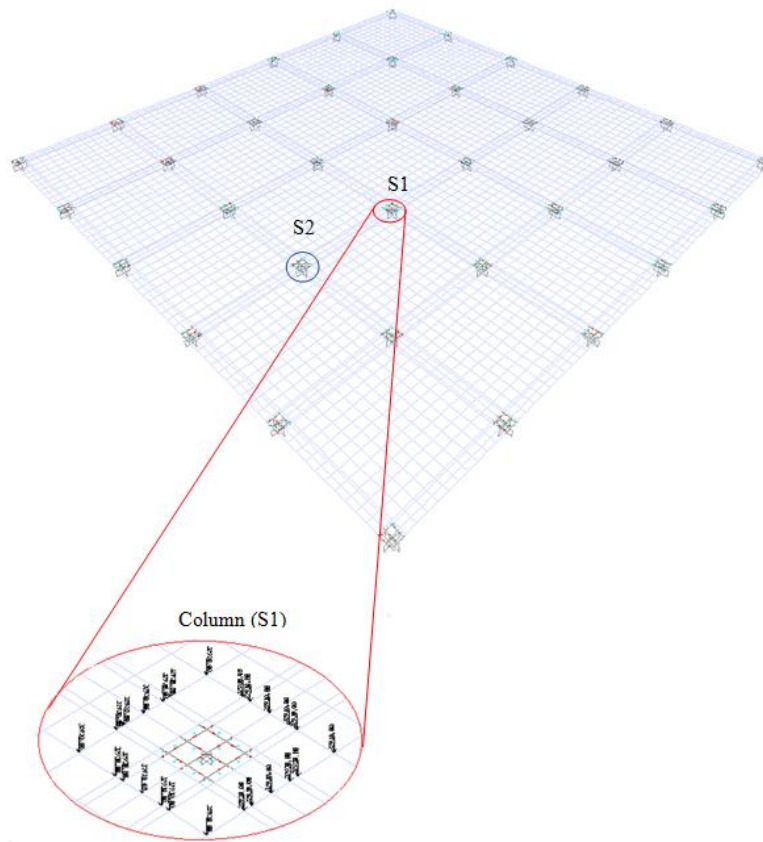
**Figure 4.2 The general view of the system and its member**

#### **4.2. Explanation of Collapse Analysis Steps:**

To determine the punching process of the slab-column connections, middle slab-column connection was loaded in three steps. These steps are explained in detail in the following paragraphs.

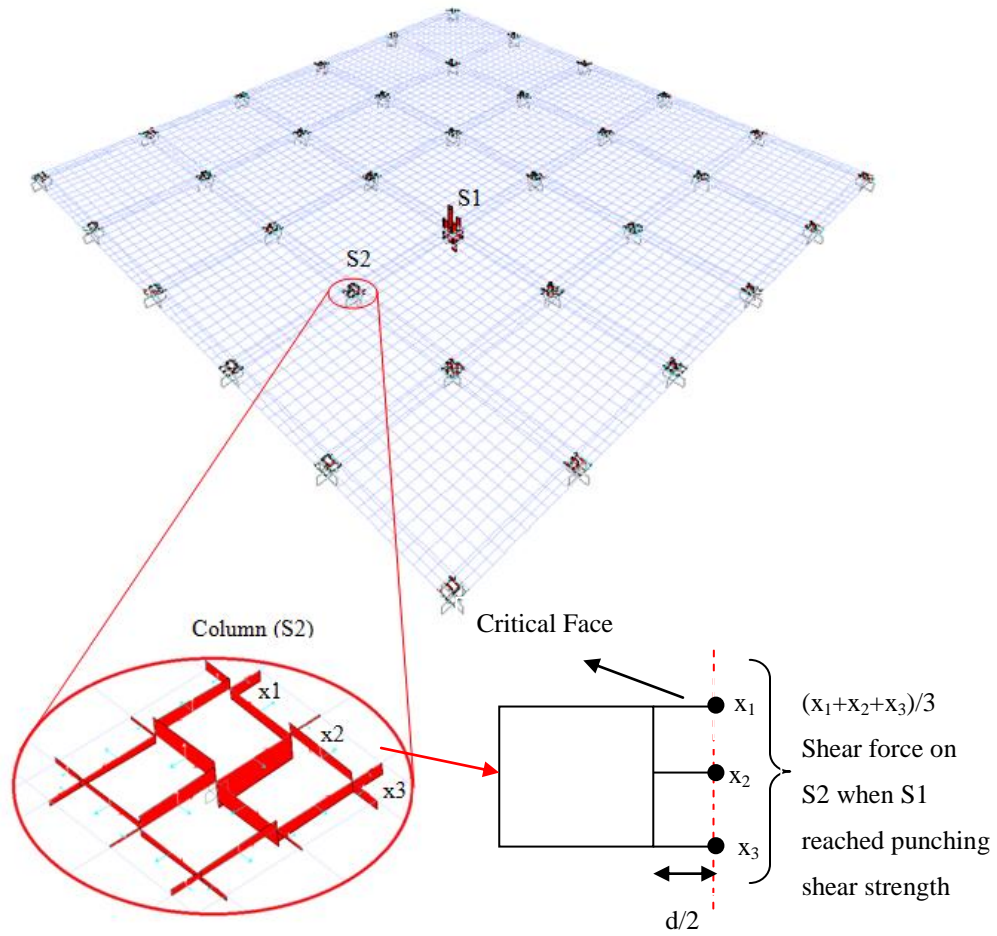
#### 4.2.1. Step 1:

Step 1 represented the elastic part of the analysis. In other words, Step 1 had ended when the loaded connection reached the punching capacity. In this step, initially both live and reduced dead loads were applied on the whole floor, where the live load was assumed as  $195.28 \text{ kg/m}^2$  and the reduced dead load was assumed as  $976.88 \text{ kg/m}^2$ . In the presence of these loads, an extra load was imposed to the slab column connection around the column S1 (see Figure 4.3), and its value was increased until the connection reached the punching point in the load combination  $DL+LL+Point$  Load, such that end of this step (Point A in Figure 4.6) the slab-column connection under consideration experienced punching failure. At the end of this step, the highest mean shear force (S2 column in Figure 4.3) was recorded in the neighboring connection as  $R_1$ .



**Figure 4.3 Applied Load to the column S1**



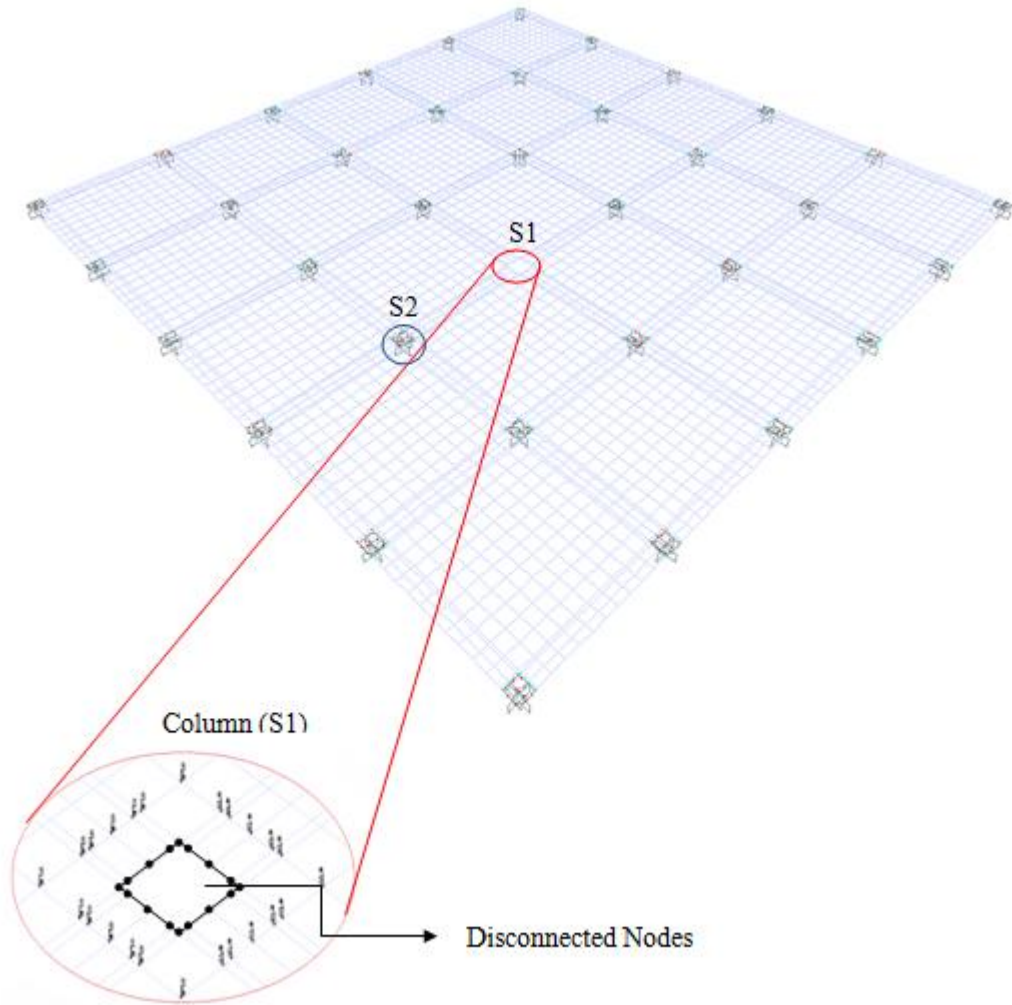


**Figure 4.4 Shear distribution of the system**

#### 4.2.2. Step 2:

After the loaded slab column connection reached the punching state in Step1, the connection was assumed to carry no additional shear force. For this reason, the connection was redefined by disconnecting the nodes around the connection, as seen in Figure 4.5. The aim of Step 2 was to simulate the yielding behavior of the connection prior to punch through action. After determining the ductility value of the slab-column connection by using Equation 3.2, load  $V_2$  was applied around S1 slab column-connection until the displacement at punching value was reached. This was referred as point B in Figure 4.6. Then the maximum mean shear forces of the edge

closest to the loaded column of the neighbor slab column connection (around column S2) was recorded with the same procedure in Step1 as  $R_2$ .



**Figure 4.5 System View and Loading Path of Step 2**

#### **4.2.3. Step 3:**

The post-punching mechanism of the loaded slab column connection was simulated in this step. A load with a value of  $V_3 + (V_p - V_{pp})$  was imposed to the same area that was used in the previous two steps. Here,  $V_p$  is the punching shear capacity of the slab column connection and  $V_{pp}$  is the post-punching shear capacity of the

connection.  $V_{pp}$  value was taken initially as 0% and it was increased till the neighbor connection did not punch. In other words,  $V_3$  was assigned to be equal to  $V_f - V_1 - V_2$ , where  $V_f$  was considered as the punching shear capacity ( $V_p$ ). It means that, the slab system was loaded with  $D+L+V_{pp}$  around the slab column connection region (S1). Under these loads, our aim was to observe the  $V_{pp}$  required so that punching did not occur in the neighboring connection S2. When a load of  $V_3 + (V_p - V_{pp})$  was applied to the system, post-punching behavior of the connection could be observed and on the load deformation curve point C was reached (Figure 4.6). Finally, the mean value of the shear forces on the critical side of the S2 was recorded as  $R_3$ .

Summing  $R_1$ ,  $R_2$  and  $R_3$  the total shear force demand (reactions) on the neighboring connection was calculated. This reaction force was compared to the 1/3 of the punching shear strength according to TS500 using Equation 4.1:

$$V_p(\text{hinge}) = \left( \frac{b+d}{3} \right) \frac{\sqrt{f_c} * d}{3} \quad (4.1)$$

Whenever the punching load ( $R$ ) from the analysis was smaller than punching load value obtained from the previous formula, the set of analysis was stopped and that post-punching value was considered as the critical punching value.

Above procedure was applied to 18 slab systems by changing  $V_{pp}$  from 0 to 100% of  $V_p$  in increments.




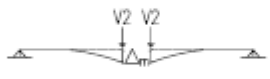
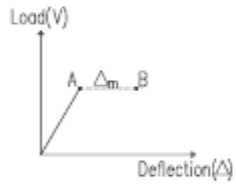


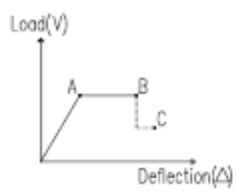
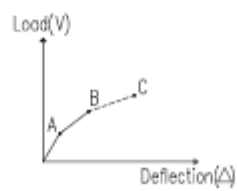
Step Name	Load Assign	Applied Load	Load Deflection Curve of Loaded Connection	Load Deflection Curve of Neighbor Connection
Step 1:	 <p> <math>V_1</math> <math>V_1</math>  <math>V = V_p</math>            Increase <math>V_1</math> when reaction <math>V = V_p</math> </p>	$V_1$		
Step 2:	 <p> <math>V_2</math> <math>V_2</math>  <math>\Delta_m</math>            Increase <math>V_2</math> when <math>\Delta = \Delta_m</math> </p>	$V_2$		
Step 3:	 <p> <math>V_3</math> <math>V_3</math>  <math>V_p - V_{pp}</math>  <math>V_1 - V_1 - V_2 = V_3</math> </p>	$V_3 + (V_p - V_{pp})$		

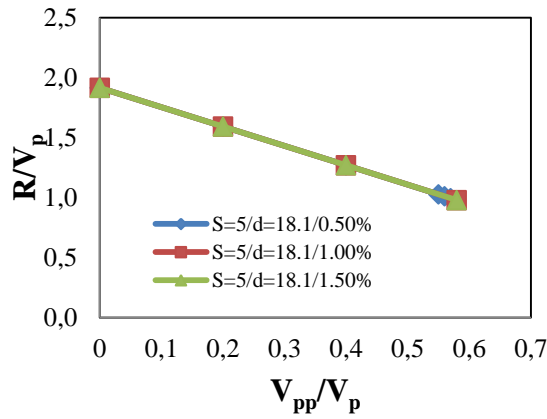
Figure 4.6 Summary of Steps1-2 and 3

### 4.3.Results:

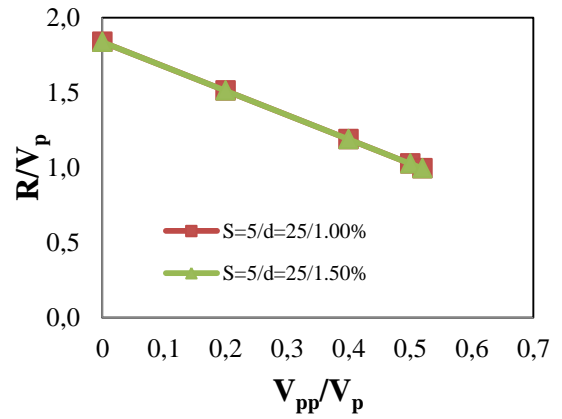
In Figure 4.7 the relationship between  $V_{pp}/V_p$  and  $R/V_p$  is shown for every combination of bay widths (S) and slab depth (d). As it can be seen from this figure,  $V_{pp}/V_p$  versus  $R/V_p$  lines for all reinforcement ratio are similar when the bay width and slab depth are kept constant. This means that the reinforcement ratio, which affects the stiffness and the ductility, has almost no effect on punching. However, the other two parameters, bay width and slab depth, change the post-punching values dramatically. So on the contrary of reinforcement ratio, these two parameters are highly effective on punching behavior. If a general  $V_{pp}/V_p$  versus  $R/V_p$  graph is intended to be drawn, the effect of reinforcement ratio can be ignored and for each combination one line can be drawn instead of three. In the light of this information, Figure 4.8 can be counted as the summary of the combinations of space length and slab depth.

When a slab column connection has low reinforcement ratio it means that it has high ductility level. If the slab thickness is high enough the neighboring slab column connection does not reach to the punching point even 0% postpunching value, since in existence of the total of the  $V_1$  and  $V_2$  loads the connection reached already the final state ( $V_{pp}+DL+LL$ ) . So this event shows the importance of the ductility.

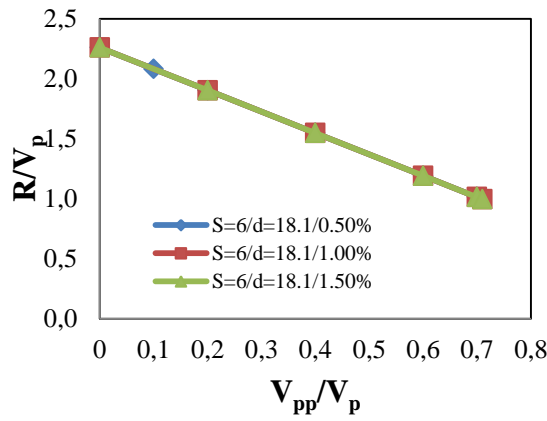
Figure 4.8 shows that around 50% of  $V_p$  should be provided as  $V_{pp}$  to avoid progressive punching. The more ductile the connection is the higher the load carrying capacity. Therefore punching shear failure of the slab column connections can be eliminated through a ductile connection and sufficient post punching based design philosophy.



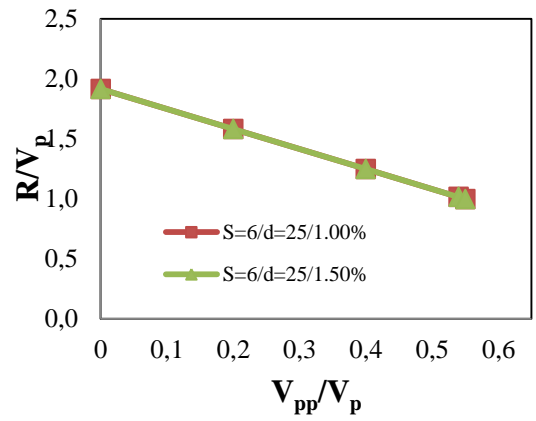
a. S = 5 m, d = 18.1 cm



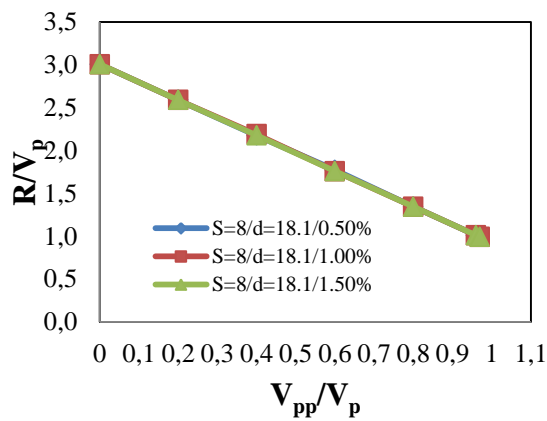
b. S = 5 m, d = 25 cm



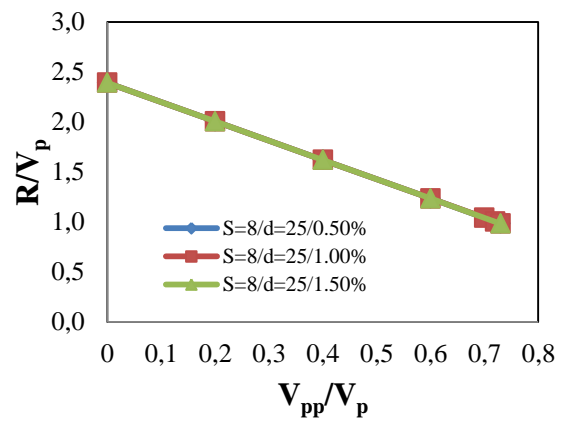
c. S = 6 m, d = 18.1 cm



d. S = 6 m, d = 25 cm

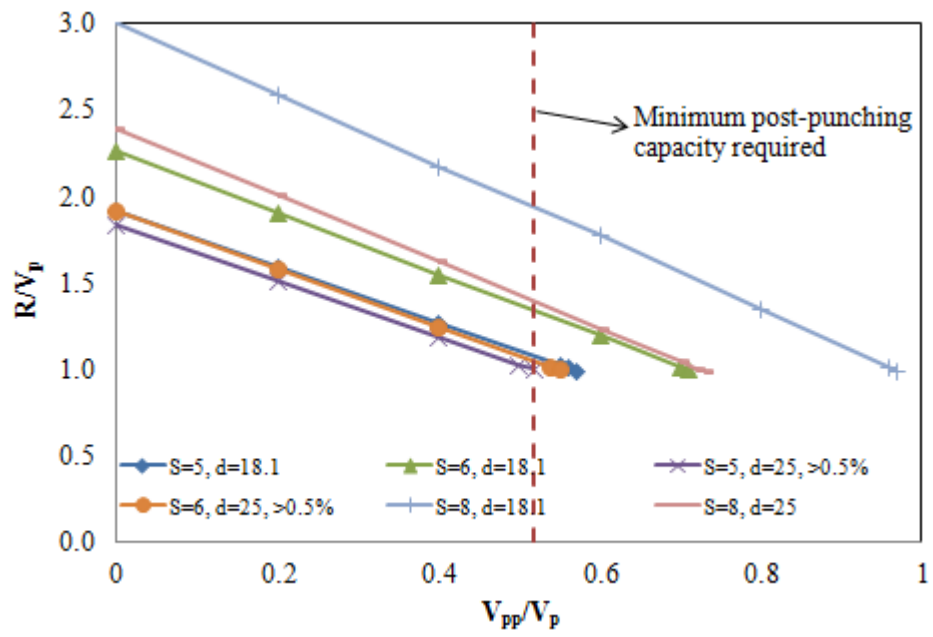


e. S = 8 m, d = 18.1 cm



f. S = 8 m, d = 25 cm

**Figure 4.7 The relationship between  $V_{pp}/V_p$  and  $R/V_p$**



**Figure 4.8** The summary of the relationship between  $V_{pp}/V_p$  and  $R/V_p$

## CHAPTER 5

### CONCLUSIONS AND RECOMMENDATIONS

The safety levels inherent in the three current design codes (ACI-318, Eurocode-2 and TS500) were examined in light of test results both for eccentric and concentric type of loading cases in Chapter 2. Obtained results can be summarized as follows:

- For the interior slab column connections under concentric type of loading, Eurocode-2 is found to have the least amount of safety excluding material strength reduction factors. The best estimate of  $V_{exp}/V_{code}$  was obtained upon employing the equations given in TS-500.
- However, for estimating the strength of interior slab column connection under eccentric loading, ACI was found as the most accurate guideline in the average sense. TS500 was the safest among the three codes for interior slab column connections.
- When the experimental data for exterior slab column connection under eccentric loading were compared with the design codes, although TS500 turns out to provide the safest estimations among the three codes, ACI-318 is found to be the most accurate code in the average sense. Compared to the other type of loadings, the accuracy of strength predictions for exterior slab column connections are less accurate and shows wider scatter. This calls for further research on better strength prediction models of exterior slab column connections.
- TS500 provides satisfactory estimation for concentric interior slab-column connection and eccentric interior slab-column connection, whereas it lacks



sufficient information for exterior slab-column connection. In addition, for eccentric type of loading the  $W$  value should be given in TS500.

- None of the codes provides an uniform level of safety for different loading cases, despite that same failure mode are considered.

Failure mechanism of a slab-column connection was simulated with simple models in Chapter 4. For this purpose, the load deformation behavior of a slab-column connection was simulated by using both shell and beam methods. Following major results were obtained:

- For both shell and beam methods, the use of  $E_c I/3$  stiffness to simulate slab cracking provided a good match for the initial stiffness but when such a stiff initial loading branch was used, the ductility was grossly overestimated.
- A new stiffness definition was proposed, which gives more reliable and proper results for deformability estimations.

The minimum post-punching capacity required to avoid progressive punching failure in a flat plate system was investigated in Chapter 4. The conclusions from the analyses are as follows:

- Bay width and effective slab depth are found to be the most important parameters effecting the punching shear force acting on a slab column connection.
- Providing 50% of punching shear strength as post punching capacity at a slab column connection may help to avoid progressive punching failures taking place after one sudden punching failure. A ductile connection and sufficient post punching capacity based design philosophy may help to avoid progressive collapse in flat plate structures.

- Additional continuous rebars passing through the slab-column connections may be supplied to provide additional post punching resistance through dowel action (Currently only two bars are needed according to ACI). Further experiments are needed to further quantify this conclusion.

## REFERENCES

- ACI Committee 318. (2011). *Building Code Requirements for Structural Concrete (ACI318-05) and Commentary (ACI 318R-05)*. Farmington Hills, Michigan: American Concrete Institute.
- Arnold, R. L. (1994). The Quake of '94. *Disaster Recovery Journal*.
- Bertero, V. V. (June 1982). State of the Art in Seismic Resistant Construction of Structures. *Proceedings of the Third International Earthquake Microzonation Conference. II*, pp. 767-805. Washington: University of Washington.
- CEB/fib Task Group. (2001). *Punching of Structural Concrete Slabs*. Stuttgart: International Federation of Structural Concrete.
- Corley, G. W. (2010). *Collapse of Harbour Cay Condominium*. Structural Engineering Institute.
- Dewey, J. (1994, January 17). *U.S. Geological Survey*. Retrieved February 4, 2012, from U.S. Geological Survey Web site: <http://www.ngdc.noaa.gov>
- Durrani, A. J., Du, Y., & Luo, Y. H. (1995, July-August). Seismic Resistance of Nonductile Slab-Column Connections in Existing Flat-Slab Buildings. *ACI Structural Journal*, 92, 479-487.
- Elstner, R. C., & Hognestad, E. (1956, July). Shear Strengths of Reinforced Concrete Strengths. *Journal of American Concrete Institute*, 28, 29-58.
- Eurocode 2-2003. (2003). *Eurocode 2: Design of concrete structures-Part 1.1: General rules and rules for buildings*. Brussels: European Committee for Standardization.
- Farhey, D. N., Adin, M. A., & Yankelevsky, D. Z. (1993, June 6). RC Flat Slab-Column Subassemblages Under Lateral Loading. *Journal of Structural Engineering*, 119, 1903-1916.
- Hueste, M. B., Browning, J., Lepage, A., & Wallace, J. W. (2007, July-August). Seismic Design Criteria for Slab-Column Connections. *ACI Structural Journal*, 104, 448-458.

- Kang, T. H.-K., Wallace, J. W., & Elwood, K. J. (2009, February). Nonlinear Modeling of Flat-Plate Systems. *Journal of Structural Engineering*, 147-158.
- McLean, C., Andreson, B., Peterlin, C., & Del Vecchio, K. (n.d.). Wikispaces. Retrieved February 10, 2012, from <http://failures.wikispaces.com/Sampoong+Department+Store>
- Mirzaei, Y. (2010). *Post-Punching Behavior of Reinforced Concrete Slabs*. Lausanne: École Polytechnique Fédérale de Lausanne. Retrieved Mai 12, 2010
- Moehle, J. P., Kreger, M. E., & Leon, R. (1988). Background to Recommendations for Design of Reinforced Concrete Slab-Column Connections. *ACI Structural Journal*, 636-644.
- Pan, A. D., & Moehle, J. P. (1992, November-December). An Experimental Study of Slab-Column Connections . *ACI Structural Journal*, 89, 626-638.
- Pan, A., & Moehle, J. P. (1987). *Lateral Displacement Ductility of Reinforced Concrete Flat Plates*. Berkeley, California: University of California .
- Park, H.-G., & Choi, K.-K. (2006, May 5). Improved Strength Model for Interior Flat Plate-Column Connections Subject to Unbalanced Moment. *Journal of Structural Engineering*, 132, 694-704.
- Park, H.-G., & Choi, K.-K. (2007). Strength of exterior slab-column connections subjected to unbalanced moments. *Engineering Structures Vol. 29*, 1096-1114.
- Park, T. W. (2011). Inspection of collapse cause of Sampoong Department Store. *Science Direct*, 119-126.
- Parking Garage Collapse*. Reinsurance Company, Munich.
- Rashita, Hamid A.; Yeng, Ai Chun; Beh, Yen Hui; Kumar, M.; Tan, Karr Wei. (2009). *Jaya Supermarket collapses*. The Stao Online.
- Robertson, I. N., & Durrani, A. J. (1992). Gravity Load Effect on Seismic Behavior of Interior Slab-Column Connections. *ACI Structural Journal*, 37-45.
- Rosenblueth, E., & Meli, R. (1986). The 1985 earthquake: causes and effects in Mexico City. (23-36, Ed.) *ACI* , 8.

- The Constructor Org.* (n.d.). Retrieved October 22, 2011, from The Constructor Organization Web site: <http://theconstructor.org/structural-enng/flat-slab>
- Turkish Standards Institutes. (2000). *Requirements for Design and Construction of Reinforced Concrete Structures*. Ankara: Turkish Standards Institutes.
- USGS. (1996, November 16). *USGS Response to an Urban Earthquake -- Northridge '94*. Retrieved February 9, 2012, from U.S. Geological Survey: <http://pubs.usgs.gov/of/1996/ofr-96-0263/introduc.htm#impacts>
- Zee, H. L., & Moehle, J. P. (1984). *Behaviour of Interior and Exterior Flat Plate Connections Subjected to Inelastic Load Reversals*. Berkeley: National Science Foundation.